1976

Electrosorption Effects Of Carboxylic Acids On The Kinetics Of Copper Electrodeposition

Robert Steven Salter

ELECTROSORPTION EFFECTS OF CARBOXYLIC ACIDS ON THE KINETICS OF COPPER ELECTRODEPOSITION

by

Robert Steven Salter

Department of Chemistry

Submitted in partial fulfillment

of the requirements for the degree of

Doctor of Philosophy

Faculty of Graduate Studies

The University of Western Ontario

London, Ontario

October, 1975

To my Wife.

ABSTRACT

The effect of neutral, electroinactive organic adsorbates on the kinetics of copper electrodeposition on a copper electrode was studied using the galvanostatic method. In general, the presence of these additives gave rise to an increase in cathode overpotential and a decrease in the apparent symmetry factor of the charge-transfer process. A theoretical examination of the kinetics of copper deposition in the presence of organic additives predicted that these effects could be explained by a physical blocking of the surface by adsorbed additive. The adsorbates were considered not only to block part of the surface to deposition thereby increasing the geometric current density but also to interfere with the transport of reacting ions at the interphase. A modified blocking equation was developed to enable the calculation of "blocking" surface coverages of adsorbed organics from kinetic data.

The adsorption of six normal monocarboxylic and eight dicarboxylic acids was studied in relation to their effects on the cathode overpotential and Tafel slope for copper deposition. The modified blocking equation was used to calculate surface coverages and hence plot adsorption isotherms.

A theoretical adsorption isotherm was developed to enable the calculation of standard free energies of adsorption from "blocking" surface coverages. Consideration was given to three orientations of adsorbate on the surface and standard free energies of adsorption were calculated for the aliphatic carboxylic acids for each of these orientations. In all cases the free energy was found to vary with

coverage. This coverage dependence of the free energy was attributed to the lateral interaction, dipole-dipole effects, within the adsorbed phase.

Calculated values of the interaction free energy were plotted against the theoretical functional dependencies of the surface coverage for the different orientations and modes of adsorption. The best agreement with the "normalized", linear predicted behaviour was obtained for localized adsorption, parallel orientation for adsorption of the mono-carboxylic acids.

The adsorption of the dicarboxylic acids also appeared to be localized, however, the orientation of adsorption appeared to depend on the length and flexibility of the compound, and the surface coverage.

The adsorption of four homologous aromatic carboxylic acids was studied in relation to their effects on the kinetics of the deposition process using the same techniques employed for the aliphatic acids. The adsorption isotherms for benzoic, 3-phenyl-propanoic, and 4-phenyl-butanoic acids were "S" shaped. A sharp decrease in the Tafel slope was observed at additive concentrations corresponding to the inflections in the isotherms. These effects were attributed to strong attractive interaction in the adsorbed phase causing the formation of a condensed adsorbed layer.

Phenyl-acetic acid exhibited a Langmuir isotherm and an increase in Tafel slope over the concentration range studied. An examination of the structure of this compound showed that the formation of a condensed layer was not possible.

The electrode capacitance was studied as a function of bulk concentration of aromatic acid by the overpotential decay method. A minimum in capacity was observed at concentrations corresponding to the decrease in Tafel slope and isotherm inflection regions. These minima and subsequent increase in capacity were attributed to adsorption "pseudo" capacitance due to the irreversibility of the adsorption process brought on by the strong intermolecular attraction in the adsorbed phase.

Phenyl-acetic acid, as expected, showed a gradual decrease in capacitance over the entire range of concentrations studied.

ACKNOWLEDGEMENTS

Sincere thanks are expressed to Dr. A. J. Sukava for his helpful suggestions, constant encouragement, and appreciated direction during the course of this work.

Thanks are also extended to Dr. J.W. Lorimer, Dr. E. Sherman, Dr. F.P. Dieken and Dr. D. Gannon of the Chemistry Department for their useful discussions.

The assistance and time given the author by the support staff of the University community is also greatly appreciated.

The financial support of the National Research Council, Department of University Affairs of Ontario and the Department of Chemistry is gratefully acknowledged.

TABLE OF CONTENTS

LIST OF TABLES

LIST OF FIGURES

LIST OF SYMBOLS

SYMBOL	
a	Tafel intercept or interaction constant
a_i	activity of species i
b	Tafel slope
C,Cap	electrode capacity
C_{org}	bulk concentration of organic
e	electronic charge or exponential
F	Faraday constant
ΔG	free energy of reaction
ΔG_+^*, ΔG_-^*	free energy of activation of forward, reverse reaction
ΔG°_{ads}	standard free energy of adsorption
$\Delta G^\circ_a(0)$	standard free energy of adsorption at the zero coverage limit
g(θ)	lateral interaction free energy
h	Planck constant
i	net current density
i_a	anodic current density
i_c	cathodic current density
i_g	geometric current density
i_o	exchange current density
i_+,i_-	current density of forward,reverse reaction
k	Boltzmann constant
K	specific conductance or rate constant
K_+,K_-°	rate constant of forward, reverse reaction
n	solvent displacement number

SYMBOL	
n^*	blocking projection number
NHE	normal hydrogen electrode
N_i	number of solvent lattice sites on the surface occupied by species i
O.H.P.	outer Helmholtz plane
P	pressure
pzc	potential of zero charge
q	charge density
q_1, q_2	internal partition functions of solvent, adsorbate
R	universal gas constant or resistance
T	temperature
t	time
v_+, v_-	rate of forward, reverse reaction
w	work
X_i	site fraction of species i
Y_i	mole fraction of species i
Z	impedance
α	cathodic charge-transfer coefficient
α'	apparent charge-transfer coefficient
β	symmetry factor
β_o	symmetry factor when overpotential equals zero
β'	apparent symmetry factor
γ	surface tension
γ^*	activity coefficient of activated complex

SYMBOL	
η	overpotential
θ	fractional surface coverage
ϵ	dielectric constant
μ_i	chemical potential of species i
$\bar{\mu}_i$	electrochemical potential of charged species i
ϕ	Galvani potential
ϕ_1	potential at inner Helmholtz plane
ϕ_2	potential at outer Helmholtz plane
$\Delta\phi$	Galvani potential difference
$\Delta\phi_r$	reversible electrode potential
$\Delta\phi_{r_c}$	reversible electrode potential across compact double layer
$\Delta\bar{\phi}_r$	reversible electrode potential on the rational scale
$\Delta\phi^m_{q=0}$	potential of zero charge
Γ_i	surface excess of species i
ω	angular frequency
χ	surface potential
ψ	Volta potential
δ	roughness factor

CHAPTER 1

INTRODUCTION

1.1 REVERSIBLE ELECTRODE POTENTIALS

There are many types of electrodes, all of which share one common property: they function as sites for the transfer of electrical charge (electrons or ions) across a phase boundary. In one of the phases, charge moves by electronic conductive processes, whereas in the other, it moves by an electrolytic mechanism through the transport of charged particles (ions). The concept of electrode potential therefore involves the existence of a difference in charge density or energy of electrons in the two phases [1].

Immersing a metal electrode M in a solution of its ions M^{z+} involves the reaction

$$M^{z+}\ (l) + ze \rightleftarrows M\ (s) \qquad (1)$$

where l represents the liquid (solution) phase and s the solid (metal) phase. The electrode potential of this simple metallic electrode system may be regarded as the work required to move a metal ion from the solution phase across the boundary into the metal phase.

Consider each phase separately. An excess of ions or electrons in the surface imparts an electric potential ψ to that phase. This potential, called the external or Volta potential of the phase, is defined as the work done in bringing a unit point charge infinitely slowly from an infinite distance up to the surface of the phase [2].

The inner or Galvani potential ϕ of the phase, however, is defined as the work done in moving a unit charge from infinity to the interior of the phase. One can now write

$$\phi = \psi + \chi \qquad (2)$$

where χ is defined as the surface potential and is independent of the excess charge on the phase.

It is now necessary to examine the conditions of interphase equilibrium. If a neutral substance i is capable of passing freely from one phase to another, a condition of equilibrium will be reached when the chemical potential of this component μ_i is the same in the two phases. In an electrochemical system, however, in which only one type of charge carrier can cross the boundary, equality of the electrochemical potential $\bar{\mu}_i$ must be achieved before the phases are at equilibrium. The term electrochemical is used to signify that the potential may formally be regarded as arising from the sum of (a) energies of interactions of a chemical type between the particle and the material of the metal phase M (s) and (b) electrical energies associated with interaction of the particle with any net coulombic charge q on the phase, plus (c) any energy involved in the passage of the particle across the interface of the phase where surface dipoles or a surface field may exist [3,4]. Therefore, the electrochemical potential may be defined as

$$\bar{\mu}_i = \mu_i + z_i F \phi \qquad (3)$$

where F is the faraday. The Galvani potential difference at equilibrium $\Delta\phi$ of the process (V) becomes

$$\Delta\phi = \phi_s - \phi_l = \frac{\mu_l - \mu_s}{z_i F} \qquad (4)$$

Usually the difference of inner potentials $\Delta\phi$ cannot be measured except in the case of two identical electrodes of the same composition. At the same time, it is evident from equations (3) and (4) that the difference of chemical potential of a single charge species in two different phases is indeterminate. These difficulties have led to the conventional definition of "single electrode potentials" in terms of Galvani potential differences within a single phase rather than in terms of $\phi_s - \phi_l$ [1].

1.2 ELECTRICAL DOUBLE LAYER

The term electrical double layer is used in electrochemistry to describe the distribution of electrons, ions, solvent molecules, and other species at the interface between a metal and an electrolyte solution. Knowledge of this distribution is especially important because it strongly influences the mechanism and kinetics of electrochemical reactions occurring on the electrode.

The first models for the distribution of species at the electrode interface date back to Perrin [5] and Helmholtz [6] in the late nineteenth century. They pictured the double layer as a simple parallel plate condenser. This model was criticized by Gouy [7] and Chapman [8] because it failed to account for the thermal motion

of ions and solvent molecules causing some diffuseness of the charge on the electrolyte side of the double layer. The expressions derived by Gouy and Chapman for the distributions of ions and potential within this layer were only capable of qualitative agreement with experiment and Stern [9] attributed the discrepancies to neglect of the finite size of the ions. Recently Parsons [10] questioned Chapman's use of the mean dielectric constant of water in the theory. Investigations of Malsch [11] and Booth [12] indicated that the dielectric constant of water changes at high field strengths at the metal-solution interface.

Stern [9] combined the Perrin and Gouy-Chapman models into a model which formed the basis of all modern concepts of double layer structure. This model, improved upon by Grahame [13], is shown in Fig. 1. The diffuse layer ions were assumed to be of finite size and could approach the electrode only to a certain critical distance, determined by the size of the solvent molecules. The potential at this outer plane of ions was denoted by ϕ_2. Any specifically adsorbed ions could approach the electrode without interference from solvent and the centres of these ions were located at the inner Helmholtz plane. The potential at this layer was denoted by ϕ_1. Calculated values of the differential capacitance based on the Stern-Grahame double layer show excellent agreement with observed values for dilute solutions in the absence of specific adsorption. A comparison of the potential variation across the electrical double layer according to the Perrin, Gouy-Chapman, and Stern models is given in Fig. 2.

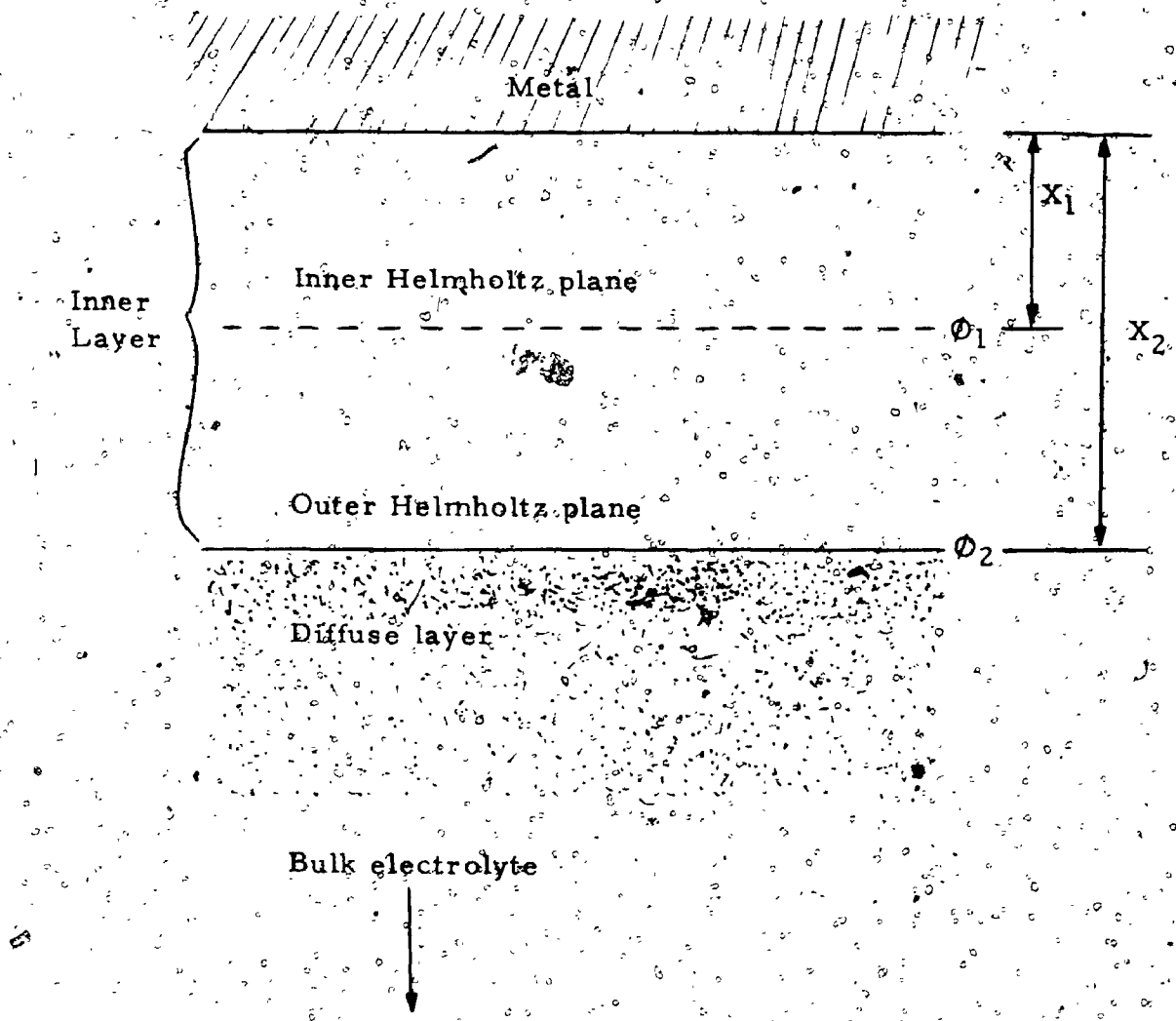

Fig. 1. Schematic diagram of Stern's model of the double layer as modified by Grahame. Specifically adsorbed ions populate the inner layer with their centers located at the inner Helmholtz plane. Diffuse layer ions penetrate no closer than the outer Helmholtz plane.

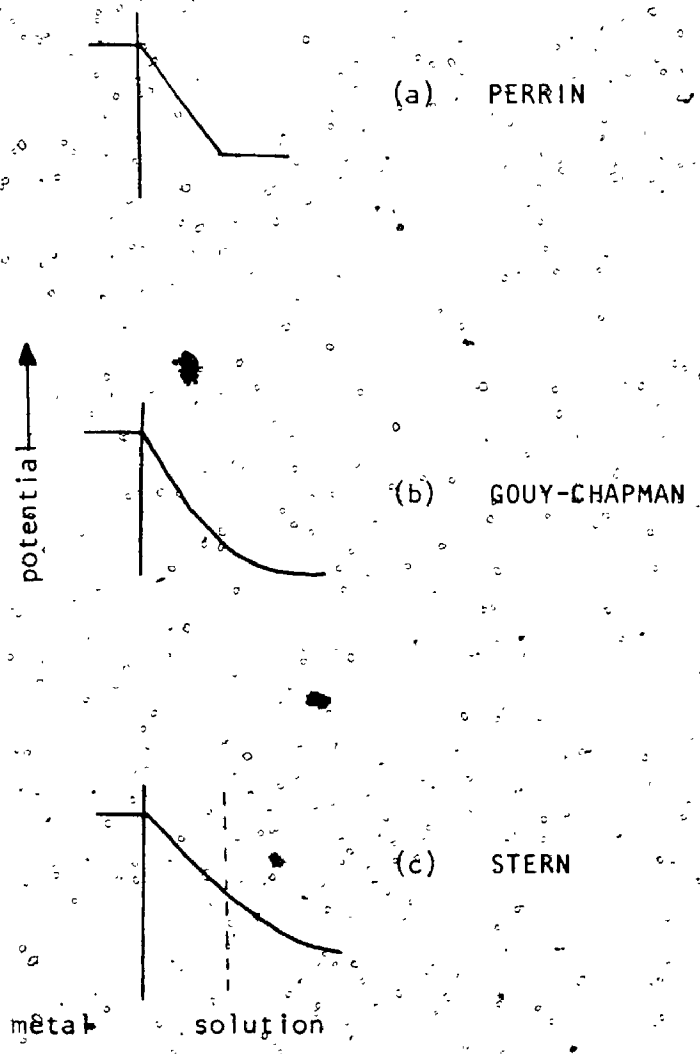

Fig. 2. Schematic representation of the variation of potential across the electrical double layer according to the model of (a) Perrin, (b) Gouy and Chapman, and (c) Stern.

Bockris, Devanathan, and Muller [14] pointed out the lack of consistency of these early treatments with the following experimental facts: (i) The minimum on the capacity-charge relation at -12 to -13 $\mu C\ cm^{-2}$ (or about -1.2 V on the normal calomel scale, Devanathan 1954) for mercury in contact with solutions containing cations of largely varying size is dependent on ion size, (ii) the degree of specific adsorption, i.e. the situation in which ions are adsorbed to an amount greater than that of the charge on the metal, of halide ions runs opposite to the order of the Hg -X bond strength, (iii) the degree of anionic adsorption as a function of charge undergoes an inflection at intermediate positive charges, (iv) a capacitance maximum occurs at positive rational potentials, (v) the maximum of the adsorption of aliphatic organic compounds occurs at a charge of about -2 $\mu C\ cm^{-2}$ (this charge is independent of the molecular structure of the organic compound, but depends on the metal), and (vi) water dipoles are adsorbed on electrodes, and the fraction of them which has a particular orientation in contact with the metal depends on the field in the double layer. Devanathan et al [14] considered adding a third layer to the Stern-Grahame model. They realized that the insertion of a layer of solvent molecules, oriented with respect to the electric field, between the metal surface and the solvated cations would make the model consistent with the capacitance data. Large polarizable anions are regarded as being able to penetrate this inner solvent layer since they are most capable of losing their solvation sheaths on approaching the inner layer. Electronic-image interactions were then regarded as responsible for the super-equivalent adsorption.

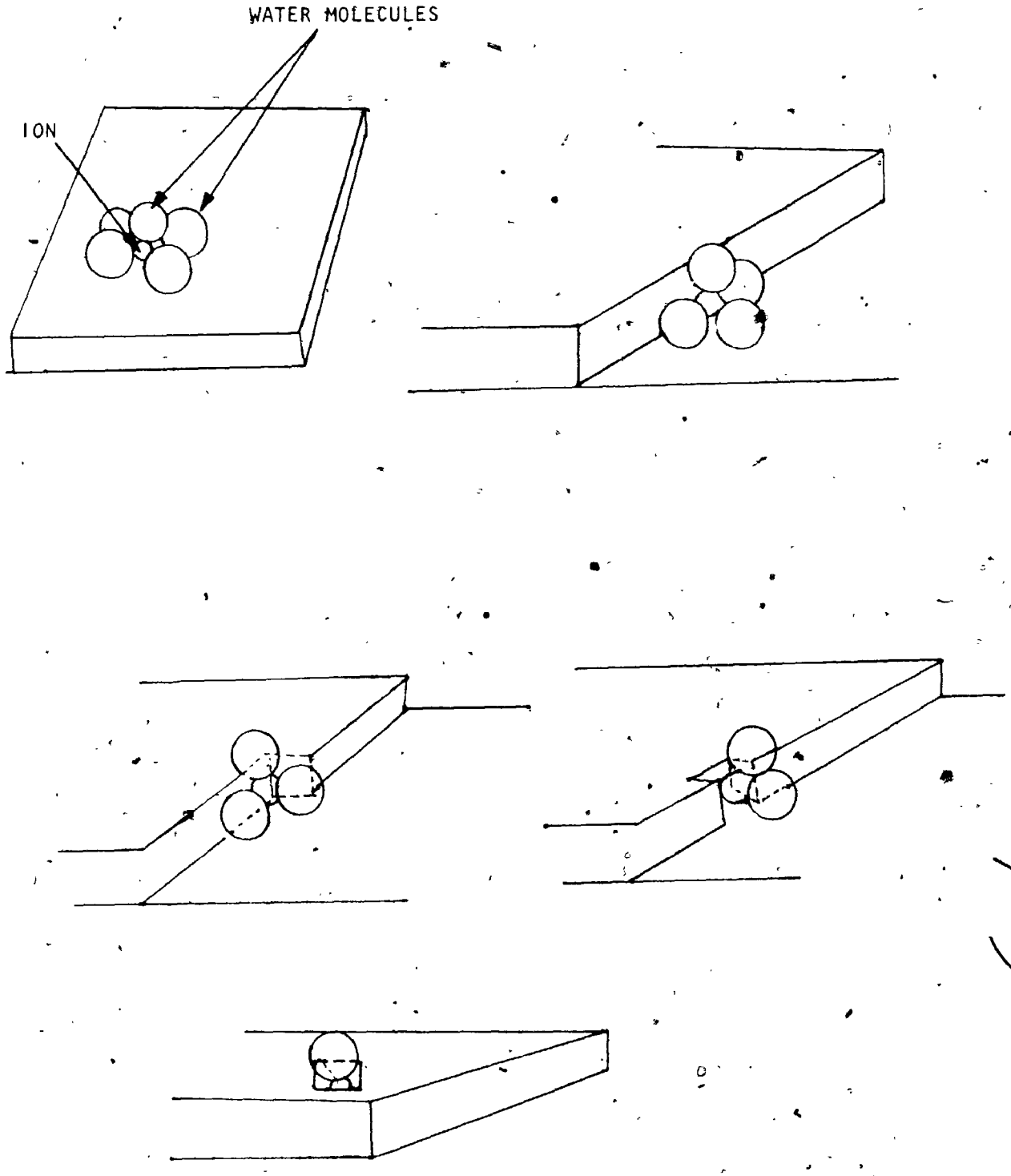

Fig. 5 Diagrammatic representation of possible modes of hydration of transferred adions at various sites upon the metal surface.

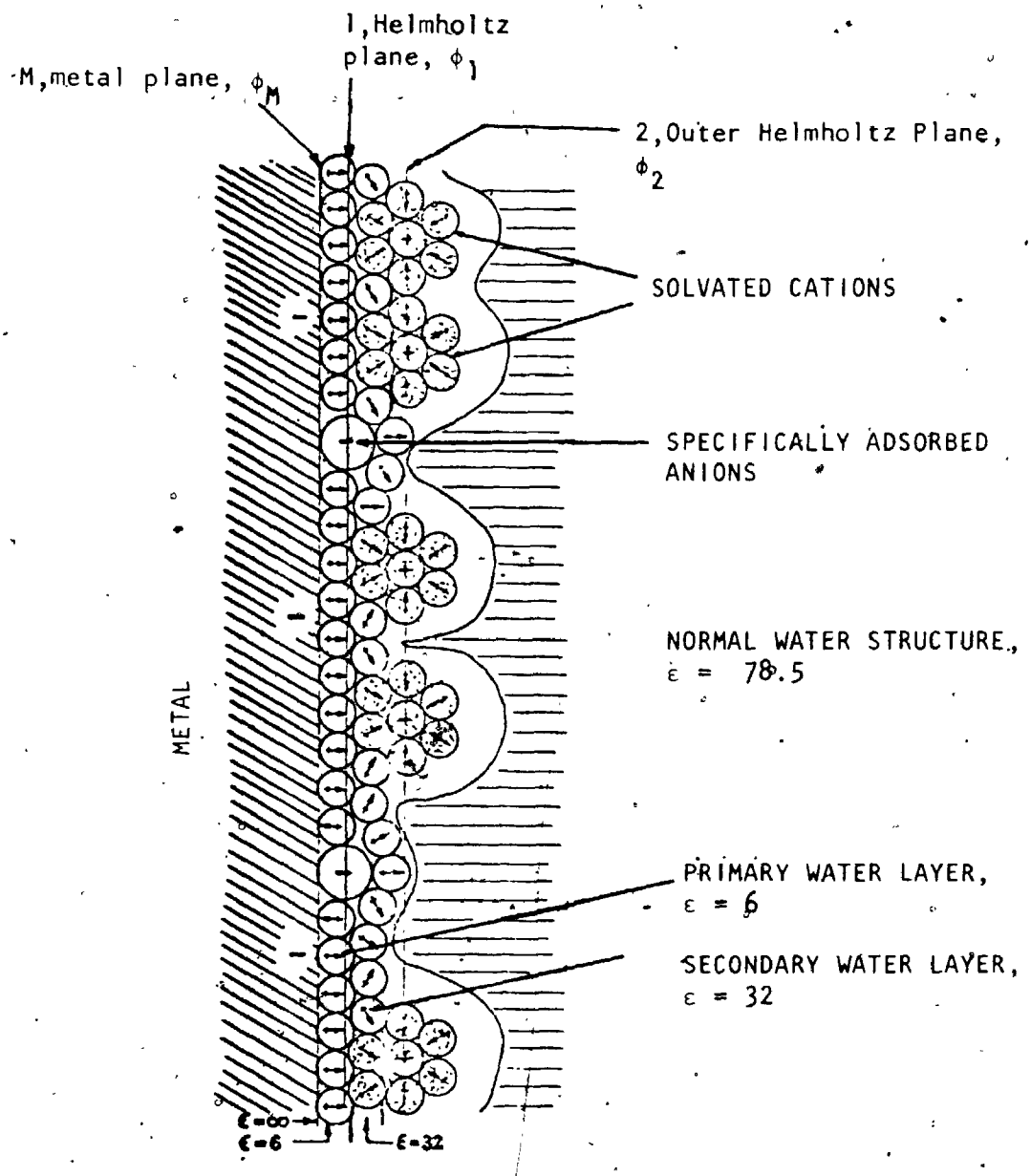

Fig. 3. Bockris, Devanathan, and Müller Triple Layer

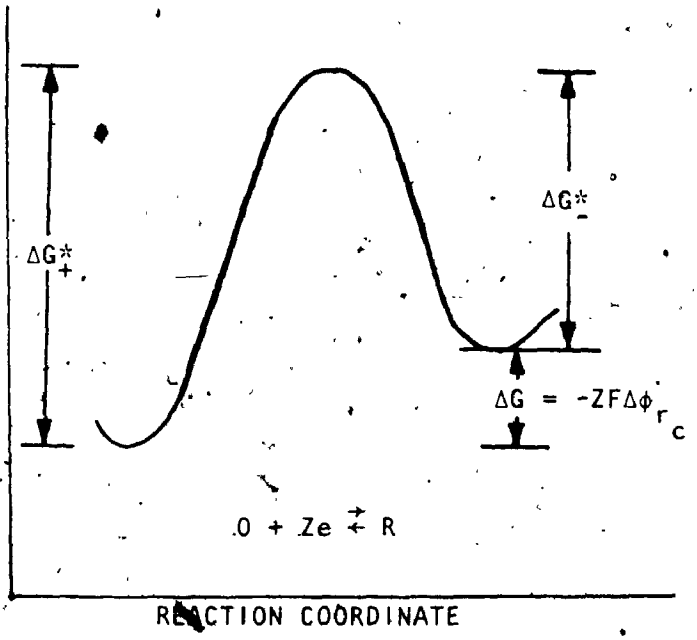

Fig. 4a. Activation energy curve for a reversible electrode process

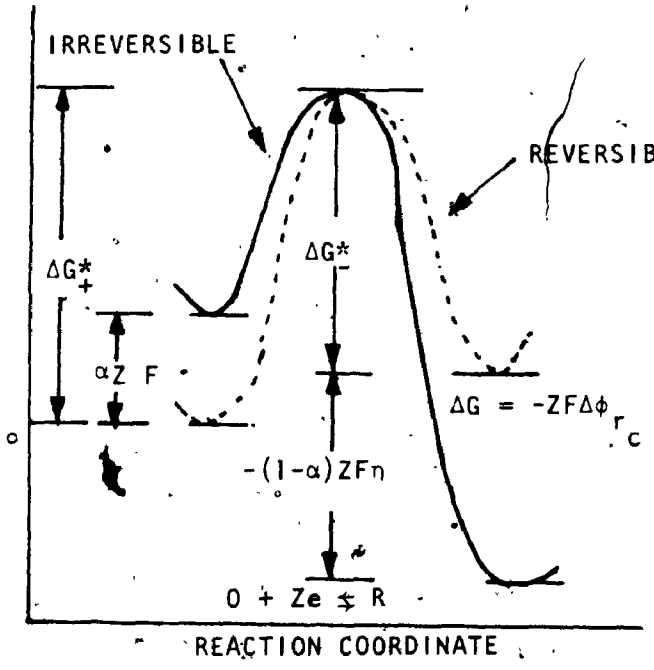

Fig. 4b. Activation energy curve for an irreversible electrode process.

a free energy of activation for the reverse process ΔG^{*}_{-}. The difference between these two free energies of activation is the free energy of reaction, ΔG, which is related to the reversible electrode potential across the compact double layer, $\Delta\phi_{r_c}$ by the expression,

$$\Delta G = \Delta G^{*}_{+} - \Delta G^{*}_{-} = -z\,F\,\Delta\phi_{r_c} \tag{6}$$

where F is the Faraday constant.

The specific rate constants of the forward and reverse reactions, at reversible equilibrium are respectively

$$K_{+} = \frac{kT}{h} \exp\left[\frac{-\Delta G^{*}_{+}}{RT}\right] \tag{7}$$

and

$$K_{-} = \frac{kT}{h} \exp\left[\frac{-\Delta G^{*}_{-}}{RT}\right] \tag{8}$$

where $\frac{kT}{h}$ is the universal frequency factor [18]. The rate of reaction and, in addition, the current density must be proportional to the concentration of the reacting species immediately at the electrode surface. If a hypothetical ideal solution at unit concentration is chosen as the standard state of the species and the rates of reaction, v, are in equivalents per second per unit area of electrode surface, then it follows that the current density of the forward reaction, i_{+}, is [19]

$$i_+ = z F v_+ = z F K_+ a_0 \quad (9)$$

and similarly the current density of the reverse reaction, i_-, is

$$i_- = z F v_- = z F K_- a_R \quad (10)$$

where a_0 and a_R are the activities of the oxidized and reduced species.

If a potential is applied to the metal solution interface such that the forward reaction is made faster than the reverse, a net reaction occurs. This irreversible situation is depicted in Fig. 4b. The electrode potential across the compact layer departs from the equilibrium value by an amount η_A called the activation overpotential.

$$\eta_A = \Delta\phi_c - \Delta\phi_{r_c} \quad (11)$$

Generally η_A is one of the three different types of overpotential comprising the total measured overpotential. Accordingly,

$$\eta_T = \eta_{IR} + \eta_{Conc} + \eta_A \quad (12).$$

where η_A is the activation overpotential, which arises from the hindrance of one or more of the reaction steps, η_{Conc} is the concentration overpotential, which is the overpotential due to concentration changes at the electrode surface (or more rigorously, immediately adjacent to the double layer), and η_{IR} is the ohmic overpotential, said to arise from electrical resistance (i.e. IR potential drop in the solution) to the passage of the reacting species to the surface of the electrode [19].

A fraction of the activation overpotential accelerates the reduction of O and the remainder retards the oxidation of R. These respective effects are accomplished by decreasing the free energy of activation for the reduction process from ΔG_+^* to $\Delta G_+^* + z\,\beta\,F\,\eta_A$ and increasing the free energy of activation for the oxidation process from ΔG_-^* to $\Delta G_-^* - z\,(1-\beta)\,F\,\eta_A$, where β is the symmetry factor and z the number of electrons transferred in the rate determining step. It should be noted that the overpotential, η_A is negative in a reducing process. Incorporation of the activity coefficients of species O and R into the specific rate constants yields the following expressions for the current densities of the reducing and oxidizing processes respectively,

$$i_+ = z\,F\,k_+\,C_O \exp\left[\frac{-z\,\beta\,F\,\eta_A}{RT}\right] \tag{13}$$

and

$$i_- = z\,F\,k_-\,C_R \exp\left[\frac{z\,(1-\beta)\,F\,\eta_A}{RT}\right] \tag{14}$$

where C_O and C_R are concentrations and where the factors k_+ and k_- include the activity coefficients.

If the applied potential is small, the reverse reaction remains kinetically significant; that is, the reverse rate cannot be neglected in the net cathodic rate, i.e.,

$$i_c = i_+ - i_- \tag{15}$$

or

$$i_c = zFk_+C_0 \exp\left[\frac{-z\beta F\eta_A}{RT}\right] - zFk_-C_R \exp\left[\frac{z(1-\beta)F\eta_A}{RT}\right] \quad (16)$$

When no potential is applied, that is the electrode is behaving reversibly, ($\eta_A = 0$), then

$$i_+ = i_- = zFk_+C_0 = zFk_-C_R \quad (17)$$

The exchange current density is thus defined as

$$i_o = zFk_+C_0 = zFk_-C_R \quad (18)$$

Substitution of equation (18) into equation (16) yields

$$i_c = i_o \left[\exp\left(\frac{-\beta\eta_A zF}{RT}\right) - \exp\left(\frac{z(1-\beta)F\eta_A}{RT}\right)\right] \quad (19)$$

Under highly irreversible conditions, i.e. $\eta_A >> \frac{RT}{zF}$, the second term in equation (19) can be neglected and the following expression is obtained

$$i_c = i_o \exp\left[\frac{-z\beta F\eta_A}{RT}\right] \quad (20)$$

By a simple transformation of equation (20), the overpotential can be expressed in terms of current density by

$$\eta_A = \left(\frac{RT}{z\beta F}\right) \ell n i_o + \left(\frac{-RT}{z\beta F}\right) \ell n i_c \qquad (21)$$

$$= a + b \ell n i_c \qquad (22)$$

Equation (22) corresponds to the empirical Tafel equation [20]. The "Tafel slope" b is, therefore, given by

$$b = \frac{-RT}{z\beta F} \qquad (23)$$

Parameters "a", "b", and "i" are very necessary in the elucidation of the mechanism of electrode processes.

1.4 THE MECHANISM OF METAL DEPOSITION

Metal deposition differs from most electrode reactions in that the reactants and products are in different phases. Thus the manner in which the product is incorporated into the solid (metal) phase must be considered as well as the charge-transfer process itself.

Erdey-Gruz and Volmer [21] suggested that ionic discharge is the slow or rate-controlling step in the overall deposition process. From the slow discharge mechanism, two hypotheses resulted: (i) the electronic mechanism, where the elementary process consists of a jump of an electron from the metal to an ion in solution, which simultaneously dehydrates and deposits as a neutral atom on the electrode, and (ii) the ionic mechanism, where the ion in its hydrated state migrates to the electrode where it is neutralized.

It is necessary to consider the structure of the growing crystal lattice in any discussion of the ionic mechanism. The transfer of an ion from its fully hydrated state in solution to an adsorption site on the metal surface may occur (a) by direct transfer to a given site (e.g. a surface vacancy or a kink site) from which it migrates no further, or (b) by transfer at first to a surface phase, and subsequent migration (surface diffusion) through the adsorbed water layer to a growth site, e.g. a kink site in a step [22-25]. During the transfer process, the ion has to displace part of its hydration sheath. The amount of displacement which has to be done depends on the site. Clearly, the more the displacement of the hydration sheath for a given type of site, the greater the energy needed to surmount the barrier for discharge at the type of site concerned. Other factors may compensate for the hydration sheath distortion. The greater degree of co-ordination of the transferred ion with the substrate's metal ions in a site where distortion is particularly large is one possible factor. Fig. 5 shows the co-ordination of the adion with respect to the metal atoms at various sites.

Many authors [23,24,26,27] have investigated the effect of the distortion energy on the energy of activation. Libby [28] and Marcus [29] applied quantum mechanical theory to show that electron transfer processes are very rapid compared to the reorientation of the solvent and shell around the reactive species. They concluded that "only weak electronic interaction of the electrode and an ion is required for a simple electron transfer to occur". Hush's calculations [27] also indicate the predominant effect of the distortion

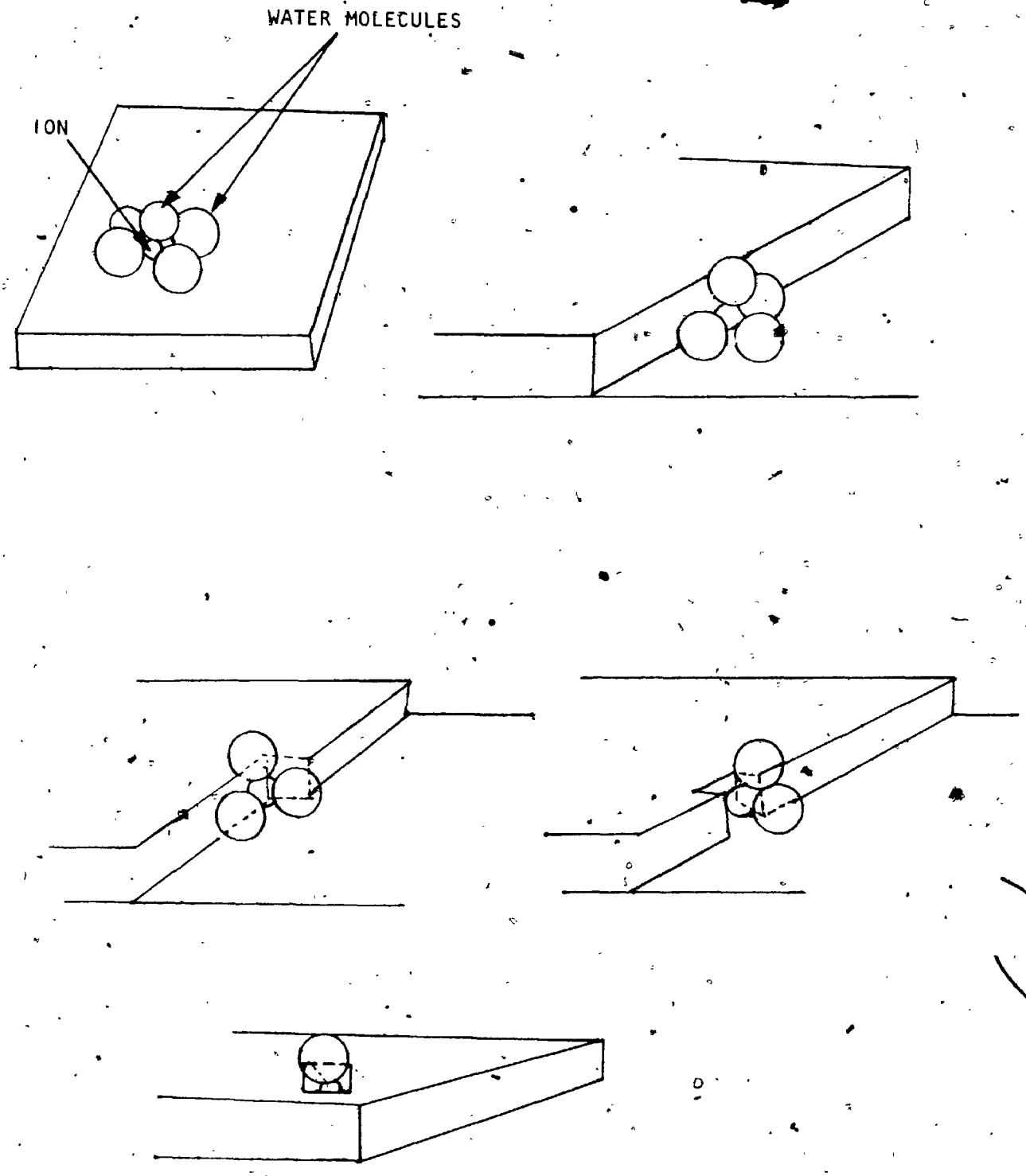

Fig. 5 Diagrammatic representation of possible modes of hydration of transferred adions at various sites upon the metal surface.

energy. Dielectric reorientation outside the first co-ordination shell around the ions appeared to cause most of the activation energy. Bockris and Conway's [23,24] calculations showed that a tendency to compensation by substitute atom co-ordination existed but was insufficient to compensate the distortion energy. As shown in Table 1, the direct ion transfer from solution to a planar surface site required much less energy than that to an edge (of a growing layer), to a kink, or to a vacancy in an edge or in a surface. Accordingly, the mechanism of metal deposition can be written as:

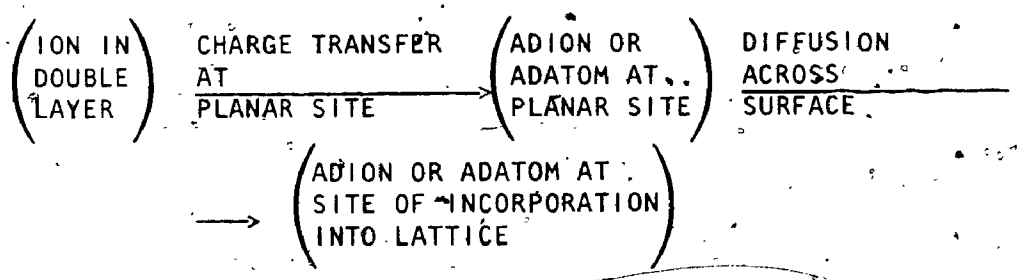

There is considerable debate as to which term, adion or adatom, better represents these species. The degree of ionic character for Ag^+ "adions" was estimated to be about 50 per cent [23-25]. Gerischer [30], however, concluded that these "adions" carry a potential charge of 30-40 per cent. At high overpotentials (η>50 mV), charge-transfer is generally considered to be rate-controlling [31,32], the kinetic treatment of which has already been discussed. If the overpotential and the density of active growth sites are small, surface diffusion is the slow step. As the overpotential increases the fraction of growth sites (e.g. kink sites or vacancies) which are active increases and the effective distance of diffusion across

TABLE 1

Heats of Activation (Kcal/mole), Bulk Solution to Various Sites

ION	PLANE SURFACE	EDGE	KINK	SURFACE VACANCY
Ni^{2+}	130	190	>190	>>190
Cu^{2+}	130	180	>180	>>180
Ag^{+}	10	21	35	35

the surface decreases. Bockris and Mattson [25] concluded that if the Tafel slope observed in the deposition of divalent cation is less than, or equal to, 29.5 mV then charge-transfer cannot be rate-determining.

1.5 ADSORPTION FROM SOLUTION

Adsorption from solution differs from gas phase adsorption in that there is competition for adsorption sites between solvent and solute. In the academic study of adsorption from this type of system, the following aspects have emerged as being of greatest interest and importance [33]:

(i) the shape of the adsorption isotherm and the possibility of fitting it with an appropriate equation,

(ii) the significance of the adsorption limit on the plateau found in most isotherms,

(iii) the extent to which the solvent is adsorbed,

(iv) a consideration of whether adsorption is confined to a single molecular layer or extends over several layers,

(v) the orientation of the adsorbed molecules,

(vi) the existence of both physical and chemical adsorption.

Aspects (ii) through (vi) may be studied from an examination of (i), the slope of the isotherm, but first it is necessary to differentiate between physical and chemical adsorption.

The forces involved in physical adsorption are the dispersion (London), short-range repulsive and dipole forces in the order of magnitude of heats of condensation of gases (about 1 to 10 Kcal/mole). In chemisorption, a transfer of electrons occurs between the electrode and the chemisorbed layer. Heats of reaction are therefore comparable to heats of chemical reactions (10 to 100 Kcal/mole). The most important difference between these two types of adsorption to the electrochemist is the irreversibility of the chemisorption process as compared to reversible physical adsorption.

1.6 THE ADSORPTION ISOTHERMS

The adsorption isotherm is the relationship between surface concentration and chemical or electrochemical potential, generally expressed as a function of the concentration in the bulk phase or the potential across the interface. The commonest shape of isotherm for adsorption of a solute from solution is shown in Fig. 6a. Giles et al [34, 35] classified the shapes of isotherms observed according to the scheme shown in Fig. 6b. The main classification is based on the initial slope of the isotherm, and the sub-classification on the slope at higher concentrations.

Class S isotherms are found when (i) the solvent is strongly adsorbed, (ii) there is strong inter-molecular attraction within the adsorbed layer, (iii) the adsorbate is mono-functional, i.e. there is a single point of strong attachment in an aromatic system or a long hydrocarbon chain.

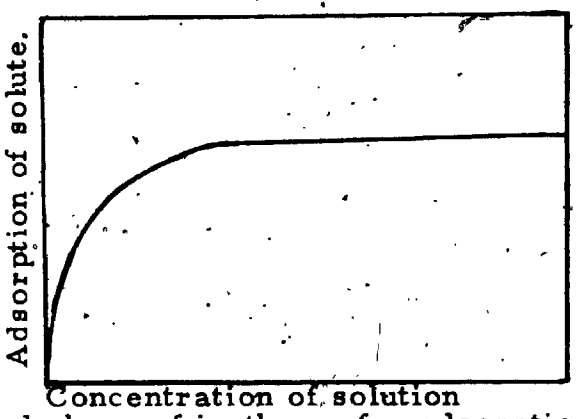

Fig. 6 a. Typical shape of isotherm for adsorption of a solid from solution.

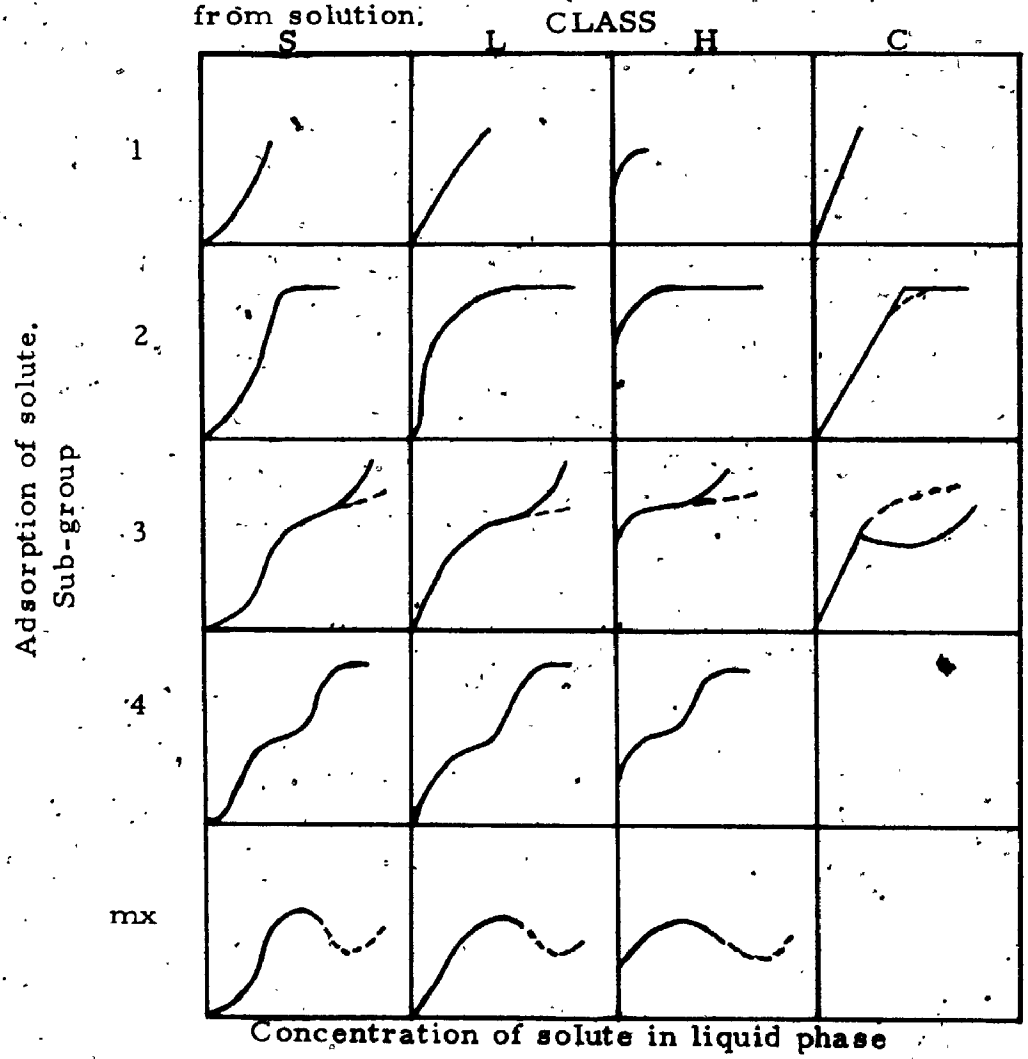

Fig. 6 b. System of classification of isotherms.

The L class or Langmuir type curve is obtained if there is no strong competition from the solvent for surface sites or if the major axis of linear or planar adsorbate molecules lies parallel to the surface.

The H class curve occurs as a result of chemisorption or from the adsorption of polymers.

Class C curves indicate constant partition of the adsorbate between the solution and the adsorbent.

Several of the sub-groups show stepped isotherms. These steps generally appear to mark a phase change in the adsorbed layer (re-orientation of the adsorbate) or the onset of the formation of a second molecular layer after completion of the first.

The adsorption of an organic molecule from aqueous solution may be represented [36,37] by the following quasi-chemical substitution process in the interphase:

$$\underset{\text{(in solution)}}{\text{Organic}} + n\,H_2O_{\text{(ads)}} \rightleftarrows \underset{\text{(ads)}}{\text{Organic}} + n\,H_2O_{\text{(in solution)}} \qquad (24)$$

There are several ways in which a theoretical isotherm may be derived for process (24). As usual, the chemical potentials μ of the entities on the l.h.s. and r.h.s. of (24) must be equated but μ can be expressed either (a) directly in terms of site fractions X equivalent to fractional surface coverage θ or (b) in terms of mole fractions [36,37,38] with subsequent algebraic conversion of mole fractions to site fractions. These two approaches are not identical

because the forms of the statistics initially expressing the composition variables in the μ terms are not the same [39].

1.6.1 Isotherms In Terms of Site Fractions

Neglecting all interactions in the adsorbed and solution phases, the electrochemical and chemical potential terms $\bar{\mu}$ and μ, respectively, for the organic (0) and water (W) in the interphase and in solution can be written:

$$\bar{\mu}_{0,ads} = \bar{\mu}^{\circ}_{0,ads} + RT \ln X_{0,ads}, \tag{25a}$$

$$\bar{\mu}_{W,ads} = \bar{\mu}^{\circ}_{W,ads} + RT \ln X_{W,ads}, \tag{25b}$$

$$\mu_{0,soln} = \mu^{\circ}_{0,soln} + RT \ln Y_{0,soln}, \tag{25c}$$

$$\mu_{W,soln} = \mu^{\circ}_{W,soln} + RT \ln Y_{W,soln}, \tag{25d}$$

where $X_{0,ads}$ and $X_{W,ads}$ are the site fractions of 0 and W in the interphase and $Y_{0,soln}$ and $Y_{W,soln}$ the mole fractions in solution corresponding to N_0 and N_W mole/l of organic and water. The standard states for the adsorbed species are unit site or fractional coverage (X or $\theta = 1$) for the adsorbate and solvent, while the standard states for the solution phase are unit mole fractions of organic or solvent [39,40,41,42].

The condition for interphase-bulk phase equilibrium in adsorption is:

$$\bar{\mu}_{0,ads} - n\bar{\mu}_{W,ads} = \mu_{0,soln} - n\mu_{W,soln} \tag{26}$$

The standard free energy of adsorption may be written as:

$$\Delta G^{\circ}_{ads} = \bar{\mu}^{\circ}_{0,ads} - \mu^{\circ}_{0,soln} - n(\bar{\mu}^{\circ}_{W,ads} - \mu^{\circ}_{W,soln}) \tag{27}$$

or in terms of site fractions of components in the interphase using equations (25), as:

$$\Delta G^{\circ}_{ads} = -RT \ln \left[\frac{(X_{0,ads})\ (Y_{W,soln})^{n}}{(X_{W,ads})^{n}(Y_{0,soln})} \right] \tag{28}$$

If a solvent lattice site in the interphase is defined as a position of finite area equivalent to that of a solvent molecule adsorbed, amongst other solvent molecules, with a certain co-ordination number and local 2-dimensional structure, then the total number of such solvent sites is

$$N_T = N_{org} + N_W \tag{29}$$

where N_{org} is the number of solvent lattice sites on the surface occupied by organic. For dilute solutions, the following relations hold:

$$Y_{W,soln} \simeq 1, \tag{30a}$$

$$Y_{0,soln} = C_{org}/55.5 \tag{30b}$$

$$X_{0,ads} = N_{org}/N_T \tag{30c}$$

The experimental surface excess quantities Γ (assumed to be identical with surface concentrations at low bulk concentration) can be expressed in terms of the site fraction X [39]. Since

$$N_T = n\Gamma_{org} + \Gamma_W \tag{31}$$

where Γ is expressed in molecules cm^{-2}, $N_{org} = n\Gamma_{org}$, and $N_W = \Gamma_W$. Noting that

$$\Gamma_{org} = \theta\Gamma_{org,max} \text{ (for saturation)} \tag{32}$$

$$\Gamma_W = \Gamma_{W,max} - n\Gamma_{org} \tag{33}$$

and

$$\Gamma_{W,max} = n\Gamma_{org,max} \tag{34}$$

it can be shown that

$$\frac{n\Gamma_{org}}{n\Gamma_{org} + \Gamma_W} = N_{org}/N_T \tag{35}$$

and this is the site fraction $X_{0,ads}$, equivalent to θ. The site fraction of solvent in the interphase may be written as:

$$X_{W,ads} = 1 - \theta \tag{36}$$

The quantities in (28) are now defined and (28) becomes

$$\frac{\theta}{(1-\theta)^n} = \frac{C_{org}}{55.5} \exp\left[\frac{-\Delta G^\circ_{ads}}{RT}\right] \qquad (37)$$

This isotherm was first developed by Dahms and Green [43] and was used to explain the adsorption of aromatic compounds on Au electrodes.

If the solution is regarded as a 3-dimensional lattice in which relative size of solvent and solute is also taken as n, then the bulk concentration term in mole l^{-1} appears as a 3-dimensional site fraction, as in Flory-Huggins theory [40,41,44,45], giving at low C_{org}

$$\frac{\theta}{n(1-\theta)^n} = \frac{C_{org}}{55.5} \exp\left[\frac{-\Delta G^\circ_{ads}}{RT}\right] \qquad (38)$$

Equation (38) is commonly known as the "Flory-Huggins isotherm". Since its first appearance [46], equation (38) has found wide acceptance for explaining electrosorption behaviour.

Recently Dhar, Conway, and Joshi [39] pointed out that equation (38) is not the resulting isotherm when Flory-Huggins statistical approximations are used. The chemical potentials of O and W in the interphase must be calculated "ab initio" by the method of lattice statistical mechanics when the adsorbate occupies several lattice sites [40,41,47,48]. Dhar et al [39] developed an isotherm using the well-known statistical mechanical basis of the Langmuir equation [45] for n = 1 and extending it to apply to adsorption of flexible linear n-mers which can occupy contiguous lattice sites along a

"random-walk" amongst the lattice sites. This approach has no effect on the surface coverage terms but a configuration term, exp [n-1], is added to the expressions (37) and (38). The resulting isotherms are:

$$\frac{\theta}{e^{(n-1)}\,(1-\theta)^n} = \frac{C_{org}}{55.5}\,\exp\left[\frac{-\Delta G^\circ_{ads}}{RT}\right] \qquad (39)$$

when the chemical potentials in the solution phase are written in terms of mole fractions and

$$\frac{\theta}{ne^{(n-1)}\,(1-\theta)^n} = \frac{C_{org}}{55.5}\,\exp\left[\frac{-\Delta G^\circ_{ads}}{RT}\right] \qquad (40)$$

when the solution is regarded as a 3-dimensional lattice. The standard free energy of adsorption is defined by

$$\Delta G^\circ_{ads} = (-RT\ell nq_2 - \mu^\circ_{0,soln}) - n\,(RT\ell nq_1 - \mu^\circ_{W,soln}) \qquad (41)$$

where q_1 and q_2 are the internal partition functions of solvent and adsorbate respectively.

1.6.2 Isotherms in Terms of Mole Fractions

When the chemical potentials of the reactants and products in equation (24) are expressed in terms of mole fractions the equilibrium constant is

$$K = \frac{(Y_{0,ads})\;(Y_{W,soln})^n}{(Y_{W,ads})^n\;(Y^\circ_{0,soln})} \qquad (42)$$

Relations (30a) and (30b) hold for dilute solutions but on the surface

$$Y_{O,ads} = \frac{\Gamma_{org}}{\Gamma_{org} + \Gamma_W} \tag{43}$$

Equation (43) is analogous to equation (35).

Substituting equations (32) and (34) into equation (43) yields

$$Y_{O,ads} = \frac{\theta}{\theta + n\,(1-\theta)} \tag{44}$$

and

$$Y_{W,ads} = \frac{n(1-\theta)}{\theta + n\,(1-\theta)} \tag{45}$$

All terms in equation (42) are now defined and recognizing that $\Delta G^{\circ}_{ads} = -RT \ln K$, one has

$$\frac{\theta\,[\theta + n\,(1-\theta)]^{(n-1)}}{(1-\theta)^n\; n^n} = \frac{C_{org}}{55.5}\; \exp\left[\frac{-\Delta G^{\circ}_{ads}}{RT}\right] \tag{46}$$

This isotherm, commonly referred to as the Bockris-Swinkels Isotherm [36,37], was successfully applied to the adsorption of naphthalene [36], n-decylamine [36] and monocarboxylic acids [49] on Cu electrodes as well as the adsorption of butyric acid on Hg [50].

It should be pointed out that all the isotherms (37), (38), (39), (40), and (46) are consistent in the case n = 1. The resulting

expression is the general Langmuir isotherm [51].

$$\frac{\theta}{(1-\theta)} = \frac{C_{org}}{55.5} \exp\left[\frac{-\Delta G^{\circ}_{ads}}{RT}\right] \qquad (47)$$

1.7 METHODS FOR STUDYING ELECTROSORPTION

Many methods [52] are now available for the study of electrochemical adsorption at metallic electrodes. The choice of a suitable method for studying any electrochemical system depends on many factors: (i) the phase of the electrode (solid or liquid), (ii) the solution (e.g. pH, solvent, conductivity, supporting electrolyte, refractive index), (iii) the adsorbate (e.g. organic, ionic, electroactivity), (iw) the electrochemical parameters of interest. A few of the most common methods will be discussed below.

1.7.1 Direct Optical Methods

The three main optical methods that have been applied to the study of adsorption at electrode interfaces in recent years are ellipsometry, attenuated total reflection spectroscopy, and specular reflection spectroscopy.

Ellipsometry is especially useful in processes of anodic passivation and inhibition of anodic dissolution. The technique provides an "in situ" method of obtaining information not only on film thickness but on dielectric or high-frequency conductivity. Essentially, an ellipsometer measures the change of condition of elliptically polarized light as it passes from one medium into another through a thin film and is reflected back into the original

medium. The technique is therefore very useful in studying thin oxide or halide films but as yet very little has been published on studies of adsorption of organic substances at electrodes by this means. One of the difficulties is that the changes of optical properties of the interphase are small unless the adsorbate has a refractive index greatly different from that of the solvent. Reviews of the work on the development and application of this technique may be found in Refs. [53], [54], and [55].

Specular reflection spectroscopy (electroreflectance) is beginning to find wide application in studies of adsorption phenomena [52]. Originally longitudinal electric field modulation of reflectivity was used in studying electronic band structures in semiconductors, but later was extended to metal hard structure and double-layer phenomena. This technique has been used to study the adsorption of pyridine, quinoline, and phenol at gold electrodes as a function of potential [56]. In the case of phenol, polymerization to form a permanent film of considerable thickness has been followed by this method. Modulated reflection also shows great promise for studying chemisorption where electron transfer or interchange is involved.

The attenuated total reflection spectroscopy method does not unambiguously give information about species adsorbed at the electrode surface but rather characterizes species in a deeper boundary layer near the surface. In addition the electrodes must be optically transparent. Due to this selectivity of applications, this technique will not be discussed further.

1.7.2 Interfacial Tension and Related Methods

Several workers [57-60] have shown by independent methods that the thermodynamic laws of Gibbs, which give the relation between surface tension, γ, the electrode potential, $\Delta\phi$, and the activities of the adsorbate in solution, a_i, and at the surface, Γ_i, are applicable to the electrode-solution interface. The repulsion between similar electric charges present at a surface lowers the surface tension. Direct measurements of the surface tension, however, are only possible on liquid electrodes.

Lippmann [61] and Gouy [62] were the first to develop the capillary electrometer. A potential difference is applied across the mercury-electrolyte interface and the resulting change in surface tension is measured. Under the conditions of constant pressure and temperature, the fundamental electrocapillary equation can be written in the form [63,64]

$$d\gamma = -qd(\Delta\phi) = RT\sum_i \Gamma_i d\,na_i \qquad (48)$$

where q is the charge density residing inside the metal phase. The charge density q and surface excess, Γ_i, can be obtained by differentiating the experimental electro-capillary curves.

$$q = -\left(\frac{\partial\gamma}{\partial(\Delta\phi)}\right)_{a_i,T,P} \qquad (49)$$

$$\Gamma_i = -\frac{1}{RT}\left(\frac{\partial\gamma}{\partial\&na_i}\right)_{\Delta\phi,T,P,a_i} \qquad (50)$$

Drop-weight [65] and drop-time measurements [66,67] can also be used to directly obtain the interfacial tension.

As mentioned previously, direct interfacial tension measurement is limited only to liquid electrodes. A novel technique, applicable to solid metals, has been developed by Gokshtein [68] and Beck [69] and is based on the extent to which a very thin wire can be stretched by an applied force. If the surface/volume ratio is relatively appreciable, then surface forces can significantly affect the modulus of elasticity so that with changing potential and hence interfacial tension, the extension of the wire under the influence of a given force can be potential dependent. The interfacial tension is given by Hooke's law

$$d\gamma = \left(\frac{AE}{PL}\right) dL \qquad (51)$$

where L and A are the length and cross-sectional area of the immersed wire respectively, P the periphery and E the elastic modulus. This method has produced electrocapillary curves (γ versus $\Delta\phi$) for gold and platinum.

Another technique involving the mechanical properties of solid metals is the pendulum method [70-72]. It is based on the principle that the coefficient of friction at an interface depends on the surface charge density and double layer distribution of ions. The decrement of successive swings of a pendulum depends (in part) on the coefficient of friction at the pivot.

Some other techniques under development which depend on the interfacial tension depend on the contact angle between metals and gas bubbles in the presence of surface active organic substances [73]. These techniques, to date, are little developed and experimentally very difficult.

1.7.3 Radioactive Tracer Methods

Equilibrium adsorption at solid electrodes can be studied by means of radioactive tracers by two methods: (i) monitoring of the change of activity in solution due to adsorption at the electrode, (ii) direct monitoring of the surface of the electrode by a counting procedure operating through a thin-film window on a proportional counter with the window itself made the electrode under study. Radioactive tracer techniques are restricted to ions and molecules which adsorb strongly since only in these cases can relatively dilute solutions ($<10^{-3}$M) resulting in minimal background activity be used.

The solution monitoring method has found wide use in studies of the adsorption of ions that are strongly adsorbed to the extent that the amount adsorbed is comparable in magnitude to the actual number of molecules of adsorbate in the solution. "In situ" techniques have been developed for halide ion adsorption by Balashova and her co-workers [74,75].

The electrode monitoring method is most commonly employed for systems of the more weakly adsorbing organic adsorbates. For electrodes that can be obtained in the form of very thin foils an "in situ" technique of monitoring through a thin-window-type electrode was

developed by Blomgren and Bockris [76-79].

General methods for any solid electrode have been developed by Hackerman and Stephens [80] and Green et al [81] whereby the amount of substance adsorbed is determined after withdrawal of the electrode from the solution. These techniques are commonly called tape methods as the electrode is in the form of a continuous metal tape and is slowly drawn through the electrolytic cell. Hackerman and Stephens [80] then washed the electrode with an inactive solution and monitored its activity. This method is only applicable when the adsorption is highly irreversible. Green et al [81] monitored the electrode by passing the wetted tape through two proportional counters, determining the total amount of radioactive material present. The thickness of the wetting layer (and therefore the amount of radiotracers in it)was calculated from the change in the capacity of a condenser between the plates of which the tape passes. The adsorption of some aromatic ^{14}C hydrocarbons on gold [43,77], of n-decylamine on Cu, Ni, Fe, Pb and Pt [36], and of naphthalene on Cu, Ni, Fe and Pt [37], has been studied using these methods. The withdrawal techniques, however, are limited in that a certain loss of potentiostatic control is necessitated.

1.7.4 Electrode Capacity Methods

The differential capacity of the electric double layer is extremely sensitive to adsorption of organic molecules on the electrode surface. However, for a rigorous determination of surface coverage from capacity measurements it is necessary to know the potential of zero charge and the value of the interfacial tension at this potential.

Several approximate methods have been suggested for use with solid electrodes where the electrocapillary curve cannot be measured. These methods have recently been reviewed by Frumkin and Damaskin [82]; according to one method the surface coverage, θ, in simplified form is given as follows:

$$\theta = (C_{\theta=0}-C_{\theta})/(C_{\theta=0}-C_{\theta=1}) + [(q_{\theta=1}-q_{\theta=0})/(C_{\theta=0}-C_{\theta=1})(d\theta/d\Delta\phi)] \quad (52)$$

where $C_{\theta=0}$ and $q_{\theta=0}$ are the differential capacitance and the charge of the uncovered surface, $C_{\theta=1}$ and $q_{\theta=1}$ those of the fully covered surface and C_{θ} the capacity at coverage θ.

Various procedures for capacity measurements have been described [83-85] employing regular C/R networks or transformer ratio arms. One such procedure is as follows.

The equivalent circuit of the measuring cell, when no electrochemical reactions are occurring at the electrode, and the area and hence the capacity of the auxiliary electrode are considerably larger than the area and capacity of the electrode under study, may be represented by the capacity (C) of the double layer and the resistance (R) of the solution connected in series. The variation of the potential difference with time is then given by [76]

$$\frac{d\Delta\phi}{dt} = R\frac{di}{dt} + \frac{i}{C} \quad (53)$$

where t is the time and i the current flowing through this network. If a current pulse which does not subsequently change with time is

applied to the cell, then i is constant, $\frac{di}{dt} = 0$, and equation (53) on rearrangement becomes

$$C = i\left(\frac{dt}{d\Delta\phi}\right) \tag{54}$$

thus the slope of the resulting charging curve gives the electrode capacity.

If, on the other hand, the electrode is polarized to a steady-state potential by a constant current and then the working circuit is instantaneously opened, the electrode capacity at the steady-state potential can be obtained by extrapolation of the potential decay curve to t = 0,

$$C = -i\left(\frac{dt}{d\Delta\phi}\right)_{t=0} \tag{55}$$

The accuracy to which the double layer capacity can be determined by these methods is limited by the inherent inaccuracy of graphical differentiation. Seto and O'Brien [86] used the theory of transmission line reflectance (time-domain reflectometry) in developing a method, not dependent on graphical differentiation, for measuring capacity at stainless steel electrodes.

Bridge methods are most commonly used in measuring capacities of ideally polarizable electrodes, i.e. no charge-transfer across the interface. These AC methods are based on the impedance of the equivalent circuit which is given by [87]

$$Z = R + \frac{1}{j\omega C} \qquad (56)$$

where $j = \sqrt{-1}$ and ω is the angular frequency.

1.7.5 Kinetic Methods

Adsorption of organic substances on electrodes leads to a decrease in the rates of various electrochemical reactions [88]. Accordingly, data on reaction kinetics have been used [49,89-105] to obtain information about adsorption processes.

In metal deposition, it is generally believed that an overpotential increment, due to adsorption of additives, arises from a partial "blocking" of the electrode, resulting in an increased current density on the uncovered fraction, hence, a corresponding increase in overpotential [98,106]. At high coverages, when the electrode surface is effectively blocked by adsorbed additive, the "sieve effect" - an increase in the activation energy required to form a pore in the adsorbed layer for the electrode reaction - becomes predominant in the inhibition mechanism [90].

In most studies [49, 102-106] the reduction in the true electrode area has been assumed to be proportional to the surface coverage. Under galvanostatic conditions, the current density in the presence of additive, i_θ, is related to the current density in the absence of organic material, i, by

$$i_\theta = \frac{i}{1-\theta} \qquad (57)$$

where θ is the fraction of metal surface unavailable for deposition due to the adsorption process. It is usually assumed that this fraction is equal to the fraction of the surface physically covered with organic particles.

Several investigators [49,102-105] transformed equation (57) by the use of the Tafel relation (equation (22)) to

$$\theta = 1 - \exp\left(\frac{-\Delta\eta}{b}\right) \qquad (58)$$

where θ is calculated, at constant apparent current density, from the increase in overpotential caused by the presence of adsorbed organic material. Equation (58) is only applicable when the presence of the adsorbate has no effect on the mechanism of the deposition process and $\Delta\eta$ is the increment in the true charge-transfer overpotential.

Niki and Hackerman [90] have recently argued that the reduction in the true electrode area is proportional to the surface coverage only for an aggregated adsorbed layer (condensation mechanism of adsorption [107]). They assumed that displacement by electroactive ions and electrochemical reaction only occurs where x water molecules aggregate, then in a mobile adsorbed layer the true electrode area is proportioned to $(1-\theta)^x$. The area occupied by the x water molecules corresponds to the cross-sectional area of the reacting ions.

1.8 OBJECTIVES OF THE PRESENT STUDY

Systematic studies of the effects of various families of organic compounds on the electrodeposition of copper have been made in this

laboratory. Recently, preliminary studies on the effects of homologous series of monocarboxylic acids, dicarboxylic acids, thioacids, and amino acids [49,104,105,108,109] have been carried out. It has been shown [107] that more accurate low-coverage data are necessary for the elucidation of the orientation and energetics of the adsorption process. It is a purpose of the present study to obtain this information and compare the results to the projections from previous work on the carboxylic acids [49,103,104,109], using a more rigorous experimental and theoretical approach.

The electrosorption of benzene and other simple aromatic molecules has been studied on ideally polarized electrodes - especially the D.M.E.* [110,111] and several solid electrodes [43,112]. The effects of aromatic adsorbates have received little attention at electrodes under deposition conditions. A major difficulty experienced in the study of the adsorption of aromatics in aqueous solution arises from their low solubilities. Substitution of a carboxyl group on these aromatic molecules effectively diminishes this difficulty. It is, therefore, another purpose of this study to study the effects of some simple carboxyl-substituted benzene derivatives on the Tafel relationship for copper deposition.

* The dropping mercury electrode.

CHAPTER 2

EXPERIMENTAL

2.1 ELECTROLYTIC CELL

There are three essential compartments to an electrolytic cell - reference (R.E.), counter (C.E.) and working (W.E.). The mass transport and concentration profiles of the reactants in the cell depend on the geometry and the interrelation of these compartments. An all-glass cell as shown in Fig. 7 was employed in this work. The C.E. compartment was separated from the W.E. compartment by a fine sintered disk intended to hinder the transport of impurities or oxidization products into the W.E. compartment. To prevent any significant concentration changes, the W.E. compartment was designed to hold a minimum of 125 ml of solution. An inner ground glass joint was fused to the large chamber and was fitted with an outer ground glass joint which served as a cap for atmospheric isolation. Centered in this cap was a long glass sleeve, through which the electrode was positioned. Further atmospheric isolation was obtained by fusing a small glass bubblet filled with solution prior to experimental runs onto the side of the cap. A tapered glass tube was fused into the W.E. compartment for bubbling high grade nitrogen gas to deaerate the solution. A small recess was made in the floor of the compartment for reproducible placement of a teflon-coated magnetic stirring bar. A thin-walled, Luggin capillary bridged the R.E. and W.E. compartments. The capillary was drawn gradually to an outside diameter of 0.7 mm at the tip, positioned about 3mm from the centre of the W.E. compart-

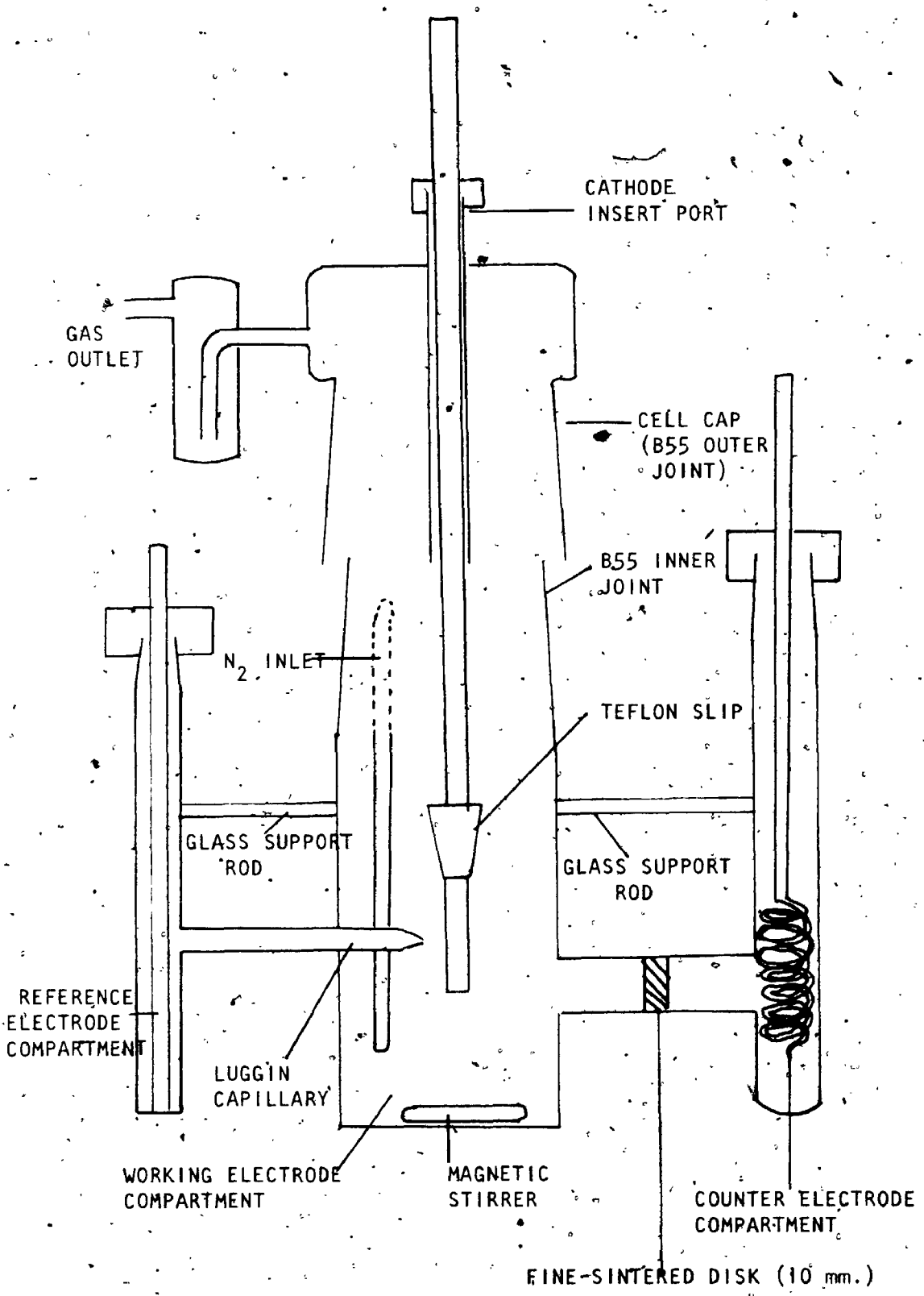

Fig. 7 Schematic diagram of electrolytic cell.

ment. Thus, with the working electrode centered in the cell, conditions are such that the current distribution is essentially not disturbed by the capillary [19].

2.2 ELECTRODES

All electrodes were of commercial copper wire, of gauge no. 12, supplied by Industrial Wire and Cable. The counter electrode (anode) was spiraled into a tight coil to increase the effective area immersed in the solution to minimize polarization. The desired surface area of the working electrode (cathode) in contact with the solution was fixed by enclosing part of the cathode in a tightly fitting tapered teflon sleeve, exposing 1.50 cm of the wire to the solution. Atmospheric isolation was obtained by forcing these electrodes through teflon caps on their respective inlet ports.

2.3 WATER PURIFICATION

All water employed in preparing solutions, cleaning glassware, and recrystallization of additives was triply distilled. Centrally supplied distilled water was fed into a slightly alkaline permanganate stage to oxidize possible surface active organic impurities. The condensate of this stage was introduced automatically into the third stage, the result of which gave specific conductances of less than 1 μmho-cm^{-1}, which was considered to be of sufficient purity for this type of work.

2.4 GLASSWARE

All solutions were prepared in special outside-capped glass volumetric flasks (Fig. 7, reference [105]). The volumetrics prevented contamination during the transfering of solution or water. All glassware was cleaned in warm chromic acid, followed by immersion for 24 hours in 1:1 HNO_3-H_2SO_4, and thorough rinsing with triply distilled water between experimental runs.

2.5 CHEMICALS

Reagent grade H_2SO_4 supplied by Allied Chemical Canada Limited was employed in cleaning solutions and in preparation of standard solution. Copper bus bar (99.9+%) employed in standard solution preparation was supplied by Anaconda Copper (Toronto). Several solutions were prepared with 99.999+% copper rod also supplied by Anaconda. The organic compounds employed in this work are listed with the supplier in Table 2. All organics were of reagent grade.

2.6 STANDARD SOLUTION

Electrolyte containing 0.5 M $CuSO_4$ and 1.0 M H_2SO_4 was used as standard solution. The electrolysis apparatus shown in Fig. 8 was employed in preparing the electrolyte solution from which standards were prepared. A 1.5 M H_2SO_4 solution was used as electrolyte in this apparatus. The cathode was made of heavy gauge platinum wire, tightly coiled around the glass tubing bridge. The anode was composed of four 15 cm strips of copper bus bar bound above the solution line by platinum wire. The electrodes were etched in 1:1 nitric acid for 60

TABLE 2

ORGANIC ADDITIVE	SUPPLIER
Propanoic (Propionic)* Acid	Fisher Scientific Company
Butanoic (Butyric) Acid	Fisher Scientific Company
Pentanoic (Valeric) Acid	Eastman Organic Chemicals
Hexanoic Acid	Eastman Organic Chemicals
Heptanoic Acid	Eastman Organic Chemicals
Octanoic (n-Caprylic) Acid	Eastman Organic Chemicals
Propanedioic (Malonic) Acid	BDH Chemicals Ltd.
Butanedioic (Succinic) Acid	BDH Chemicals Ltd.
Pentanedioic (Glutaric) Acid	Eastman Organic Chemicals
Hexanedioic (Adipic) Acid	Fisher Scientific Company
Heptanedioic (Pimelic) Acid	Eastman Organic Chemicals
Octanedioic (Suberic) Acid	Columbia Organic Chemicals
Nonanedioic (Azelaic) Acid	Eastman Organic Chemicals
Decanedioic (Sebacic) Acid	Eastman Organic Chemicals
Benzoic Acid	BDH Chemicals Ltd.
Phenyl-Acetic (α-Toluic) Acid	BDH Chemicals Ltd.
3-Phenyl-Propanoic (Hydrocinnamic) Acid	J. T. Baker Chemical Ltd.
4-Phenyl-Butanoic Acid	Aldrich Chemical Co.

* Common names in brackets

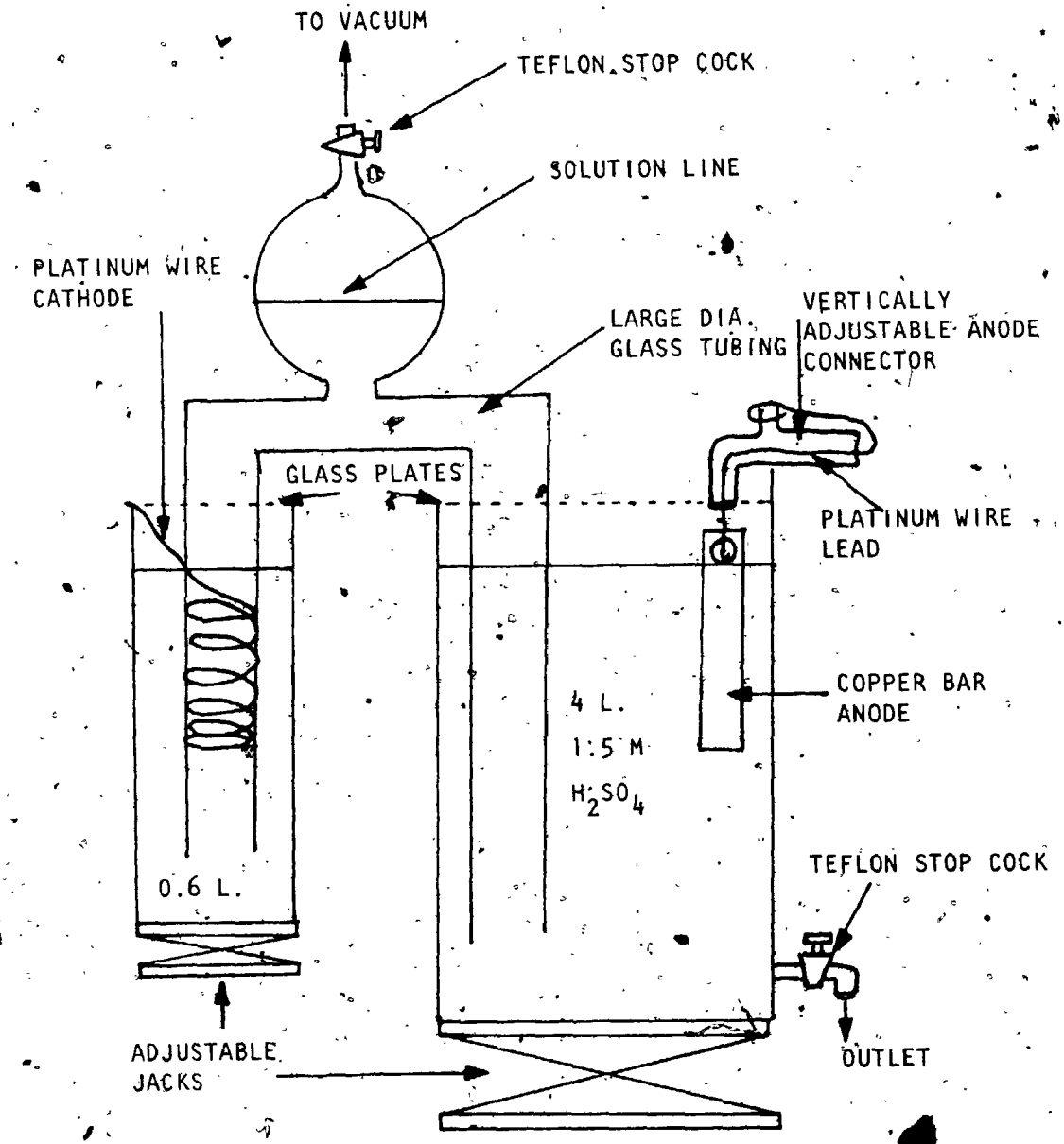

Fig. 8. Electrolytic apparatus for standard solution preparation.

seconds and rinsed thoroughly with triply distilled water before immersion in the solution. Electrolysis was performed for 48 hours at 5 amperes current at which time the sulfuric acid content in the anode compartment was less than 1.0 M and the $CuSO_4$ content greater than 0.5 M. Any insoluble impurities released from the copper during dissolution collected on the bottom of the compartment. The resulting electrolyte solution was drained into a 5 liter glass stoppered bottle through the teflon outlet stopcock. After thorough mixing the solution was further purified of remaining surface active impurities by slow filtration through a 6.5 cm wide x 40 cm long column of spectroscopic grade activated charcoal and a fine sintered glass disk [25,30-32, 113-115]. The activated charcoal was prepared by flushing the column with 2 liters of warm 1 M H_2SO_4, followed by thorough rinsing with triply distilled water.

The effluent was thoroughly stirred using a teflon coated magnetic stirring bar and analysis for Cu^{2+} and H^+ were performed.

Cupric ion concentration was determined gravimetrically using a Sargent Electrolytic Analyzer. A sample of the solution was then passed through a column of Dowex 50 W cation exchange resin, and the clear effluent titrated with standardized potassium hydroxide solution using phenolphthalein as indicator.

Standard solutions of the desired $CuSO_4$ and H_2SO_4 concentrations were then prepared by addition of H_2SO_4 and water to these solutions.

2.7 PREPARATION OF SOLUTIONS CONTAINING ORGANIC ADDITIVES

All the monocarboxylic acids used in this work were newly purchased from the suppliers ± unopened and unused other than in this work. With

this condition satisfied and from the earlier work of Loutfy [49], further purification was unnecessary. These additives were directly added to the volumetrics, and weighed on the analytic balance for solutions of high additive concentration, i.e. near the saturation concentration. Solutions of low and moderate concentrations were prepared from a concentrated solution prepared from the additive and triply distilled water.

The dicarboxylic and phenyl-carboxylic acids, all of which are crystalline at room temperature, were recrystallized twice from triply distilled water and dried thoroughly in a vacuum desiccator before use. The required amount of acid was weighed in a transfer boat on the analytic balance and introduced into the volumetrics.

2.8 PREPARATION OF ELECTRODES AND THE CELL

Each set of runs* was conducted employing a single set of electrodes. At the end of a run the electrodes were removed from the cell, rinsed thoroughly with triply distilled water and the diameter of the cathode measured with a micrometer. The cell was drained of solution, the stirrer removed, and the cell and stirrer rinsed several times with the next solution to be studied. After filling the cell with a solution, the electrodes were etched for 60 seconds in 1:1 nitric acid, rinsed first with triply distilled water, followed by a rinse with the solution. The stirrer was handled at all times with a set of clean platinum plated tongs. It should also be noted that the cathode at all times remained fixed in the glass sleeve in the working electrode

* A set of runs consisted of two runs of standard solution, followed by runs with solutions of increasing additive strength, prepared from that standard.

compartment cap. This insured as near reproducible placement of the cathode as possible. The electrolytic cell was placed in a bath of 1:1 nitric-sulfuric acid between sets of runs.

2.9 TEMPERATURE REGULATION

Control of the temperature was achieved by immersing the electrolytic cell up to the solution level in a temperature-regulated water bath. A Fisher Proportional Temperature Control operating a 500 watt heater element controlled the temperature. Cold tap water, run through a coil of copper tubing immersed in the bath, facilitated the temperature regulation. The bath was stirred by bubbling a stream of compressed air through it. The temperature of the water bath was maintained at 25± 0.1° C. All overpotentials were taken at this temperature.

2.10 ELECTRICAL CIRCUITS

The electrical arrangement for overpotential measurement is as shown in Fig. 9. Current for electrolysis was supplied by a Harrison Regulated Power Supply Model 6201 A (PS). The current was regulated by variable resistors (RV) and measured with a three-range Weston Model 934 milliammeter accurate to one percent. The overpotential was continuously monitored with a Nesco Model JY120 recorder and steady-state values obtained with a Weston Model 1294 digital voltmeter or in some cases a Corning Model 12 pH meter.

An electrical circuit similar to that of Devanathan et al [116] was employed to measure ohmic overpotential and to measure the build-up and the decay of electrode potentials at the copper cathode. After

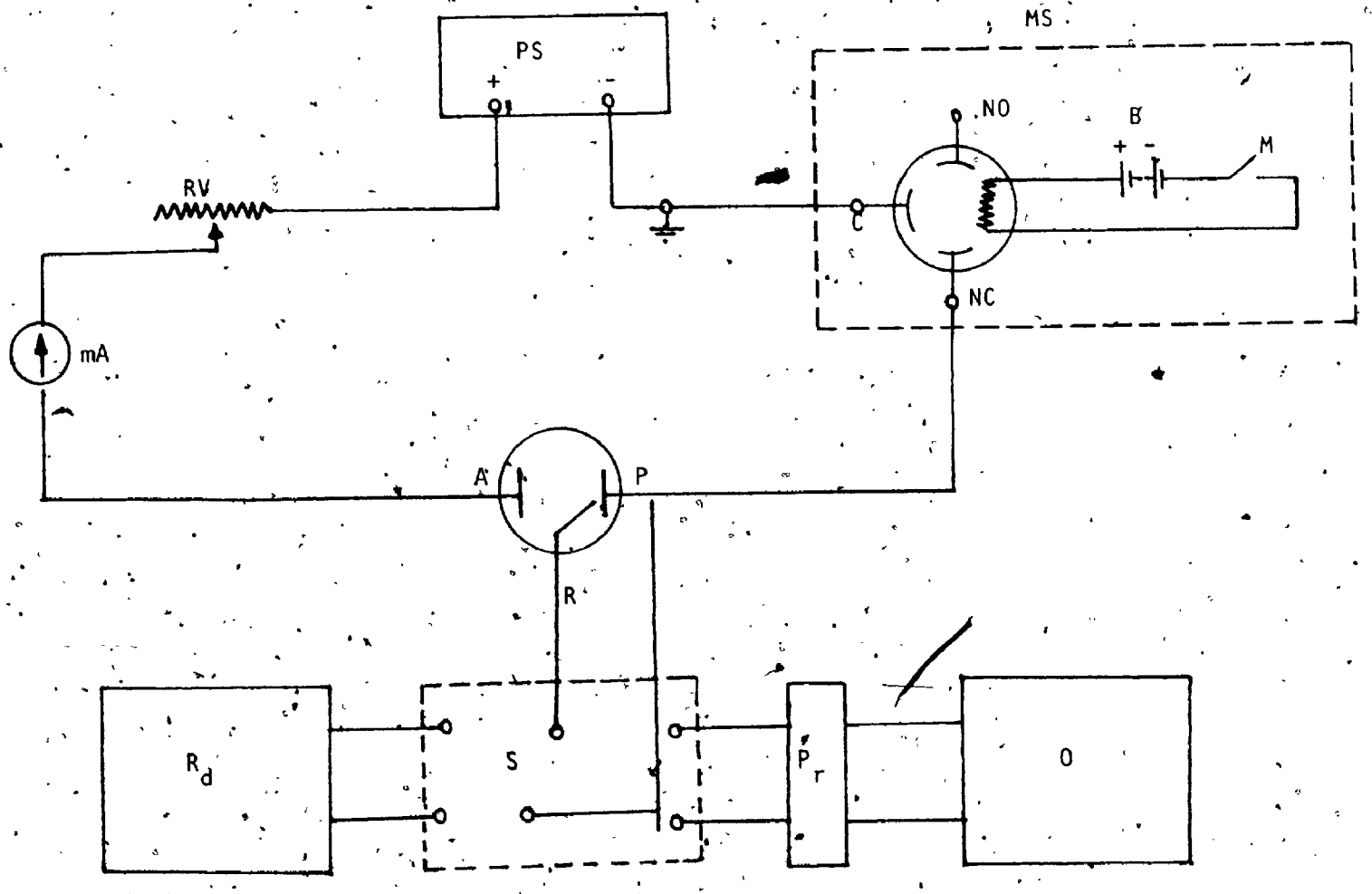

Fig. 9. Schematic diagram of electrical circuit:mA, milliammeter;RV, variable resistances; PS, power supply;MS, fast-rise mercury wetted switch;A, anode;P, polarizing or working electrode;R, reference electrode;R_d, recorder;S, DPDT switch; P_r, preamplifier; O, oscilloscope.

the Tafel curve was determined, the transient circuit was turned on by means of the DPDT switch S. After attainment of steady-state potential the cathodic current was turned on or off by means of a Northern Electric type 2758 mercury-wetted relay switch, rise time 1 μsec. The resultant potential-time transient was monitored and photographed on a Tektronix 535A cathode ray oscilloscope with Type D plug-in unit as preamplifier. All photographs were taken with a Beattie Polaroid-Land Oscillotron Camera Model 12445 using fast Polaroid type 47, speed 3000 film.

2.11 DEAERATION

Before each run the glass bubblet on the cathode compartment cap was partially filled with solution. High grade nitrogen gas was then slowly bubbled through a gas washing bottle filled with triply distilled water, through a fine sintered glass disk, and into the cathode compartment. This process was continued for 10 minutes before the beginning of the run. The gas bubbling was discontinued at the outset of the run.

2.12 ELIMINATION OF CONCENTRATION OVERPOTENTIAL

Concentration overpotentials were minimized by stirring the solution with a teflon-coated magnet bar and a Bronwill Scientific immersed magnetic stirrer. The latter was powered by compressed air. The stirring rate was controlled by a Cash Acme Type A-31 pressure reducing and regulating valve and measured by a Strobotac Type 1538-A stroboscope supplied by General Radio. It was possible to maintain

the stirring rate to within 4 percent of any desired value. It was determined from several solutions that 400 rpm minimized the concentration overpotential and no further change in the potential could be measured with stirring speeds up to 800 rpm. The stirring rate of 600 rpm was selected for all runs, unless otherwise specified.

CHAPTER 3

RESULTS

3.1 OVERPOTENTIAL DECAY CURVES

In order to separate the true charge-transfer overpotential from the total steady-state overpotential, the value of the ohmic overpotential has to be determined. The three components of the total overpotential; ohmic, charge-transfer, and concentration can be distinguished by their build-up and decay curves. If the overpotential of an electrode process proceeding galvanostatically is at steady-state and the electrolysis circuit is opened instantaneously, the ohmic, charge-transfer and concentration overpotentials will decay at vastly different rates. The ohmic overpotential decays instantaneously, the charge-transfer overpotential decay generally requires around 10 μsec. for 80% decay, the concentration overpotential decay requires a time scale in the order of msec [116]. Thus ohmic overpotential can be easily identified by means of oscillograph transients. A typical decay trace is shown in Fig. 10a.

The labelled illustration Fig. 10 b, shows clearly the region of ohmic decay, AC. The magnitude of AC increased linearly with the electrolytic current, thus indicating that AC is indeed ohmic in nature. Furthermore, the magnitude of AC increased when the distance between the polarizing electrode and the Luggin capillary tip is increased. With further increase of distance the magnitude of AC reached a limiting value as predicted by the expression [19]

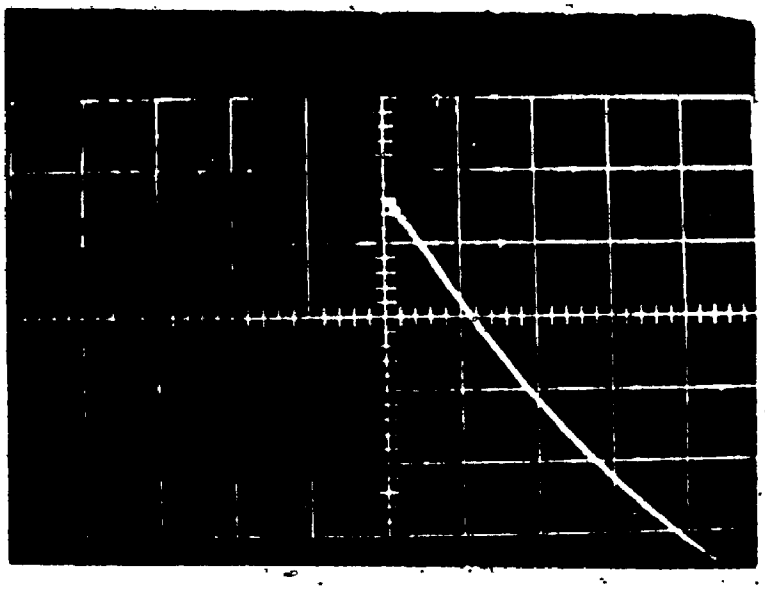

Fig. 10 a. Oscillograph of an overpotential decay curve.

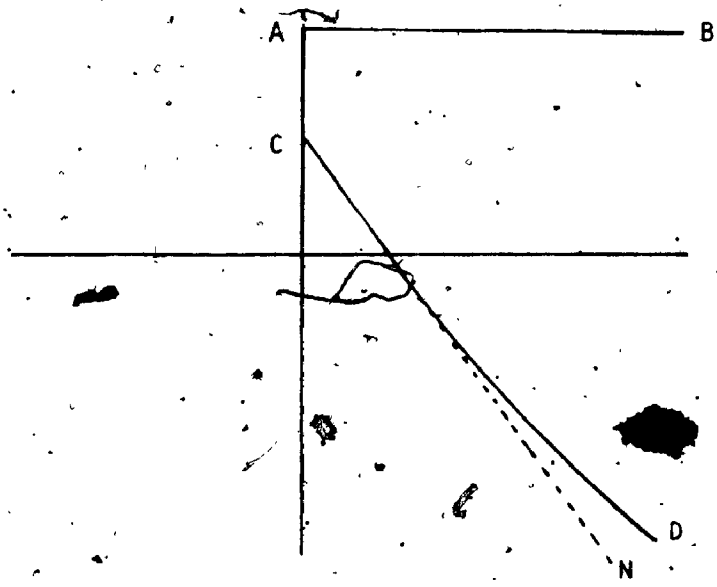

Fig. 10 b. Illustration of the overpotential decay curve.

$$R = \frac{r}{K} \ln\left(\frac{r + a}{r}\right) \qquad (59)$$

where R and a are the resistance and distance between the electrode and the Luggin capillary tip, K is the specific conductance of the solution, and r is the radius of the copper wire electrode.

The ohmic overpotential at 20 mA current for all solutions studied was in the range of 3 - 7 mV and could be measured with a reproducibility of ± 0.5 mV. The steady-state charge-transfer overpotential was then determined by direct subtraction of the ohmic value from the total value.

The differential electrode capacity described by equation (55) was calculated from the slope of the straight line CN, drawn tangent to the initial curve of CD as shown in Fig. 10 b.

Electrode capacities obtained from open-circuit overpotential decay traces, even when smooth and apparently noise free, were irreproducible, especially in the presence of additives. Due to the difficulty of considerable scatter in obtaining trend-like decreases in the electrode capacities, no attempt was made to correlate these measurements with adsorption of the mono- and dicarboxylic acids at the copper cathode during the electrodeposition of copper. Only in the adsorption of the phenyl-carboxylic acids was the electrode capacity studied, due to sudden increases in the capacity at higher coverages. The results and discussions of this behaviour are given in Appendix I.

The electrode capacity of the standard solution at 20.0 mA-cm^{-2}

apparent geometric current density and corresponding electrode potential of + 0.22V ± 0.01 V vs NHE was determined as 34 ± 6 $\mu F\text{-}cm^{-2}$ (15 results). This is in agreement with the values of around 40 $\mu F\text{-}cm^{-2}$ at this potential reported by McMullen and Hackerman [117] and Winkler [118] for the Cu electrode in 1.0 N Na_2SO_4.

3.2 VARIATION OF OVERPOTENTIAL WITH TIME

Typical total cathodic overpotential-time relations for standard solution are shown in Fig. 11 a and b under unstirred and stirred conditions respectively. These curves, even when additive was present at significant concentrations, always showed the same initial relations, i.e. the unstirred solutions show the rapid initial rise in overpotential to a maximum value, followed by a small but rapid decline and levelling to steady-state similar to the stirred solutions. The time to steady-state was generally around 10 min. and 30 min. for stirred and unstirred standard solution respectively. This value increased slightly with increasing additive concentration.

Fig. 12, shows a behaviour noticed only with certain solutions containing benzoic acid as additive. This secondary rise in overpotential was exhibited in both stirred and unstirred solutions and generally occurred at about the same additive concentration, irrespective of the convection conditions.

3.3 TAFEL BEHAVIOUR OF STANDARD SOLUTION

Typical charge-transfer overpotential-apparent current density relationships for the deposition of copper from standard solution are

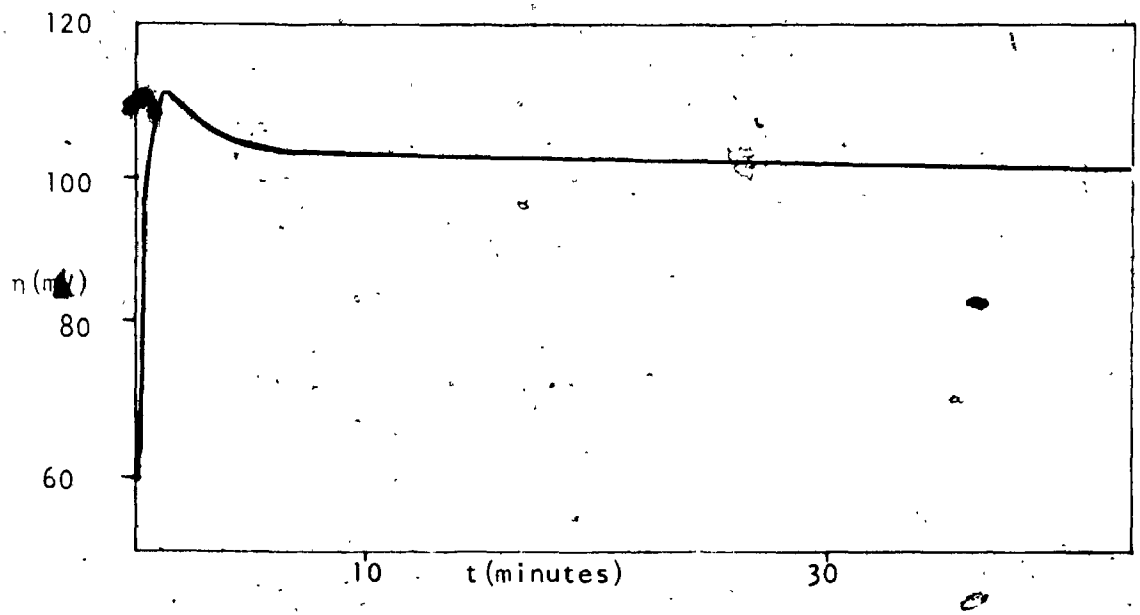

Fig. 11 a. Typical cathodic overpotential-time relation for unstirred standard solution.

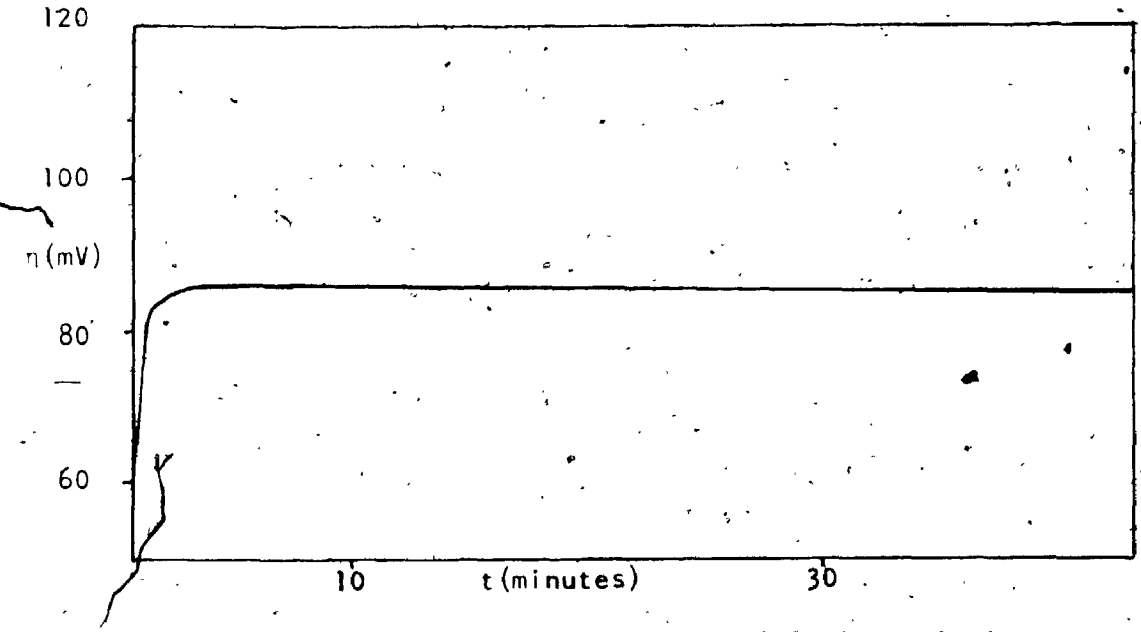

Fig. 11 b. Typical cathodic overpotential-time relation for stirred standard solution.

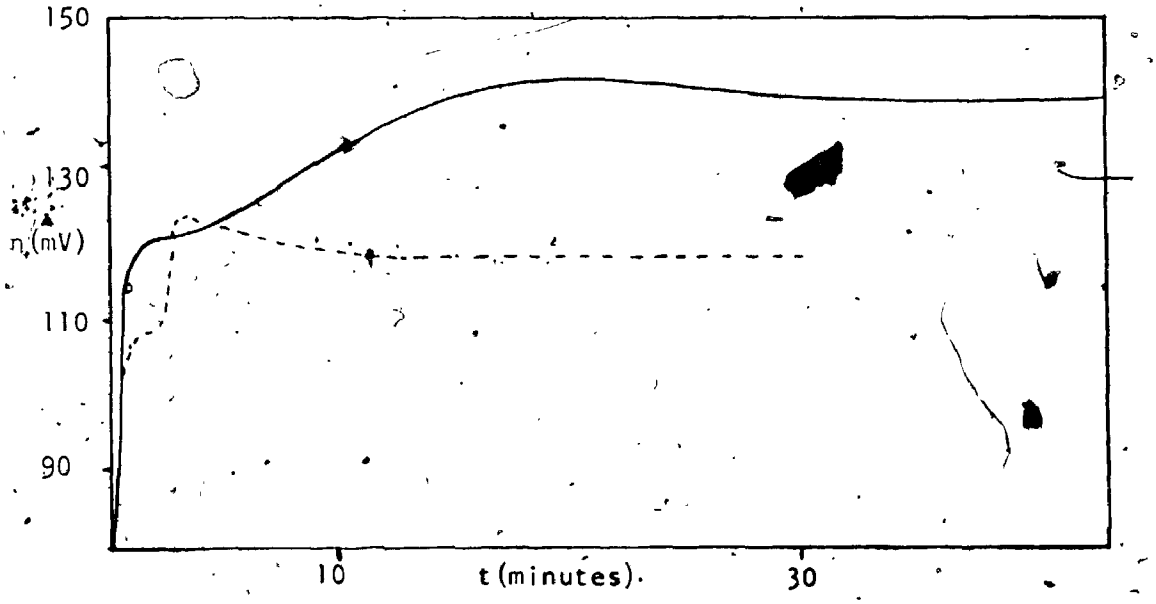

Fig. 12. Overpotential-time relation for solution containing benzoic acid as additive; solid curve, 4.09×10^{-3} M; unstirred convection; dashed curve, 4.74×10^{-3} M, stirred convection.

shown in Fig. 13 in semi-logarithm form. The Tafel (linear) region of the curve generally extended over the range 12 $mA\text{-}cm^{-2}$ to above 45 $mA\text{-}cm^{-2}$, the highest apparent current density examined for solutions under stirred conditions. In some cases under free convection however, the upper limit fell to around 40 $mA\text{-}cm^{-2}$. The theoretical slope for the deposition process is 51 mV [25]. For the many solutions studied, the average slope under forced convection was 42 mV, as compared to 64 mV for free convection. Similarly the average overpotential at 20 $mA\text{-}cm^{-2}$ was lower for stirred than non-stirred solutions; 86 mV as compared to 107 mV. The Tafel slopes and average overpotential values for runs with solutions taken from the same standard, employing the same electrodes and cell geometry, were reproducible to an extent which is reasonable for research in the electrochemical field. The average error for Tafel slopes and overpotential values were $\pm$ 0.5 mV and $\pm$ 2.0 mV respectively. The Tafel slopes and overpotential values for solutions prepared from different standards and employing different electrodes and varying cell geometry varied greatly.

Consideration of the possibility of incorporation of finely-divided carbon into the metal deposit [105,119,120] as a cause of such variation led to the following experiments; 1) Examinations of various solutions by light scattering. 2) Ultra-centrifuging of a sample of solution and performing Tafel runs on this and the stock solution. No indication of colloidal carbon was evident from the light scattering experiments and good reproducibility was obtained for the Tafel parameters for the centrifuged and stock solutions, employing the same electrodes and cell geometry.

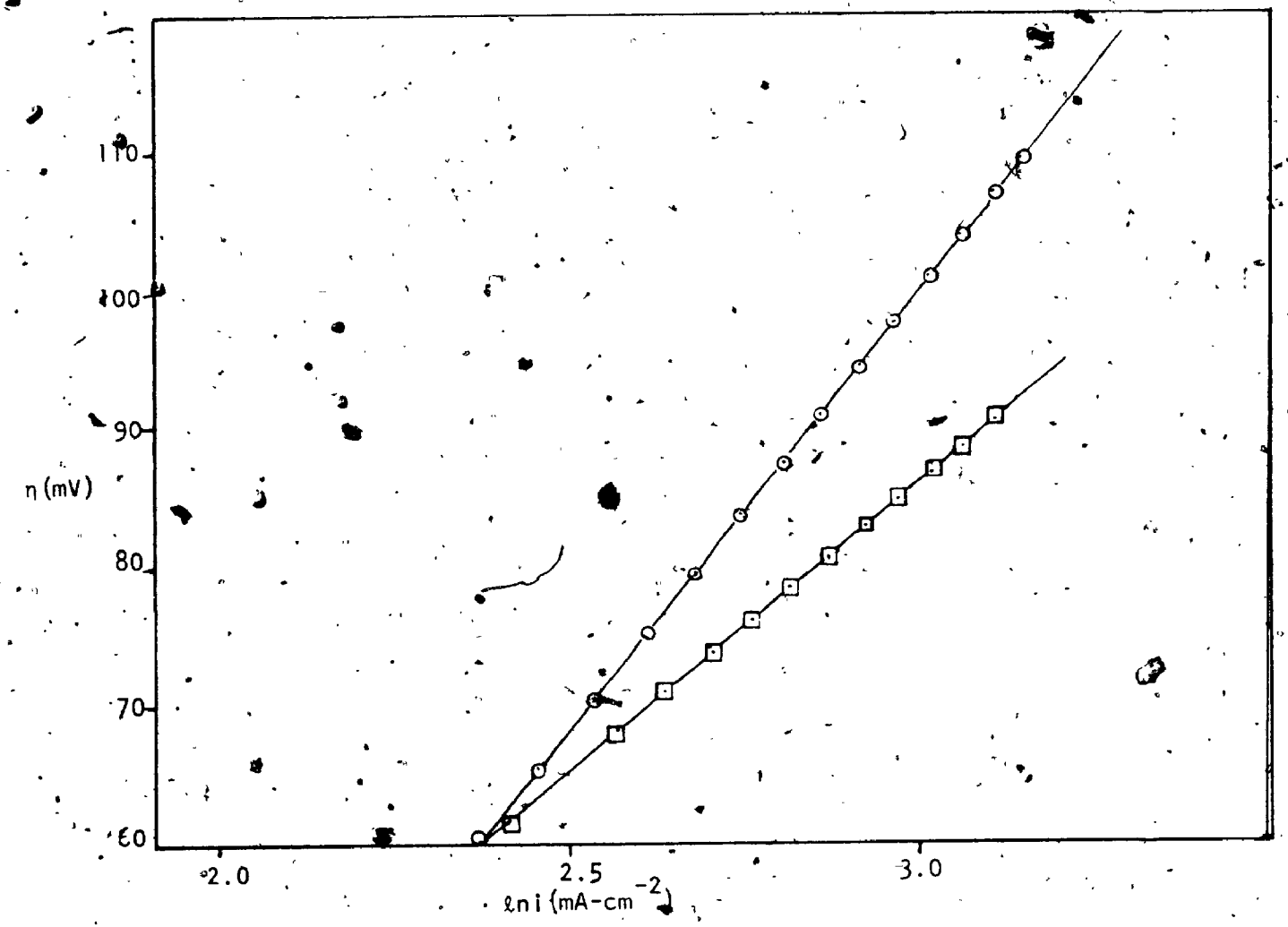

Fig. 13 . Typical activation overpotential versus ℓn apparent current density plots for standard solution: □ stirred solution ○ unstirred solution.

3.4 TAFEL BEHAVIOUR OF SOLUTIONS CONTAINING ADDITIVES

Shown in Figs. 14 a,b,c and d are the cathodic overpotential-natural log apparent current density plots for solutions containing various concentrations of propanoic, butanedioic, and benzoic acids as additives. In general the Tafel plots are linear in the charge-transfer region. The Tafel slopes tend to increase with increasing concentration of additive. This effect was more pronounced in the unstirred, than the stirred solutions. Some additives, namely the monocarboxylic acids and succinic acid, showed no apparent effect on the Tafel slope for solutions of low additive concentration (small surface coverage).

With the exception of phenyl-acetic acid, the phenyl-carboxylic acids studied showed a deviation from the trend of increasing Tafel slope with increasing concentration. At sufficiently high concentrations, the Tafel slope decreased to a value approximately 10 mV below the original standard value. Appendix II contains a tabulation of additive concentration-overpotential at constant apparent current density $i_g = 20\ mA\text{-}cm^{-2}$ - Tafel slope relationships along with the overpotential and Tafel slope of the standard solution in which this data was obtained.

3.5 VISUAL EXAMINATION OF ELECTRODEPOSITS

In general, visual microscopic examination of the electrodeposits with 200X magnification showed polycrystalline deposits in the presence of all additives studied. The electrodeposits formed in the presence of the additives at high concentration were more uniform and smoother.

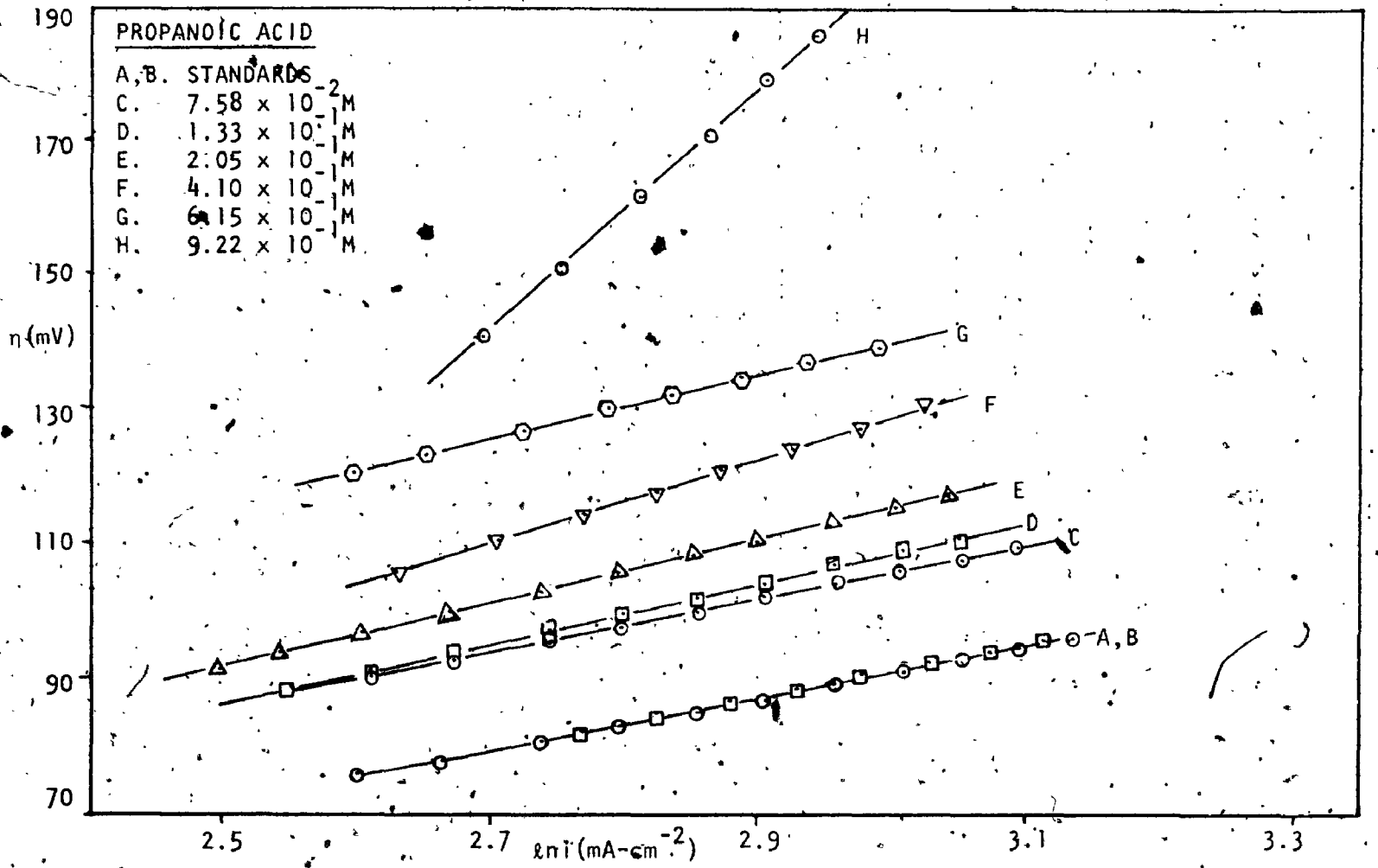

Fig. 14 a. Tafel plots for solutions containing propanoic acid as additive.

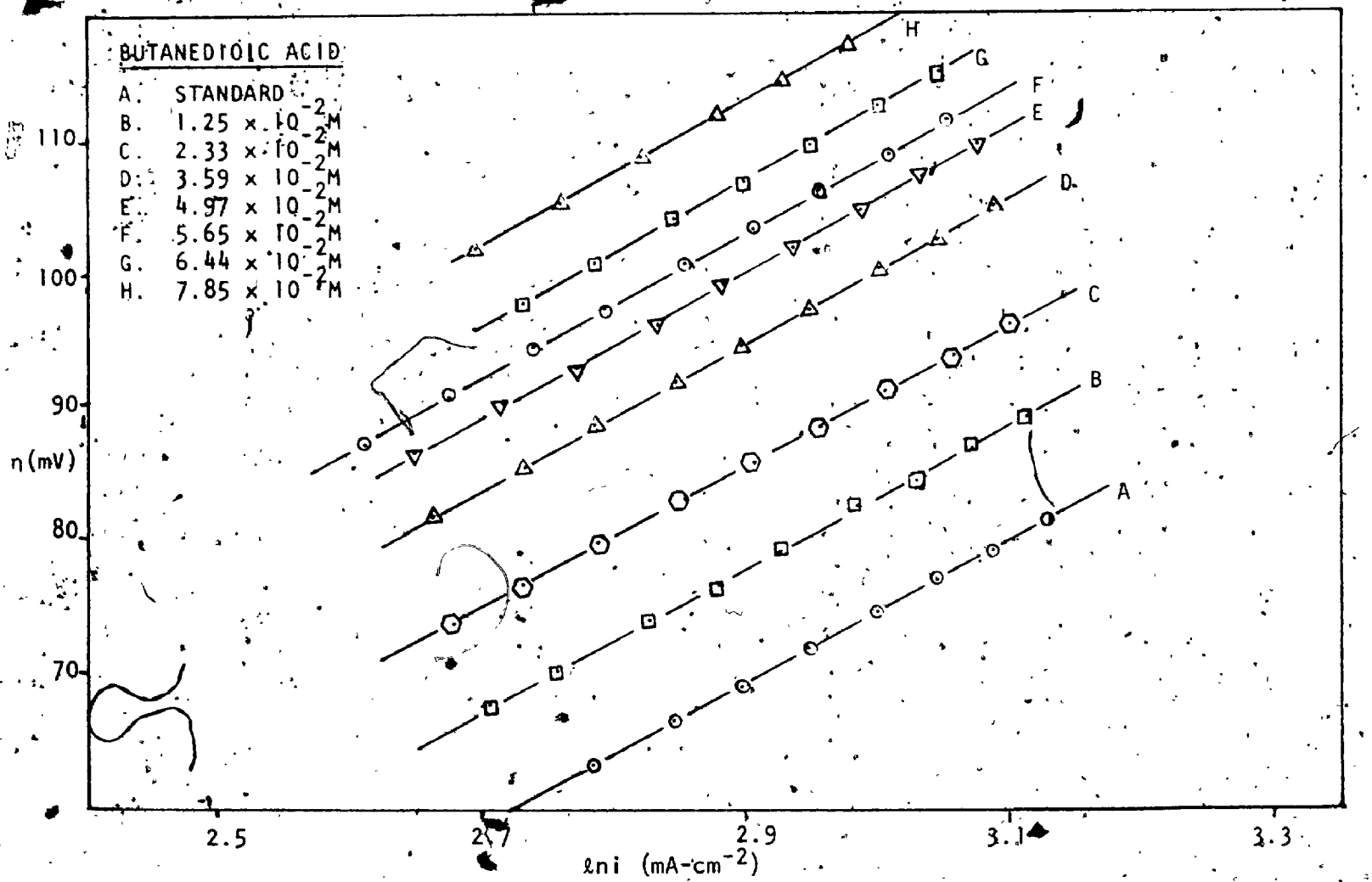

Fig. 14 b. Tafel plots for solutions containing butanedioic acid as additives.

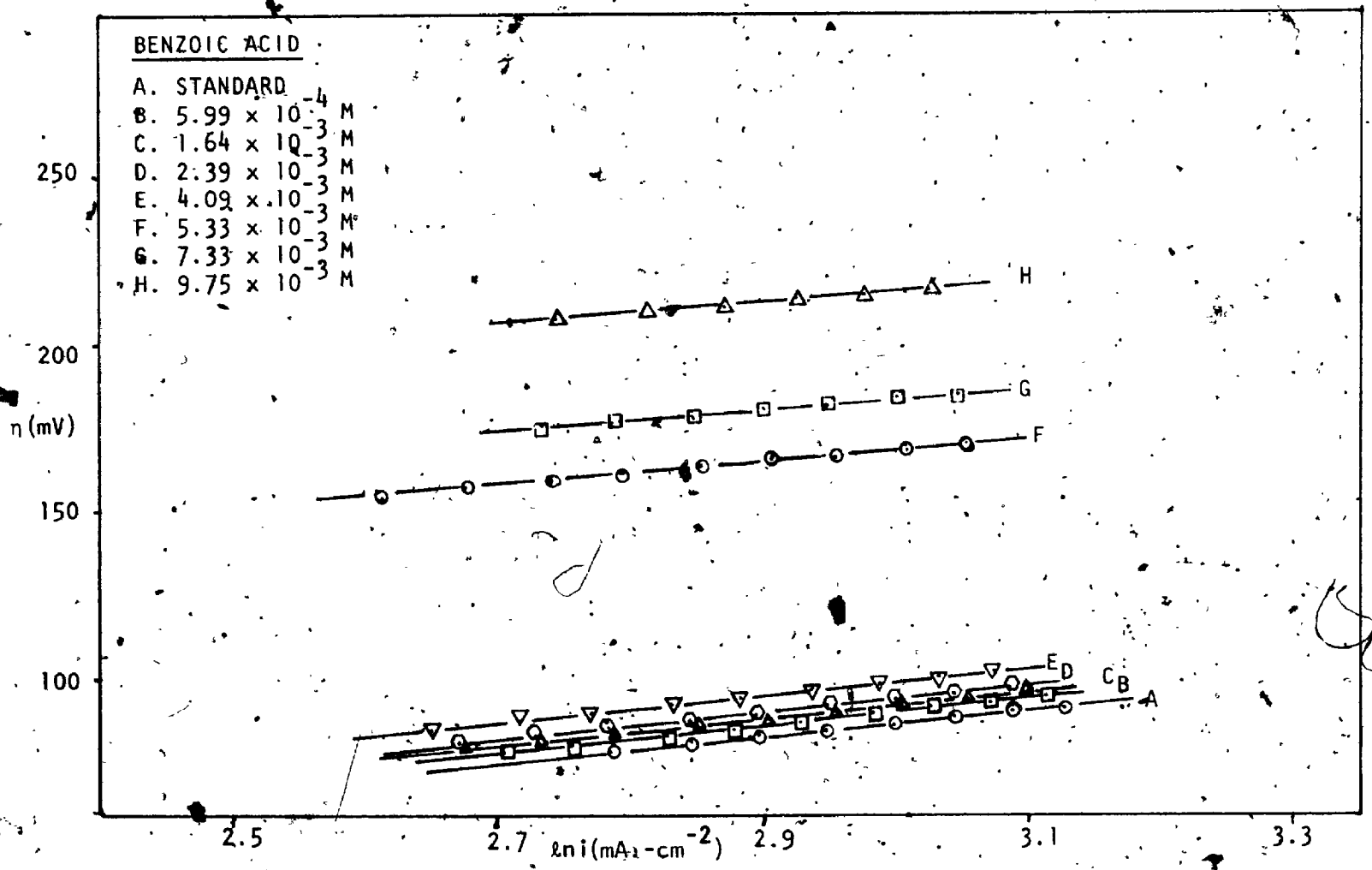

Fig. 14c. Tafel plots for solutions containing benzoic acid as additive.

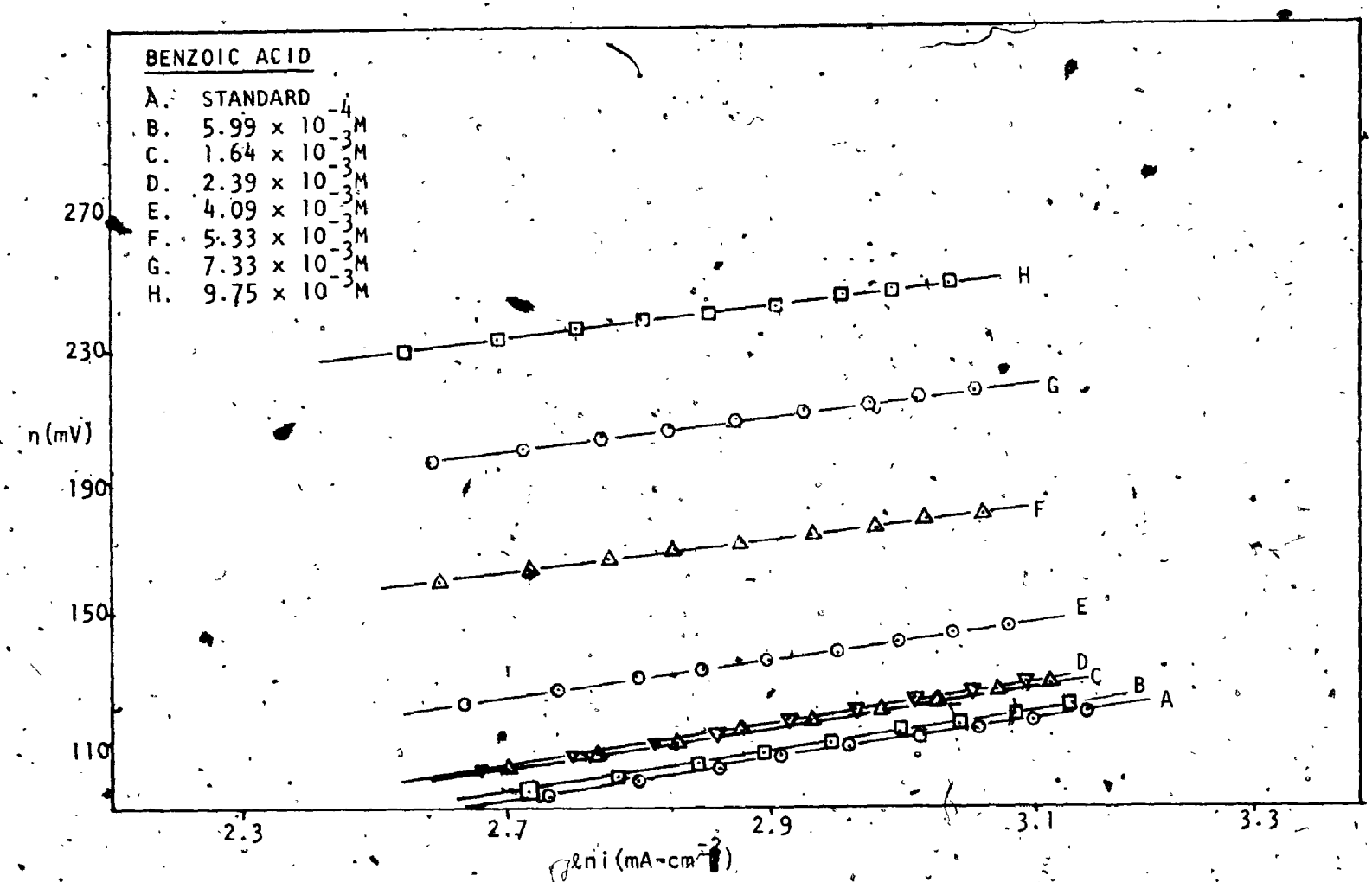

Fig. 14 d. Tafel plots for unstirred solutions containing benzoic acid as additive.

This effect was greatest when the solutions were not stirred. With larger molecules, a smoothing of the deposit became noticable at lower concentrations. As was later shown, this smoothing effect only became apparent when the fractional surface coverage by additive was greater than approximately 0.8. The presence of the phenyl-carboxylic acids at sufficiently high concentrations to increase the overpotential above 220 mV caused a blackening of the electrodeposit. Since no unusual deposits were viewed, pictorial recordings of these deposits were deemed unnecessary.

CHAPTER 4

DISCUSSIONS - PART I

4.1 DISCUSSION OF ELECTRODE KINETICS AND BLOCKING THEORY

4.1.1 Behaviour of the Standard Solution

At high overpotentials, indicative of irreversible electrode processes, the electrodeposition of copper has been shown to follow the mechanism [25]

$$Cu^{2+} + e \xrightarrow{\text{slow}} Cu^{+} \qquad (60)$$

$$Cu^{+} + e \xrightarrow{\text{fast}} Cu \qquad (61)$$

and the anodic dissolution of copper, the mechanism [25]

$$Cu \xrightarrow{\text{fast}} Cu^{+} + e \qquad (62)$$

$$Cu^{+} \xrightarrow{\text{slow}} Cu^{2+} + e \qquad (63)$$

The overall rates of deposition and dissolution of copper are given in terms of the current density i by

$$i_{dep'n} = K_{60}\, a_{Cu^{2+}} \exp\left[\frac{-\beta\Delta\phi F}{RT}\right] \qquad (64)$$

and

$$i_{diss} = K_{63}\, a_{Cu^+} \exp\left[\frac{(1-\beta)\,\Delta\phi F}{RT}\right] \tag{65}$$

respectively; where β is the symmetry factor and $\Delta\phi$ is the metal-solution potential difference.

In the anodic process the $Cu(aq)^+$ ions are assumed to be in reversible equilibrium with the electrode. Accordingly,

$$a_{Cu^+} = \frac{K_{62}}{K_{-62}}\, a_{Cu} \exp\left[\frac{\Delta\phi F}{RT}\right] \tag{66}$$

Substituting equation (66) into (65) yields

$$i_{diss} = K_{63}\left(\frac{K_{62}}{K_{-62}}\right) a_{Cu} \exp\left[\frac{(2-\beta)\Delta\phi F}{RT}\right] \tag{67}$$

The exchange current density i_o, of the charge-transfer process (60) is

$$i_o = K_{60} a_{Cu^{2+}} \exp\left[\frac{-\beta_o \Delta\phi_r F}{RT}\right] = K_{63}\frac{K_{62}}{K_{-62}}\, a_{Cu} \exp\left[\frac{(2-\beta_o)\Delta\phi_r F}{RT}\right] \tag{68}$$

where $\Delta\phi_r$ is the reversible metal-solution potential difference, β_o is the symmetry factor when the overpotential η, equals 0, i.e. when $i_{dep'n} = i_{diss} = i_o$, and K_{60}, the rate constant, is defined in equation (7). The net cathodic current for deposition is

$$i_c = i_{dep'n} - i_{dissolution} \tag{69}$$

Putting equations (64), (67), and (68) into equation (69) yields

$$i = i_o \exp\left[\frac{(\beta_o-\beta)\Delta\phi_r F}{RT}\right]\left\{\exp\left[\frac{-\beta\eta_c F}{RT}\right] - \exp\left[\frac{(2-\beta)\eta_c F}{RT}\right]\right\} \quad (70)$$

At high cathodic overpotentials, η_c, say -100 mV, equation (70) reduces to

$$i = i_o \exp\left[\frac{(\beta_o-\beta)\Delta\phi_r F}{RT}\right]\exp\left[\frac{-\beta\eta_c F}{RT}\right] \quad (71)$$

On rearrangement, equation (71) becomes

$$\eta_c = \frac{RT}{\beta F}\ell n i_o + \frac{RT}{\beta F}\left(\frac{(\beta_o-\beta)\Delta\phi_r F}{RT}\right) - \frac{RT}{\beta F}\ell n i \quad (72)$$

Equation (72) reduces to the well known Tafel equation

$$\eta_c = \frac{RT}{\beta F}\ell n i_o + \left(\frac{-RT}{\beta F}\right)\ell n i \quad (73)$$

when $\beta_o = \beta$.

The true current density, i, is related to the geometric current density i_g, by

$$i = \frac{i_g}{\delta} \quad (74)$$

where δ is the roughness factor.

Substituting equation (74) into (72) yields

$$\eta_c = \frac{RT}{\beta F} \ell n i_o + \frac{RT}{\beta F}\left(\frac{(\beta_o - \beta)\Delta G_r F}{RT}\right) + \frac{RT}{\beta F} \ell n \delta_r - \frac{RT}{\beta F} \ell n i_g \qquad (75)$$

Morphological examinations of electrode surfaces formed by metal deposition in the overpotential region, 60 mV to 140 mV, show similar types of deposits. In this overpotential range, the deposits formed on single-crystal substrates exhibit layered and pyramidal growth with no indication of truncation [121], while with polycrystalline substrates the grain size of the deposits seems constant. Accordingly, the roughness factor can be assumed to be independent of the overpotential in this overpotential range. Also, since the symmetry factor arises from the consideration of the change in activation energy of the deposition process with the change in overpotential (Fig. 4b), it also can be assumed to be independent of overpotential in this same overpotential range. This assumption can be justified by considering that the activation energy depends on the availability of sites of different types for deposition. It has been shown by Bockris and Conway (Table 1) that the heat of activation for direct ion transfer from the undistorted hydrated ion to the metal surface depends on the type of site on the surface at which this takes place. Accordingly, if the availability of each type of site is independent of overpotential, so also is the activation energy and the symmetry factor. The roughness factor is in a sense a measure of the relative number of different types of sites and since it can be assumed to be independent of overpotential in the overpotential region, 60 to 140 mV, so also can the symmetry factor. The symmetry factor will be discussed in more detail at a later point.

Accordingly, equation (75) can be assumed to be linear, for the overpotential region 60 to 140 mV, the validity of which has been shown experimentally by Mattsson and Bockris [25] and Loutfy and Sukava [104], (Fig. 13). Extrapolation of this Tafel-type relation to $\eta_c = 0$ gives $\ln i_{o_g}$, where i_{o_g} is the geometric exchange current density at an electrode with roughness factor δ and symmetry factor β (i.e. an electrode with the same morphological and double layer structure as that which is exhibited at an electrode at an overpotential between 60 and 140 mV). Thus equation (75) may be written as

$$\eta_c = \frac{RT}{\beta F} \ln i_{o_g} - \frac{RT}{\beta F} \ln i_g \qquad (76)$$

4.1.2 Effect of Adsorbed Substances on Electrodeposits

It is well known [122] that the addition of certain organic substances affects to a very large extent the physical properties and the conditions of formation of electrodeposits. Two kinds of effects produced by these additives are discernible [123]: (i) morphological effects, those resulting in changes in the microscopic (or even visible) appearance of the surface, as well as in the structural properties of the deposit (grain size, orientation, stress, dislocations); (ii) electrochemical effects, resulting in changes in the overpotential-current density relationship for the particular electrode reaction, e.g. variations in i_o and b for a Tafel relation, or even disappearance of a Tafel behaviour. These two types of effects are interrelated, but may be separately discernible for systems exhibiting Tafel behaviour.

4.1.3 Behaviour of the Standard Solution Containing Additive

When an uncharged, electroinactive substance is present on a cathode at an apparent fractional surface coverage θ, the true current density, i_θ, increases by a factor $\frac{1}{(1-\theta)}$. Equation (74) becomes in the presence of additive

$$i_\theta = \frac{i_g}{(1-\theta)\delta_\theta} \qquad (77)$$

where δ_θ is the roughness factor of the electrode when the surface is covered by a fraction θ with additive. Equation (75) becomes in the presence of additive

$$\eta_{c_\theta} = \frac{RT}{\beta_\theta F} \ln i_{o_\theta} - \frac{RT}{\beta_\theta F}\left[\frac{(\beta_{o_\theta}-\beta_\theta)\Delta\phi_{r_\theta}F}{RT}\right] + \frac{RT}{\beta_\theta F}\ln(1-\theta) + \frac{RT}{\beta_\theta F}\ln\delta_\theta - \frac{RT}{\beta_\theta F}\ln i_{g_\theta} \qquad (78)$$

where

$$i_{o_\theta} = a\,(K_{60})_\theta\,(a_{Cu^{2+}})_\theta\,\exp\left[\frac{r\beta_{o_\theta}\Delta\phi_{r_\theta}F}{RT}\right] \qquad (79)$$

and $\Delta\phi_{r_\theta}$ is the reversible metal-solution potential difference when adsorbed additive is present at a coverage θ.

Applying the same assumptions used in the discussion of the linearity of equation (75), one can assume equation (78) to be linear if θ is independent of the overpotential in the overpotential range considered (60 to 140 mV). Fig. 14 demonstrates the linearity of

2 3

OF/DE

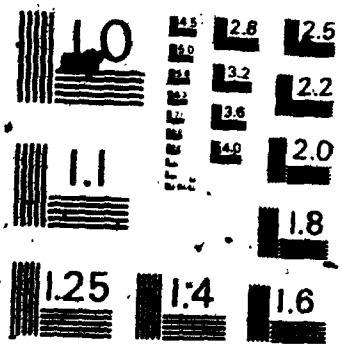

MICROCOPY RESOLUTION TEST CHART
NATIONAL BUREAU OF STANDARDS - 1963 - A

ABC - 374

equation (78) for certain additives over the specified overpotential range and the independence of θ is justified. Accordingly, equation (78) simplifies to

$$\eta_{c_\theta} = \frac{RT}{\beta_\theta F} \ell n i_{o_{g_\theta}} - \frac{RT}{\beta_\theta F} \ell n i_g \qquad (80)$$

where $i_{o_{g_\theta}}$ is the geometric exchange current density at an electrode with roughness factor δ_θ, symmetry factor β_θ, and covered by a fraction θ with adsorbed additive.

4.1.4 Correlation Between Galvanostatic Deposition Processes in the Presence of Adsorbed Additive and Processes Free of Adsorbed Additive

Substitution for i_o and i_{o_θ} from equations (68) and (79) respectively into equations (75) and (78) yields, from (75), in the absence of adsorbed additive

$$\eta_c = b \left[\ell n K_{60} + \ell n a_{Cu^{2+}} - \frac{\Delta\phi_r}{b} + \ell n \delta \right] - b \ell n i_g \qquad (81)$$

and from (78), in the presence of additive

$$\eta_{c_\theta} = b_\theta \left[\ell n (K_{60})_\theta + \ell n (a_{Cu^{2+}})_\theta - \frac{\Delta\phi_{r_\theta}}{b_\theta} + \ell n \delta_\theta + \ell n (1-\theta) \right] - b_\theta \ell n i_{g_\theta} \qquad (82)$$

where b and b_θ are the appropriate Tafel slopes, $\frac{RT}{\beta F}$ and $\frac{RT}{\beta_\theta F}$. Subtracting

equation (81) from (82) and rearranging gives the effect of adsorbed additive as

$$\left[\frac{bn_\theta - b_\theta n'_c}{b_\theta b}\right] - \left[\frac{b_\theta \Delta\phi_r - b\ \Delta\phi_{r_\theta}}{b_\theta b}\right] + \ln \frac{K_{60}}{(K_{60})_\theta} + \ln \frac{a_{Cu^{2+}}}{(a_{Cu^{2+}})_\theta} \qquad (83)$$

$$= \ln \frac{\delta_\theta}{\delta} + \ln (1-\theta)$$

since $i_g = i_{g_\theta}$ for a galvanostatic process.

4.1.5 Electrochemical Effects of Adsorption on Deposition Processes

Although the accumulation of inhibitor in a layer of solution adjacent to the electrode appears capable of affecting the deposition to some extent, the basic action of such additives seems to arise almost invariably from their adsorption on the electrode surface and, hence, a modification of the conditions of the steps of the crystallization process following that of mass transport in the solution. Correlation has been established between adsorption of some organic compounds (measured by the decrease in double layer capacities) and the modification of the electrochemical parameters [123,124].

In general, several changes in the electrochemical parameters may occur as a result of the presence of adsorbed material [123]. First, the free energy of activation for the elementary charge-transfer steps can be modified. Hence, the rate constant, i_o, the rate-determining step (60), and even the path of the reaction will depend on the amount and nature of the adsorbed substance.

4.1.6 Effect of Adsorbed Substances on Electrode Kinetics

The adsorbed material can either accelerate or retard the rate of reaction; the latter is generally termed inhibition and the former termed catalysis. Many authors [49,88-104,108,115,125] have examined the inhibition of electrode kinetics on surfaces partly covered by adsorbed films. In most cases the exchange current density or rate constant has been found to decrease linearly with surface coverage, which tends to support a simple model for the influence of such adsorption on a reaction [89, 90]. Several theories are available and these will be discussed.

4.1.7 Frumkin's Double Layer Effect [126,127,128]

It was originally assumed that the electrochemical reaction can occur when the reacting species from the solution is adsorbed at the inner boundary of the diffuse layer. According to the electrical double layer theory, this boundary is the outer Helmholtz plane (O.H.P.) (see Fig. 3), and its potential drop is ϕ_2 with respect to the bulk solution. This assumption has two consequences. First, the rate of reaction is affected, not by the whole of the metal-solution potential difference $\Delta\phi^m$, but by this potential less the potential difference across the diffuse layer, ϕ_2. It follows that the rate equation for a reduction such as (60) is of the form

$$i = K\,[A]_2\,\exp\left[\frac{-\alpha F(\Delta\phi^m-\phi_2)}{RT}\right] \qquad (84)$$

where $[A]_2$ is the concentration of the reducible species at the O.H.P.

Second, the concentration $[A]_2$ differs from the concentration in the bulk of the solution and is given by

$$[A]_2 = [A] \exp\left[\frac{zF\phi_2}{RT}\right] \tag{85}$$

where z and [A] are the valency and the bulk concentration of the electroactive species A respectively. Substituting equation (85) into equation (84) one has

$$i = K\,[A] \exp\left[\frac{-\alpha F\Delta\phi^m}{RT} + \frac{(\alpha-z)F\phi_2}{RT}\right] \tag{86}$$

The magnitude of ϕ_2 is governed by the ionic strength according to diffuse layer theory and the pzc of the metal forming the electrode. In the absence of specific adsorption its variation can be predicted with fair accuracy, but its magnitude has no simple correlation with η. Usually in concentrated solution ϕ_2 is approximately 50 mV and sufficiently constant to be taken as independent of η [128]. In dilute solution ϕ_2 is large and varies widely.

This simple theory is capable of quantitative results so long as no specific adsorption occurs on the electrode surface. When surface-active material adsorbs on the electrode surface, it may effect the theory in two ways [129]: (i) the reacting particle is still located at the OHP but the potential, ϕ_2, of the layer is altered by the presence of specifically adsorbed material; and (ii) the reacting particle moves closer to the electrode before reaction occurs and ϕ_2 must be replaced by the potential at this point. The effect of

(i) is most easily demonstrated by the adsorption of ionic species. For example, the structure of the double layer may be altered by the presence of specifically adsorbed charged species through lateral interaction with oriented solvent molecules as well as ionic interaction with the reacting ions at the O.H.P: [129-136]. In some instances, such as the reduction of $S_2O_8^{2-}$ in chloride solutions, there is reason to believe that there is some ion-pair formation between $S_2O_8^{2-}$ and the cations [129,134,137,138].

Surface-active neutral molecules are more likely to exhibit the second effect. These adsorbates may be aligned such that the negative ends of the adsorbed particles may help the reducible cations to move closer to the electrode surface, as a result of which the reaction rate may be increased to some extent [97]. The reverse may hold true if the alignment is such that the positive ends interact with the cations. Some surface-active electroinactive additives, mostly large cations such as quaternary ammonium ions, exhibit both electrostatic and blocking effects in deviations from the theory [95,99,115,139].

In some cases where the adsorbing species is neutral and its effective dipole moment is comparable to the effective dipole of the solvent in the primary layer, there may be negligible effect on ϕ_2. The electrostatic interaction with cations at the O.H.P. will not be changed by the presence of adsorbate and as long as charge-transfer cannot take place through the adsorbate (blocking effect) the reacting particle will remain at the same distance from the active part of the electrode surface.

4.1.8 Interaction Between Activated Complex and Adsorbed Particles

Recently, Parsons [129] introduced the interaction between the activated complex of the electrode reaction and adsorbed halide ions in the form of an activity coefficient into Frumkin's theory of absolute reaction rates; the rate constant is altered from equation (7) to

$$K_\theta = \frac{1}{\gamma^*}\left(\frac{kT}{h}\right)\exp\left(-\frac{\Delta G^*}{RT}\right) \qquad (87)$$

where γ^* is the activity coefficient of the activated complex. γ^* will undoubtedly depend on the extent of specific adsorption when the adsorbate is ionic [129,105] due to differences in interaction with the adsorbed species and neutral solvent and due also to changes in the ionic strength in the double layer. However, when the surface-active additive is neutral and the ionic character of the double layer is largely unaffected by its presence, γ^* can be assumed to be independent of the surface coverage.

4.1.9 Change of Heat of Activation

The heat of activation of a charge-transfer process may be affected by the presence of neutral (or ionic) adsorbate in two ways: (i) if there is preferred adsorption of adsorbate at active sites, then the transfer process may be favoured at sites where the activation energy is greater, and (ii) the separation between the outer Helmholtz plane and the electrode surface may be increased, causing a corresponding increase in the heat of activation.

A brief discussion of the Conway and Bockris theory on active sites may be found in the Introduction (1.4). This theory predicts

the rate constant for transfer to planar sites to be at least 10^6 times greater than that to any other type of site. Due to the large energy differences, transfer will most likely occur at planar sites as long as they are available, i.e. not blocked by additive or adions ($Cu(aq)^+$).

It is probable that the heat of adsorption of an organic molecule, e.g. at a kink site, can be much greater than it is on the planar surface, and this would indicate heterogeneous adsorption at growth sites. However, solvent molecules are also adsorbed at growth sites and there is no knowledge available at the present time to suggest that there will be different symmetry of adsorption of the water molecule on the growth sites [123]. In other words, the heterogeneity of the surface would tend to be masked by the equalizing effect of the adsorbed water molecules. Whether the distribution of adsorbed substance with respect to surface sites will be homogeneous or heterogeneous will depend upon the variation of $[\Delta G_v^\circ(org) - n\Delta G_v^\circ(W)]$ from one point to another on the surface ($[\Delta G_v^\circ(X)]$ is the standard free energy of adsorption of X from the pure vapour phase onto the clean metal surface). It is reasonable to expect both $\Delta G_v^\circ(org)$ and $\Delta G_v^\circ(W)$ to become more negative in going from a planar to a kink site, but whether the difference between $\Delta G_v^\circ(org)$ and $\Delta G_v^\circ(W)$ becomes more negative or does not change will depend on the particular case. Therefore, the heterogeneity of the adsorption cannot be predicted in a general sense.

The effect of increasing the activation energy at any given site by increasing the separation between the outer Helmholtz plane and the electrode surface was first proposed by Biegler and Laitinen [89]. The assumptions made in developing this model are: (i) the separation

is a linear function of coverage; and (ii) the effect of such increased separation may be represented by an increase in distance, along the reaction co-ordinate, between the potential energy curves of the type conventionally used to represent the course of electrode reaction. If the intersection of these curves occurs well above the energy minima, (Fig. 15), the increase in free energy of activation may be approximated to a linear function of the increased separation. By equating this to the free energy of activation one has

$$\Delta G^{*}_{\theta} = \Delta G^{*}_{\theta} + (\Delta G^{*}_{1} - \Delta G^{*}_{o})\theta \qquad (88)$$

where ΔG^{*}_{1} is the free energy of activation for a monolayer film. The rate constant is then given by equation (87) and the comparison of the rates in pure and contaminated solution leads to

$$\ln \frac{K_o}{K_\theta} = \frac{(\Delta G^{*}_{1} - \Delta G^{*}_{o})\theta}{RT} \qquad (89)$$

Biegler and Laitinen found a linear relationship between the logarithmic term and surface coverage for the discharge of Cd^{2+} in the presence of thymol, n-butanol, and leucoriboflavin.

It should be noted at this point, that the presence of the inhibitor on the electrode surface may hinder a step for which the adions constitute a reactant, i.e. surface diffusion or incorporation at a growth site, as well as hindering the charge-transfer process. Depending on the relative magnitudes of these two effects, there may well be an increase in surface diffusion control of the electrode process. In many cases, however, there is an increase in adion

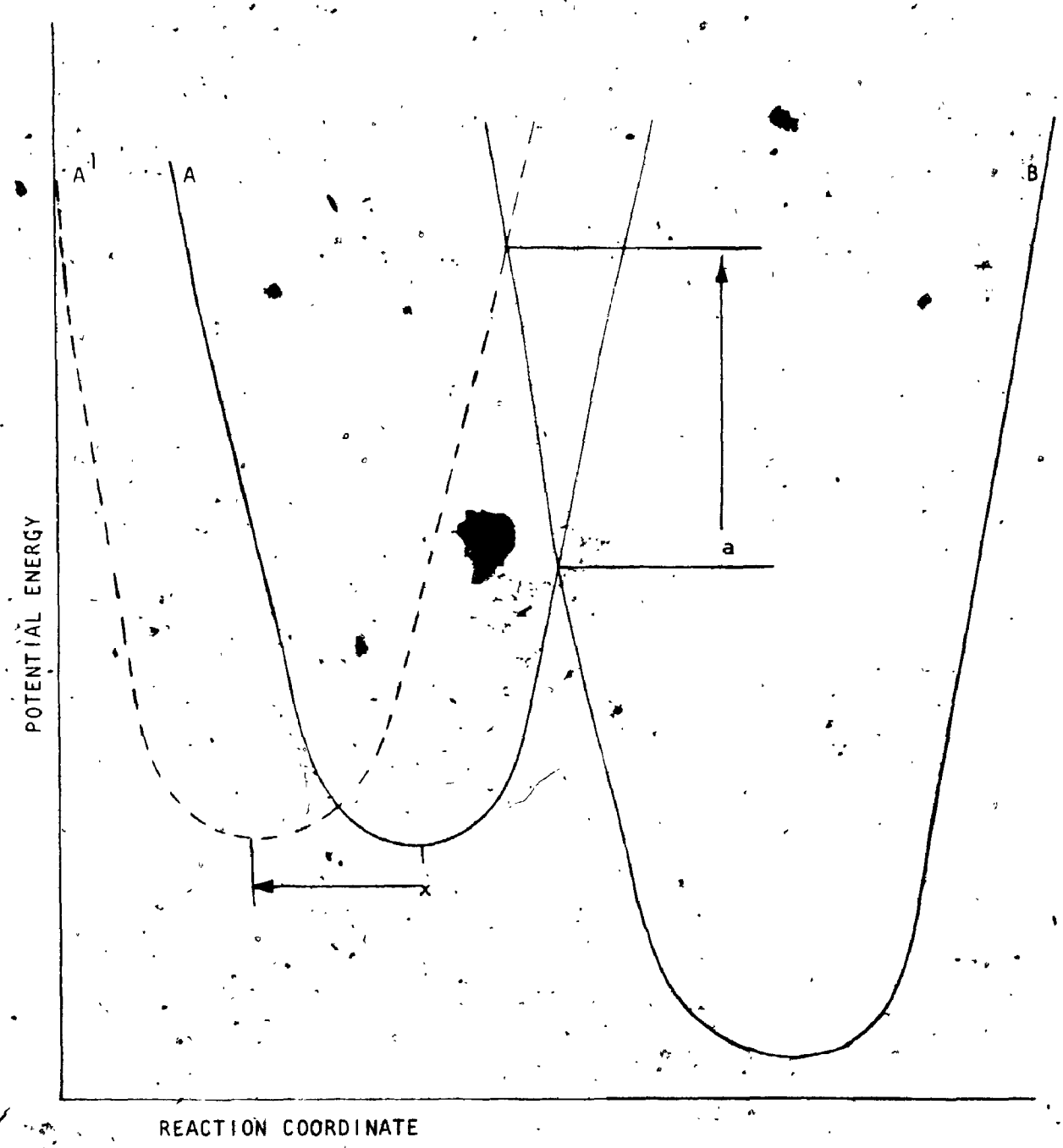

Fig. 15. Schematic energy diagram for electrode reaction. A and B are the curves for reactants and products, respectively. A is shifted by a distance of x along the reaction coordinate to A' and a is the increase in activation energy.

concentration at steady-state to a point such that the rate of two-dimensional nucleation becomes appreciable and, hence, due to the reduction in the distance between growth steps, a decrease in surface diffusion control results.

4.1.10 The Symmetry Factor

Several attempts have been made at giving a theoretical interpretation to the symmetry factor for a one-electron-transfer reaction such as (60). The first attempts [140,143-146] at interpreting β were based on Morse potential energy curves. In these treatments an increase of overpotential is assumed to increase the height of one curve relative to the other without altering the potential/distance relation. This results in the intersection point representing the energy of activation shifting both vertically and horizontally. The fractional increase in the energy of activation with respect to the electrical field energy is the factor β. Using idealized linear potential energy diagrams, it can be shown that β is given by the ratio of the potential/distance relations of the initial and the final states. If therefore, the activation energy barrier is symmetrical, the gradients will be equal and β will be 1/2. The activated state lies midway between the initial and final states. Somestimes [141, 142] this is left in the general form of "along the reaction co-ordinate", at other times [147-151] actual distances perpendicular to the electrode surface are implied. Despic and Bockris [152] have shown that under certain conditions the "Morse curve" and "distance" interpretations are roughly equivalent. Although for infinitesimally small changes of

overpotential this concept of the symmetry factor may be accepted, the non-linear nature of the Morse curves leads one to expect large variations of the symmetry factor with potential, whereas experimentally, β is insensitive to potential and even to the solvent composition [128].

More recently Hush [132], Marcus [29], Levich [153] and others used treatments based on closely similar ideas about the energy of activation for an adiabatic electron-transfer, which is attributed to changes in solvation energy of the ions during discharge.

Hush [132] derived an expression for the heat of activation for simple ions for which the energy of ion-water interaction is electrostatic. For such systems the activation energy for an electron-transfer process is almost entirely dielectric charging and is given by

$$\Delta G^* = \frac{164}{r + 2.76}\,\alpha(1-\alpha) \quad \text{Kcal./mole} \qquad (90).$$

where r is the mean ionic radius in Å and α is the transfer coefficient* of the reaction for an aqueous solution. The key concept of Hush's treatment is the variation of the electronic charge density during the course of the reaction, with the transition state charge for a one-electron-transfer denoted by $(z-q^*)$, z being the charge of the ion in the initial state and q^* the transition state charge. By assuming that the energy of the system is at a minimum in the transition state, it is seen from equation (90) that this condition is satisfied only when $\alpha = 1/2$, the value of q^* then being $(2z-1)/2$. This result follows from the mathematical requirement that $\alpha(1-\alpha)$ be a maximum and shows

* NOTE: α and β are synonymous for one-electron charge-transfer reactions.

that the symmetry factor must be regarded as a mathematical factor independent of the nature of the electrode reaction. Hush has discussed correction factors that would lead to other values of α, in order to accommodate experimental results quoted by a number of authors for one-electron-transfer reactions for which α is significantly different from 1/2, but these apparent deviations are most probably due to a combination of complex formation and diffuse layer effects [128].

Marcus [29] developed the following expression for the energy of activation

$$\Delta G^* = w^* + \frac{m^2\lambda}{2} \qquad (91)$$

where

$$\lambda \cong n^2 e_o^2 \left[\frac{1}{a} - \frac{1}{r}\right]\left[\frac{1}{D_{op}} - \frac{1}{D_s}\right] \qquad (92)$$

with

$$-(2m+1)\frac{\lambda}{2} = -n\,l_o n + w - w^* \qquad (93)$$

In these equations, w and w^* represent the work required to bring the reactants and products to the electrode respectively, a is the ionic radius and r is twice the distance between the electrode and the centre of the ion. D_{op} and D_s are respectively the optical and static dielectric constants. When the activation overpotential is small compared to the activation energy at the reversible potential, then

from equations (91) and (93)

$$\Delta G^* = \frac{w+w^*}{2} + \frac{\lambda}{8} + \frac{(w-w^*)^2}{2\lambda} - \frac{nl_o\eta}{2}\left[1 + \frac{w-w^*}{\lambda}\right] \quad (94)$$

since the term $((nl_o\eta)/\lambda)^2$ can be neglected. The apparent transfer coefficient α' is then

$$\alpha' = \frac{1}{2}\left[1 + 2\frac{(w-w^*)}{\lambda}\right] \quad (95)$$

Since $(w-w^*)$ is a term associated only with the transport of the species to the electrode it is clear that for the electron-transfer step itself α is always 1/2 according to this treatment [128].

The above interpretations all connect the symmetry factor to the energy of activation and predict that the most probable value of β is 1/2 if mass transport effects are eliminated. An expression accounting for transport effects analogous to equation (95) has been developed by Frumkin [126,154-156]. Mass transport effects can be accounted for by considering the potential drop across the diffuse layer θ_2. The relationship between the apparent and true symmetry factor for one-electron-transfer reactions follows from equation (86) and (70).

$$\beta' = \beta\left[1 + \frac{\theta_2}{\eta}\frac{(z-\beta)}{\beta}\right] \quad (96)$$

Equation (96) predicts a gradual dependence of the apparent or measured symmetry factor on the potential.

Recently an attempt has been made by Oldham [157] to make α a parameter dependent on the relative magnitude of the rate constants for electron-transfer and the ultimate rates for mass transfer. In this treatment the point is made that there is nothing in the absolute reaction rate theory that implies that the transfer coefficient should not itself be potential-dependent, but the experimental evidence indicates that usually α is nearly constant over the potential ranges studied. Oldham concluded that α is actually a continuously (but gradually) varying function of the potential such that 1/2 is the value that it happens to acquire in the vicinity of the reversible potential. Moreover, departures from the symmetrical value of 1/2, at $\Delta\phi_r$, are attributed to the inequality of the rate constants of the forward and reverse reactions and should be greatest for electrode reactions in which the reactants and products are in different phases.

4.1.11 The Symmetry Factor and Adsorption of Neutral Molecules

It has been discussed in the previous section that the basic equations for electrode kinetics must be modified to account for mass transport effects. For an irreversible reaction, adsorption of large neutral molecules on the electrode surface will interfere with the transport of the ions from the solution to the reaction site. This effect will then appear to increase the activation energy of the process as described by Biegler and Laitinen [89], but actually the effect can be accounted for by considering the change in the potential (ϕ_2) of the O.H.P. as manifested by a change in symmetry factor (equation (96)). In this manner the activation energy of the transfer

can be considered independent of adsorption. Accordingly, the rate constant, K, as defined by equation (7), may also be considered independent of adsorption (i.e., $K = K_\theta$).

For systems under conditions of forced convection and current density below the limiting value, the concentrations of reactant ions in the reaction plane (O.H.P.) will be relatively unaffected by the presence of adsorbed neutral compounds of moderate size. As discussed previously, the presence of neutral molecules has a negligible effect on the ionic strength in the double layer and accordingly the activity of the reacting ions may be assumed to be independent of adsorption of neutral molecules. Thus, equation (83) simplifies to

$$\ell n\ (1-\theta) = -\ell n\ \frac{\delta_\theta}{\delta} + \left[\frac{b\eta_\theta - b_\theta \eta_c}{b_\theta\, b}\right] - \left[\frac{b_\theta \Delta\phi_r - b\Delta\phi_{r_\theta}}{b_\theta\, b}\right] \qquad (97)$$

Effects of the diffuse layer potential, dielectric constant of the double layer, and mean distance of separation of the O.H.P. and the electrode surface, are considered to be included in the symmetry factor as discussed in the previous section. The Tafel slopes in equation (97) are therefore apparent values in that

$$b = \frac{RT}{\beta' F} \qquad (98)$$

and

$$b_\theta = \frac{RT}{\beta'_\theta F} \qquad (99)$$

4.1.12 Morphological Effects of Adsorption

Several authors have investigated the effects of organic adsorption on the type of deposit at single-crystal electrodes [113,121,158]. A summary of the work done on single-crystal copper substrates is given in Tables 3 and 4. In the present work since the substrate is polycrystalline, polycrystalline deposits resulted. Naturally since the current densities were high and the deposition time long, polycrystalline deposits would also have been obtained if the substrates were single crystals [158].

For the application of equation (97), an understanding of the effect of adsorbate on the roughness factor is necessary. Vermilyea [159,160] has presented a reasonable mechanism for the effect of adsorbed additives on grain refinement. According to the theory, organic molecules adsorbed on the crystal interfere with the motion of lattice steps on the surface. When the concentration of adsorbed molecules is above a critical value depending on the overvoltage, step motion is completely blocked and no further growth of the crystal occurs. On the other hand, molecules adsorbed on a rapidly growing surface are thought to be incorporated into the crystal as lattice steps move around and past them. A prediction of the theory [160] is that there is a critical current density for the continued growth of a metal crystal in a solution containing organic impurities. At the critical current density, there is a balance between the rate of transport of molecules to the surface and the rate of incorporation into the crystal. The equation for the critical current density for a spherical crystal of a given metal and for a given metal ion

TABLE 3

Type of Deposit as a Function of Current Density in the Presence of n-Decylamine [123]

CURRENT DENSITY ($mA\text{-}cm^{-2}$)	APPEARANCE OF CRYSTAL GROWTH IN PRESENCE OF N-DECYLAMINE	ABSENCE OF N-DECYLAMINE
5	layers (truncated pyramids)	layers, larger distances between steps.
10	layers and truncated pyramids	layers and pyramids, larger distances between steps, low tendency to form truncated pyramids.
15	layers, truncated pyramids and blocks	layers, larger distances between steps, lower tendency to form truncated pyramids.
20	polycrystalline	layers, truncated pyramids, blocks

TABLE 4

Types of Deposits from Highly Purified Solutions at Various Current Densities [121]

CURRENT DENSITY ($mA\text{-}cm^{-2}$)	TYPE OF DEPOSIT	OVERPOTENTIAL AT 10 COULOMB/cm^2
5	layer type of deposit	40 - 60
5	pyramids	60 - 80
7.5	layers and pyramid growth	110
10	layers and pyramid growth	130 - 140
15	layers, pyramid growth and truncated pyramids	140 - 160
20	layers, truncated pyramids and blocks	165
30	truncated pyramids and blocks	225
40	polycrystalline, truncated pyramids and blocks	230
50	polycrystalline	240

concentration and temperature is

$$i_c = \text{const} \left(\frac{C_{org}}{r} \right)^{1/3} \qquad (100)$$

where C_{org} is the concentration of organic material in the solution, and r is the radius of the crystal. Equation (100) is valid for crystals with radii less than about 10 μ.

Vermilyea's theory predicts that the electrode potential will rise until deposition begins to occur on most active sites of the electrode when a current is passed through the cell. Crystals would probably start growing at many points on the surface. The overvoltage required to start the deposition would be large because of the initial contamination of the electrode, and the crystals once nucleated would grow very rapidly. The resulting overpotential would decay to a steady-state value. This behaviour is observed in the deposition of copper in the presence of monocarboxylic acids, dicarboxylic acids, and aromatic carboxylic acids as additives under conditions of free convection (Fig. 11a). As the crystals grow, there would be a concentration overpotential in the vicinity of each growing crystal, around which there will be a hemispherical diffusion field, and if the crystal is small (<10 μ diameter) the gradient will be proportional to the concentration difference between the bulk of the solution and the surface of the crystal and to the reciprocal of the crystal radius. As the crystal grows a larger concentration difference is required to maintain the same concentration gradient at the surface. When the concentration of metal-ions at the surface has become essentially zero

it will no longer be possible to maintain the same gradient at the surface, and further growth of the crystal will result in a rapid decrease in current density. Therefore, eventually it will not be possible to maintain the critical current density as predicted by equation (100). Hence, the crystal will become contaminated and stop growing. On the electrode as a whole, crystals will continually nucleate, grow, reach a limiting size, become contaminated and stop growing. A uniform deposit over the electrode will result since the area around newly formed crystals will be deficient in metal ions favouring nucleation at positions far removed from these crystals. Equation (100) therefore predicts that the grain size of the crystal decreases as the additive concentration increases. The deposit should therefore become smoother and so the roughness factor decreases as the additive concentration increases. Evidence of this effect became visually noticeable in the present work at high additive concentrations under conditions of free convection. Under rapidly stirred conditions microscopic comparison of electrode deposits prepared in standard solution free of and contaminated by additive at moderate concentrations showed no evidence of this smoothing effect. This has been attributed to an increase in the critical current density and stabilizing of the concentration gradient by forced convenction. Therefore, under these conditions and for the additives studied in this work, equation (97) may be written as

$$\theta = 1-\exp\left[\frac{bn_\theta - b_\theta n_c - b_\theta \Delta\phi_r + b\Delta\phi_{r\theta}}{b_\theta b}\right] \qquad (101)$$

4.1.13 The Reversible Metal-Solution Potential Difference

The reversible electrode potential for the Cu/0.5 M $CuSO_4$, 1.0 M H_2SO_4 system is + 0.31 volt vs NHE and this does not vary by more than 4 mV in standard solution containing electroinactive neutral organics capable of physical adsorption on the electrode [49,105]. The pzc of the copper cathode was empirically calculated to be - 0.04 volt vs NHE in the absence of specific adsorption [161] and in solution with SO_4^{2-} as the anion in the electrolyte [162].

The rational scale of the potentials is referred to the potential of zero charge as zero [17]. Thus, for the Cu electrode systems studied, the reversible potential on the rational scale will be

$$\Delta\bar{\phi}_r = (\Delta\bar{\phi}_r)_\theta = \Delta\phi_r - \Delta\phi_{q=0} = (\Delta\phi_r)_\theta - \Delta\phi_{q=0} \qquad (102)$$

$$= + 0.31 - (- 0.04)$$

$$= + 0.35 \text{ volts}$$

The metal-solution potential difference is a Galvani potential difference and may be written as

$$\Delta\phi = \Delta\psi - \Delta\chi \qquad (103)$$

where $\Delta\psi$ is the difference between the Volta potentials due to free charges and $\Delta\chi$ is the surface potential difference due to oriented dipoles. At the pzc $\Delta\psi = 0$, but the value of $\Delta\chi$ depends on the solvent and the metal composing the electrode. Trasatti [163] argued that for a Cu electrode at the pzc no preferential orientation of water

dipoles is likely. The reasoning behind this statement is as follows. The shift of the pzc due to adsorption of anions for all metals other than Cu and Au is lower than on mercury and this is generally assumed to be indicative of stronger adsorption of water. For Cu and Au a lower orientation of water should be expected in as much as the experimental values of the pzc shift are higher than on Hg [164,165]. The real situation is probably not so simple, however, since a spontaneous orientation of water with hydrogen toward the metal does not seem to be likely, the hypothesis that the dipole of water would lie parallel to the metal surface (no preferential orientation) may not be unreasonable.

Thus, for copper at the pzc, the surface potential, and therefore the metal-solution potential difference, may be taken as zero.

This conclusion is in conflict with that arrived at by Frumkin [161,166]. Considering experiments [166-168] with a mercury electrode at the potential of zero charge and a 1N NaCl solution, the potential difference was estimated to be 0.33 V. It was concluded on this basis that $\Delta\phi^{m}_{q=0}$ cannot be taken equal to zero. The non-zero value of the metal-solution potential difference for the Hg-NaCl case can, however, be easily explained. The Hg electrode was maintained at a potential value equal to the pzc when no specifically adsorbed anions are present. Chloride ion is known now to be a very strong specific adsorbate. Therefore, the Hg electrode was not at the pzc. of the system, that is $\Delta\chi$ was not equal to zero. Also, in the case of Hg, preferential orientation of adsorbed water dipoles is known to

occur. This effect on Hg is moderate and believed to account for a $\Delta\chi$ of around 80 mV at the pzc [14,163].

It may be concluded on the basis of the above arguments that the rational metal-solution potential difference for a Cu electrode in aqueous SO_4^{2-} electrolyte is approximately equal to the absolute metal-solution potential difference. For the Cu/0.5 M $CuSO_4$, 1.0 M H_2SO_4 electrode, in pure solution and in solution containing electroinactive neutral molecules capable only of physical adsorption, the reversible metal-solution potential difference is

$$\Delta\phi_r = 0.35 \text{ volt}$$

and accordingly equation (101) becomes

$$\theta = 1-\exp\left[\frac{bn_\theta - b_\theta \eta_c - 0.35(b_\theta - b)}{b_\theta b}\right] \qquad (104)$$

For the special case when the Tafel slope is independent of coverage, equation (104) reduces to equation (58), the so-called blocking equation.

DISCUSSIONS - PART 2

4.2 THE ELECTROSORPTION OF THE ALIPHATIC CARBOXYLIC ACIDS

4.2.1 The Experimental Adsorption Isotherms

The application of equation (104) to the experimental data in Appendix II yields fractional surface coverage (θ) of the adsorbed species as a function of the bulk concentration (C) of the additive. Figs. 16 - 29 show this relationship. From the derivation of equation (104), it must be remembered that as the calculated coverage increases, the applicability of (104) comes increasingly into doubt. Therefore, calculated values of θ above 0.6 should not be accepted unquestioningly. Due to the low solubilities of the longer chain monocarboxylic acids, only low coverage data were obtainable for these compounds. The isotherms for the aliphatic carboxylic acids are all of the "L" or Langmuir type.

4.2.2 Free Energies of Adsorption

It is well known that the fractional surface coverage calculated from blocking theory for the adsorption of charged species is an apparent value. There may be electric interaction between electroactive ions and the adsorbed species, thereby inhibiting reaction on more of the surface than is physically blocked by the additive. Although this effect is minimal when the adsorbate carries no net charge, the θ calculated from blocking theory for these species as well, may be an apparent value. If a molecule adsorbs on the surface

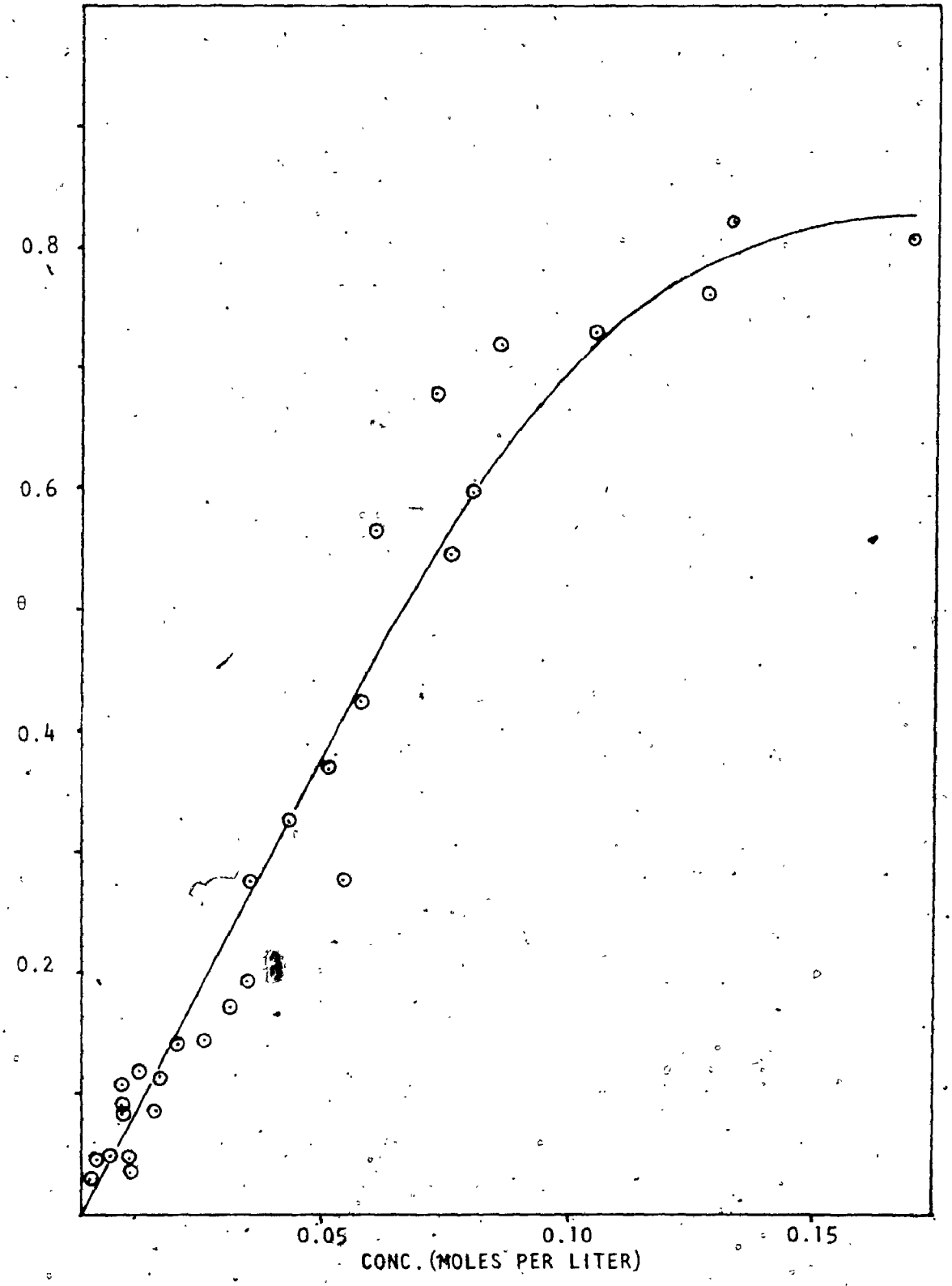

Fig. 16 Surface coverage-concentration relationship for propanoic acid.

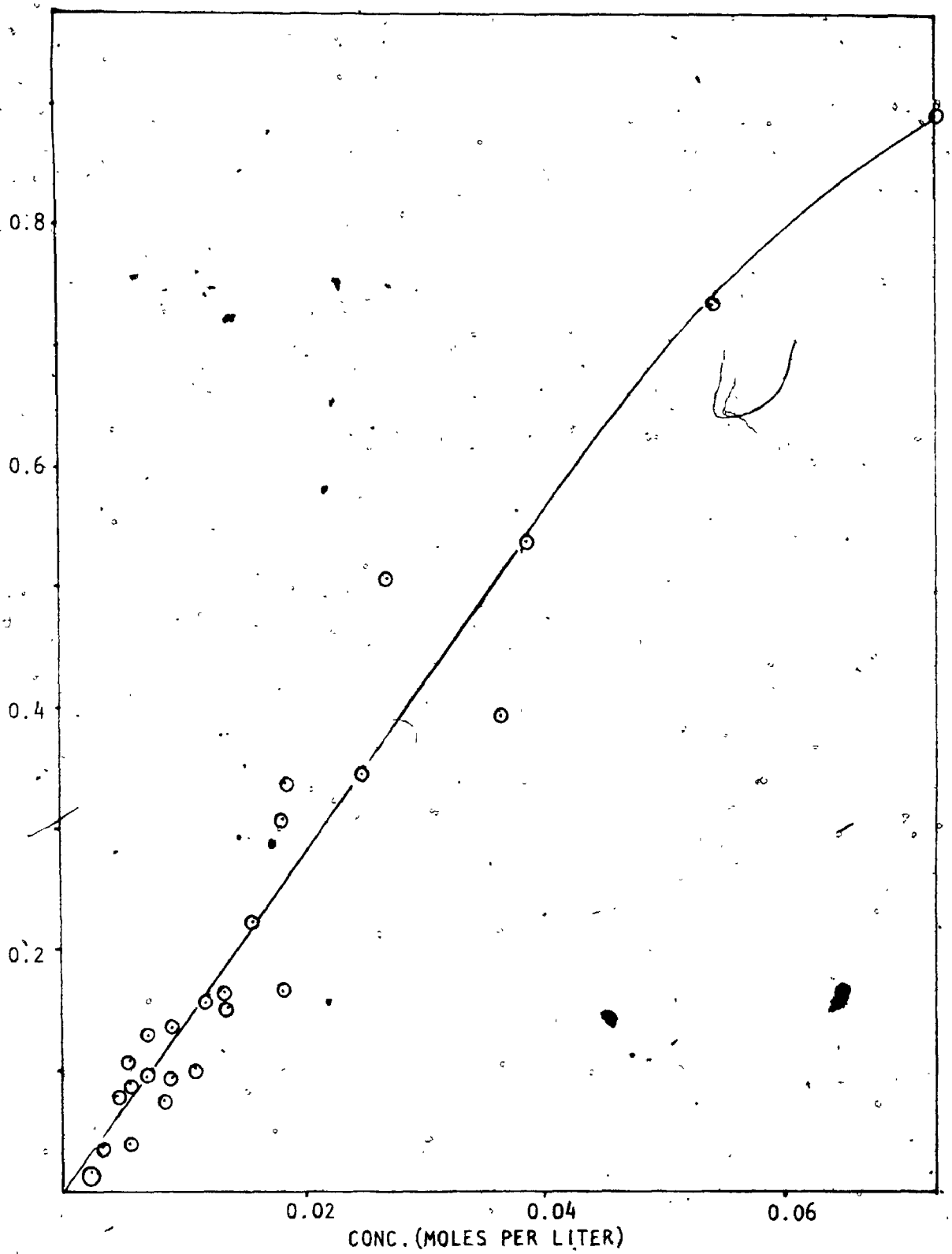

Fig. 17 Surface coverage-concentration relationship for butanoic acid.

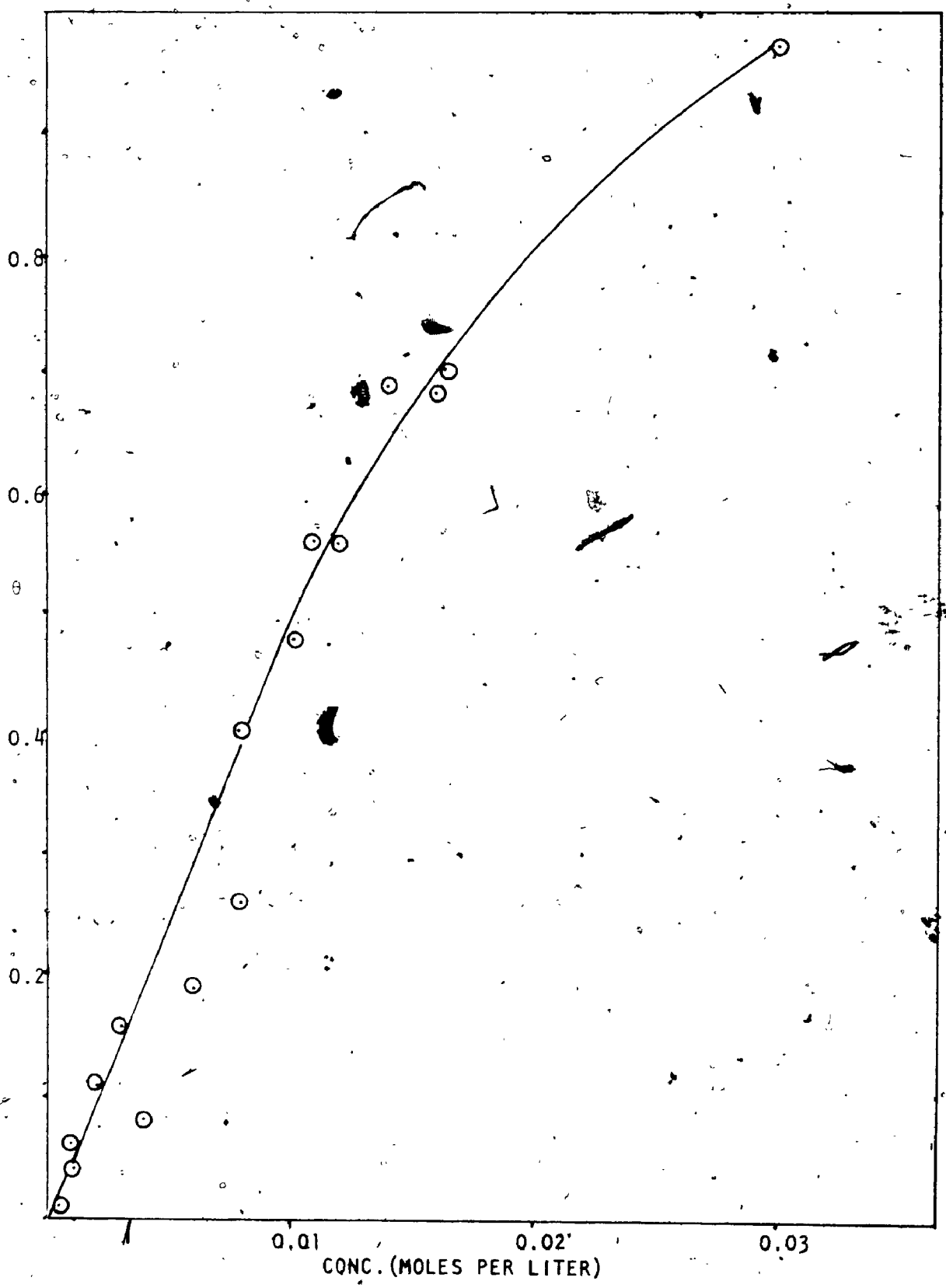

Fig. 18 Surface coverage-concentration relationship for pentanoic acid.

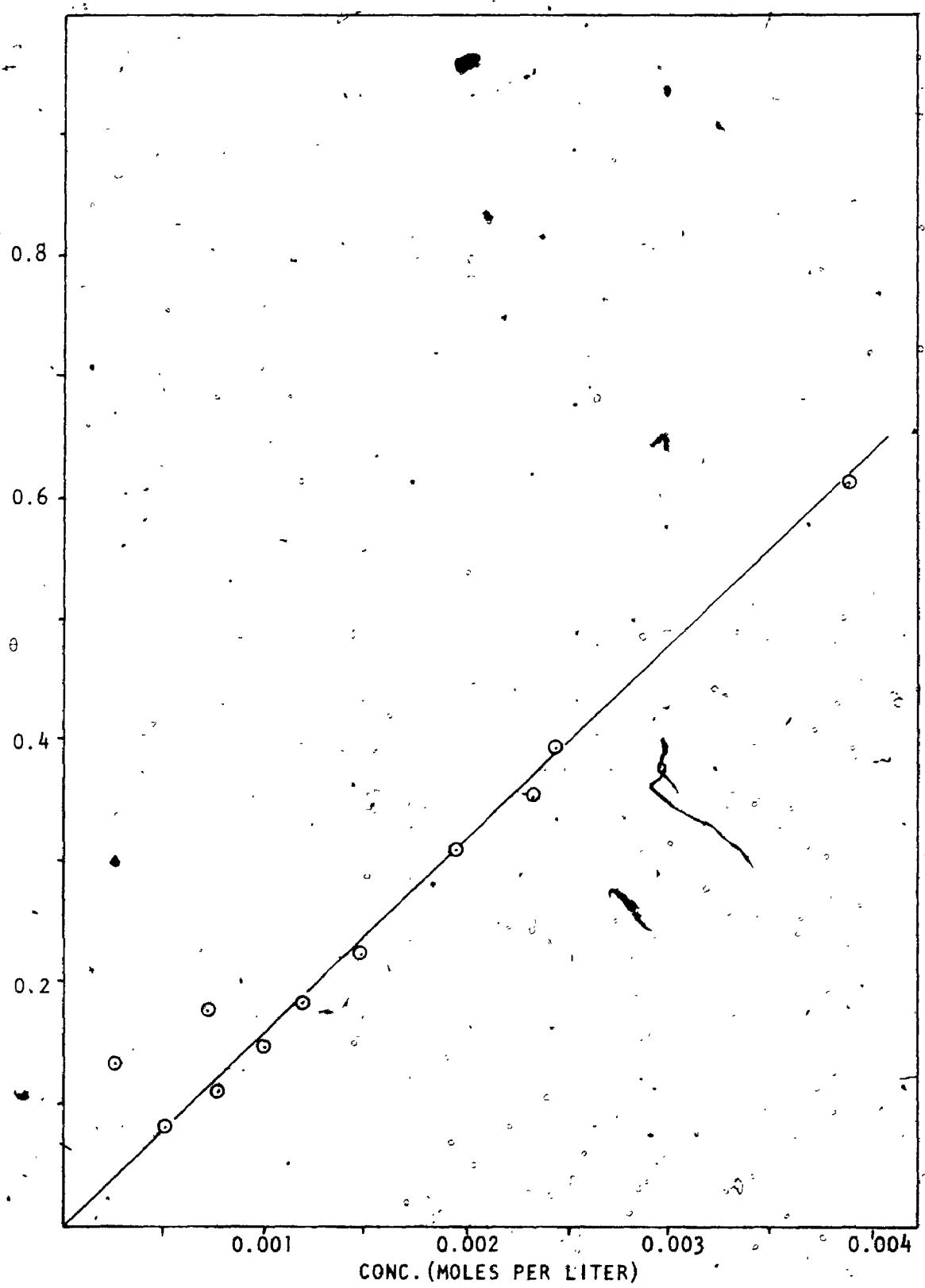

Fig. 19 Surface coverage-concentration relationship for hexanoic acid.

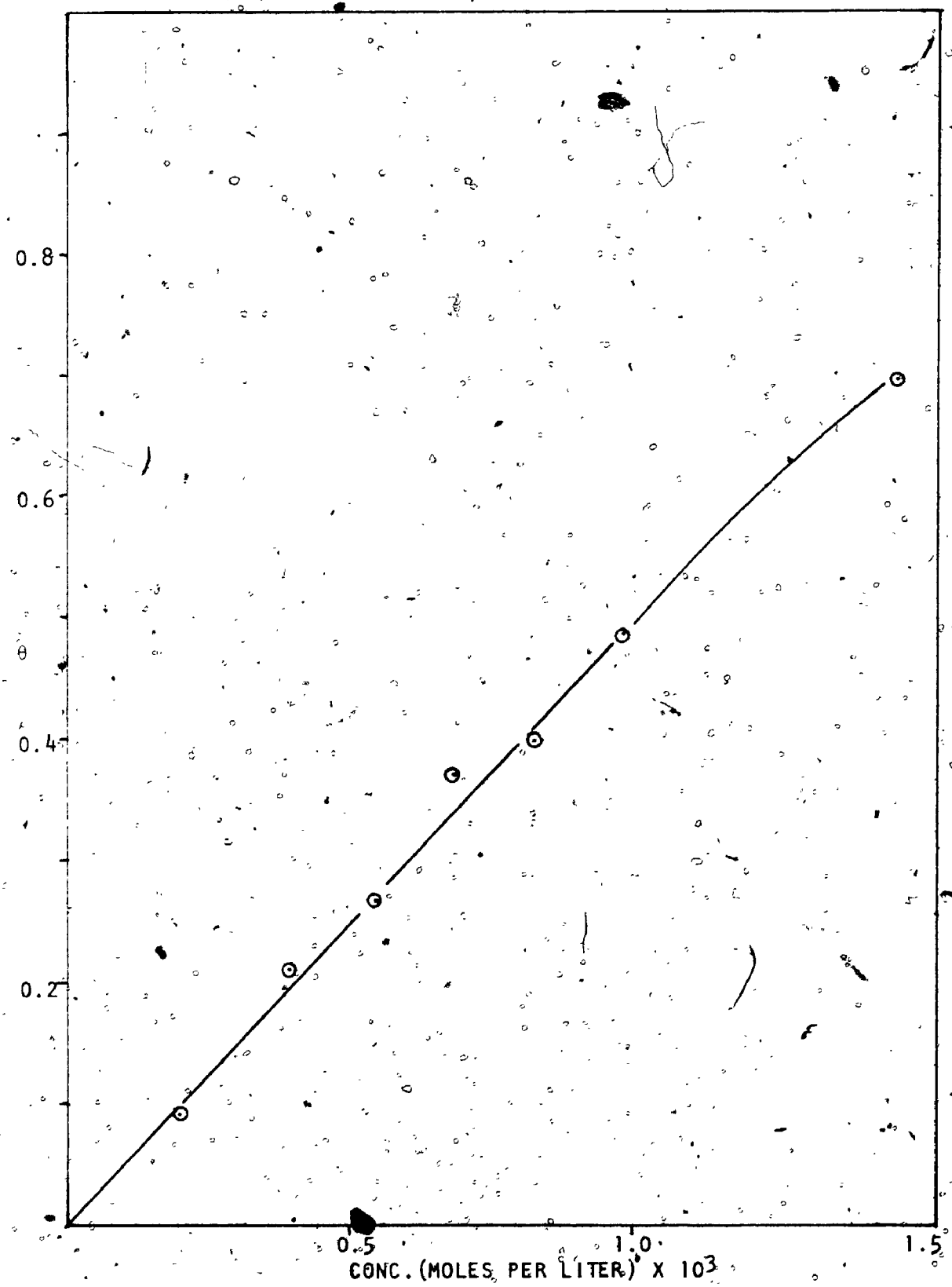

Fig. 20 Surface coverage-concentration relationship for heptanoic acid.

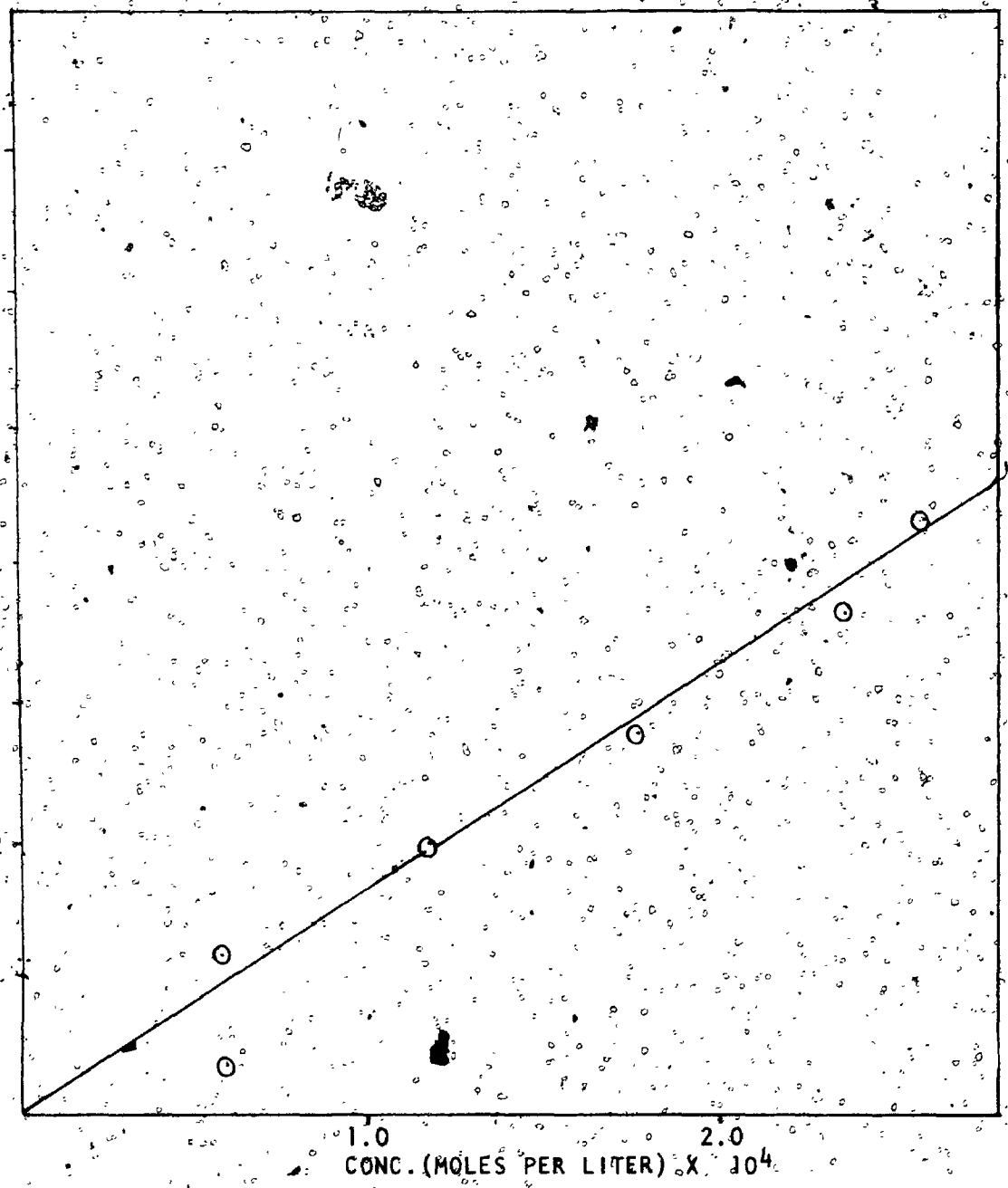

Fig. 21 Surface coverage-concentration relationship for octanoic acid.

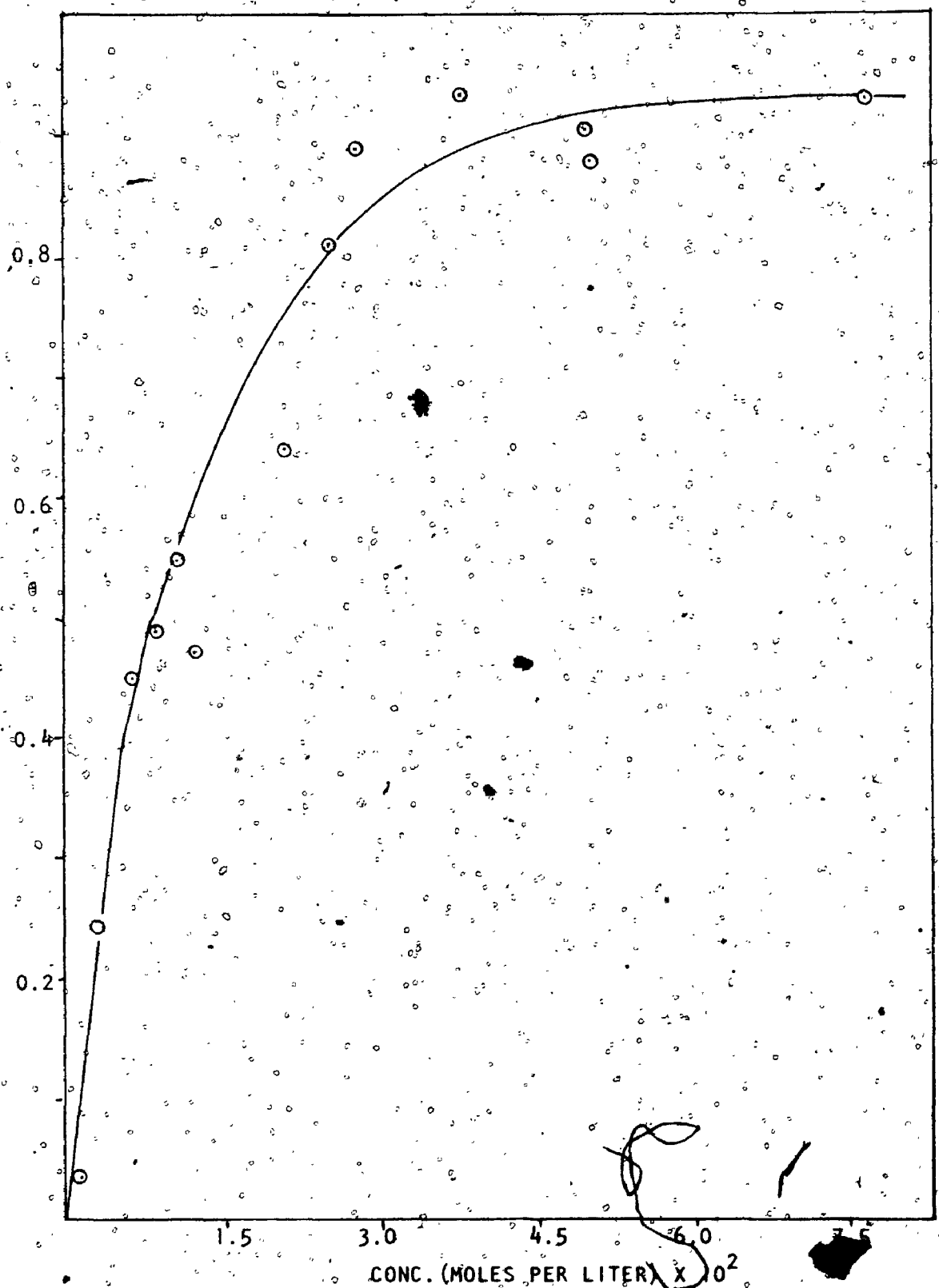

Fig. 22 Surface coverage-concentration relationship for propanedioic acid.

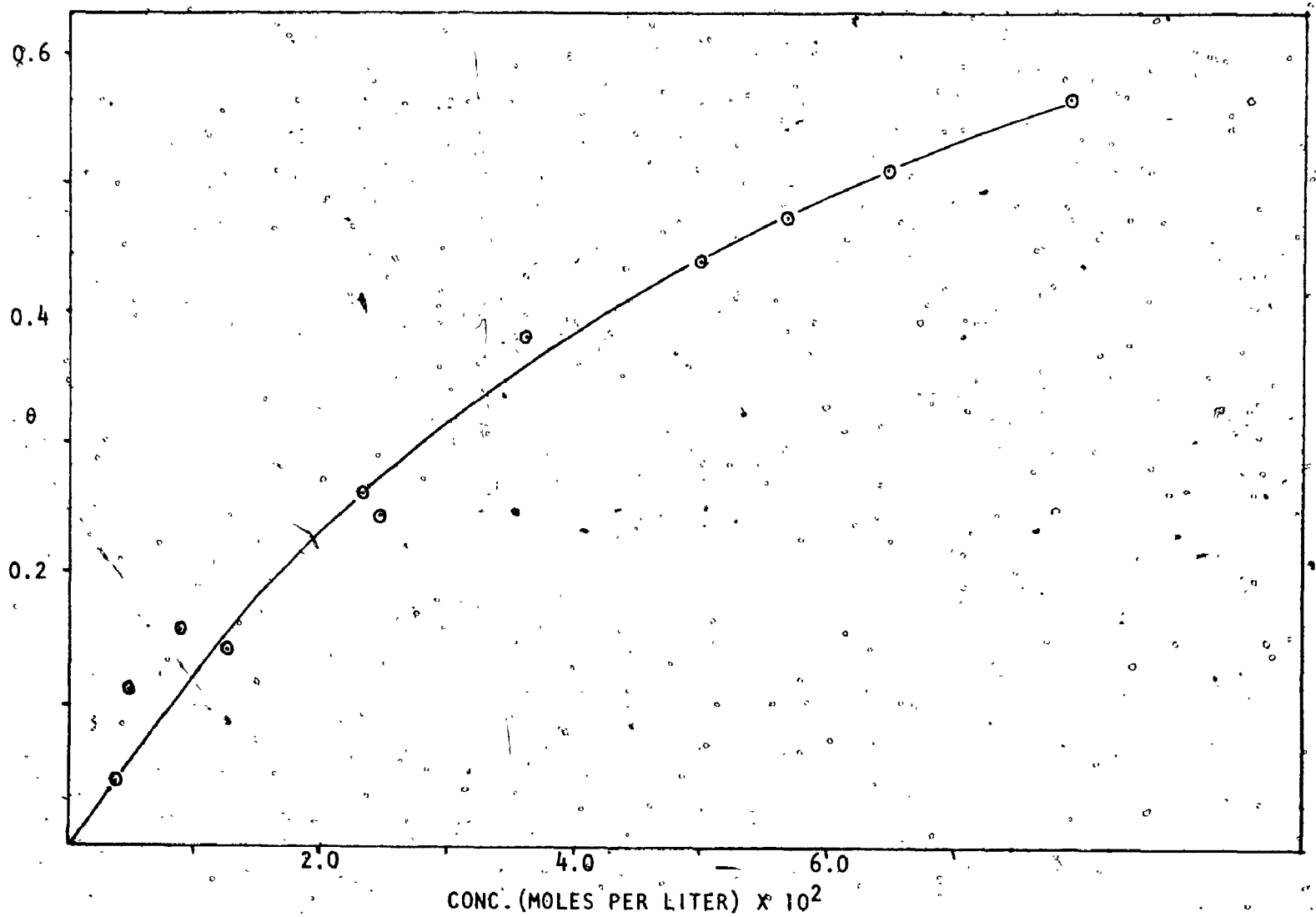

Fig. 23 Surface coverage-concentration relationship for butanedioic acid.

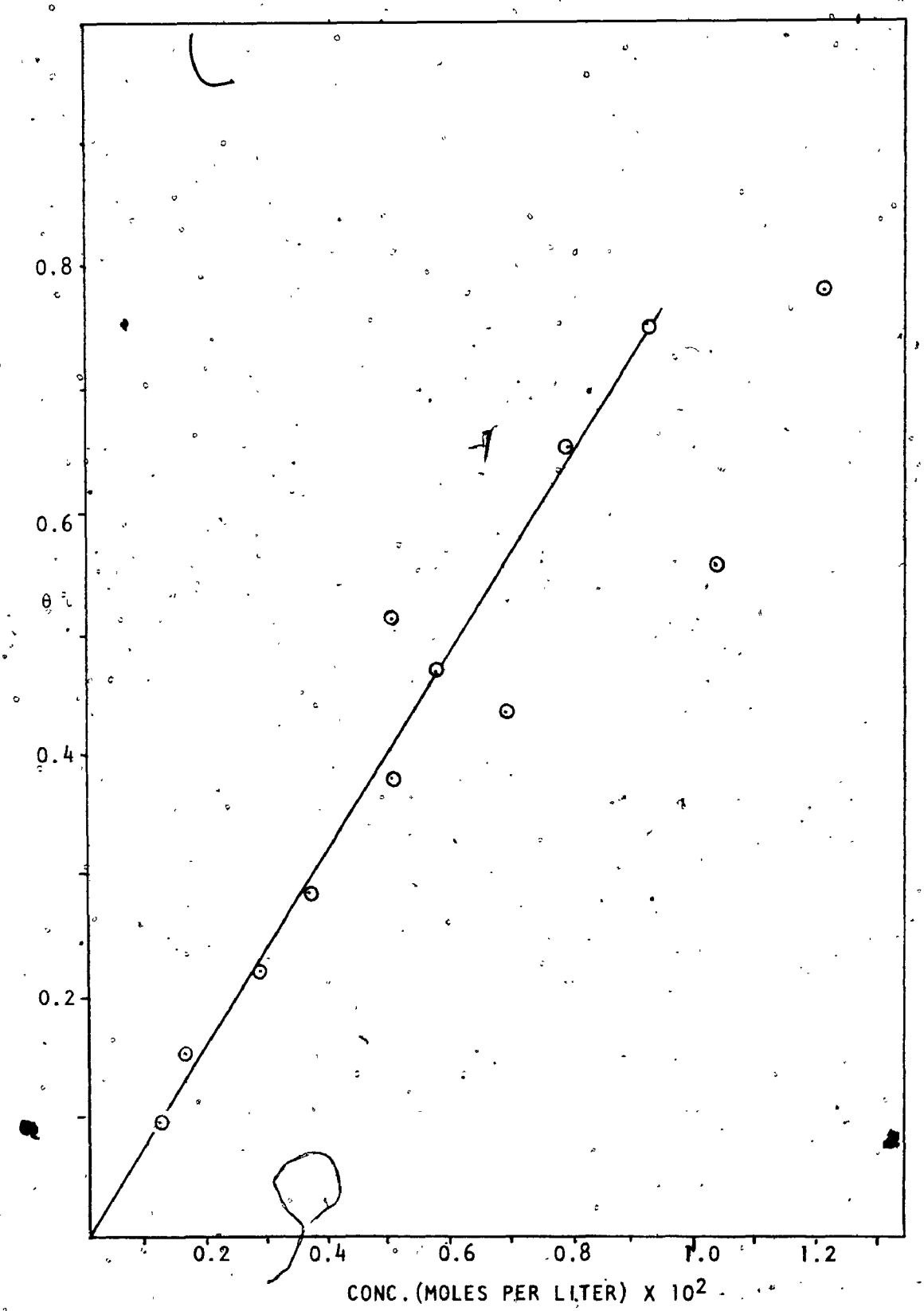

Fig. 24 Surface coverage-concentration relationship for pentanedioic acid.

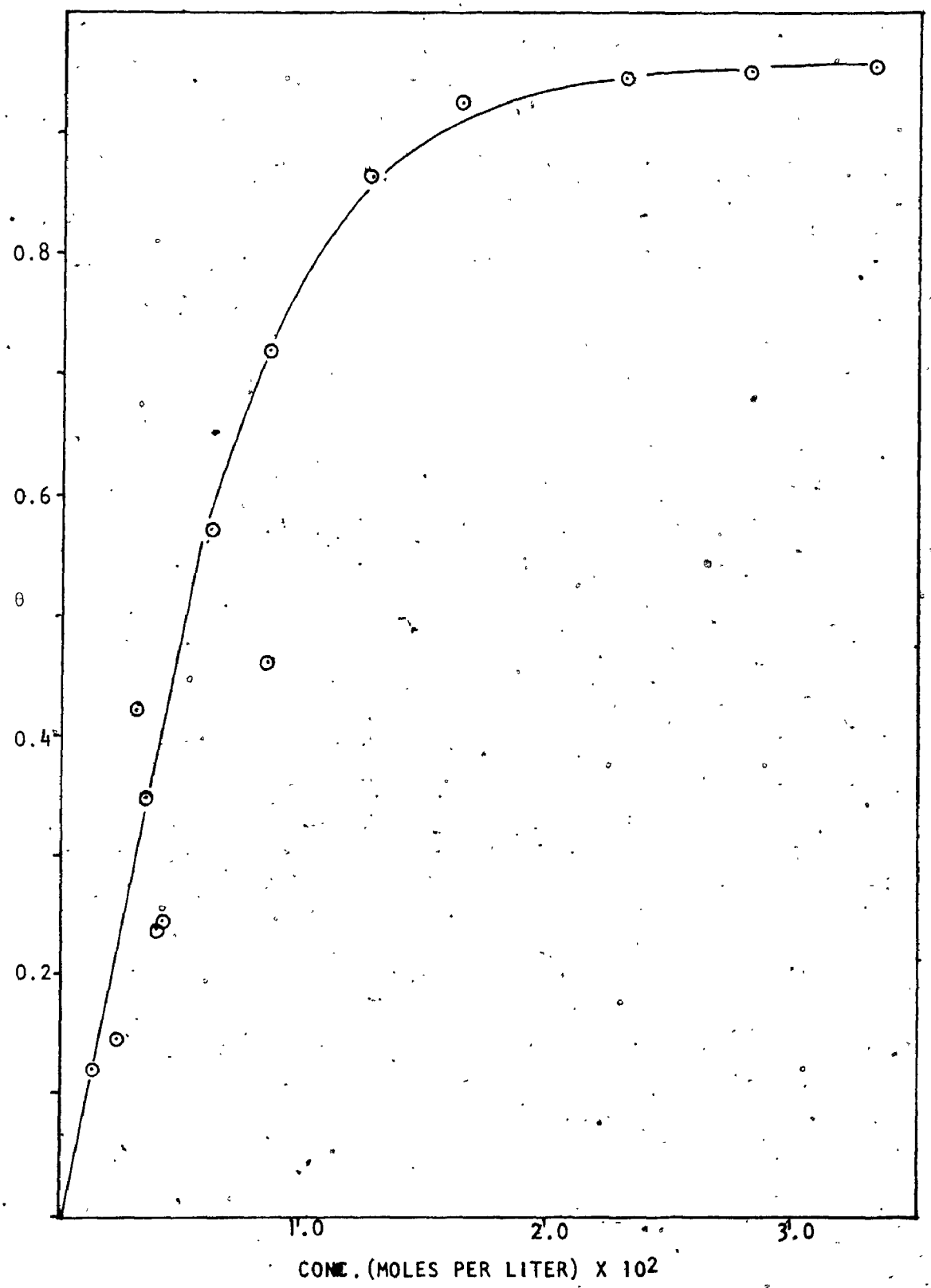

Fig. 25 Surface coverage-concentration relationship for hexanedioic acid.

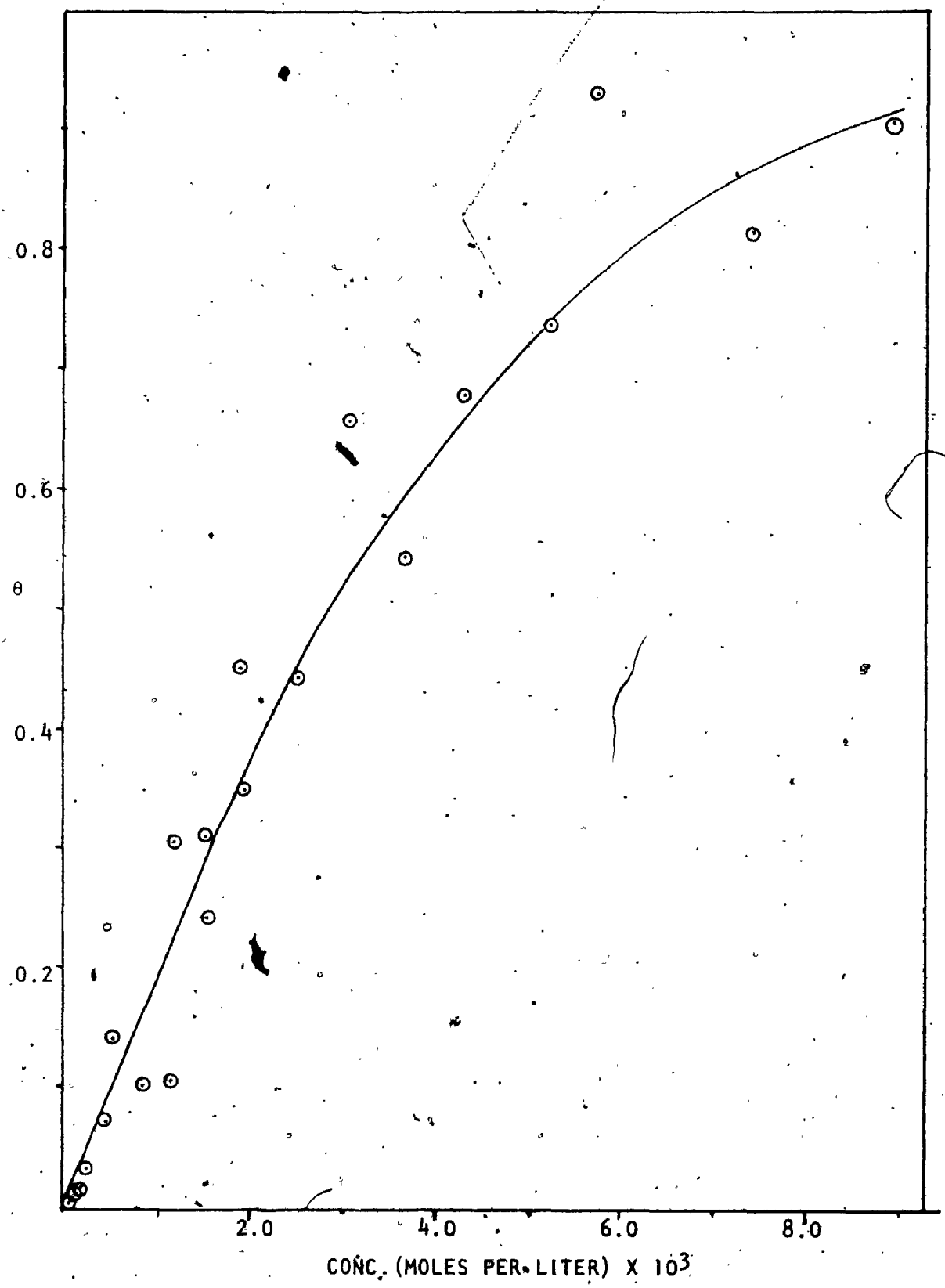

Fig. 26 Surface coverage-concentration relationship for heptanedioic acid.

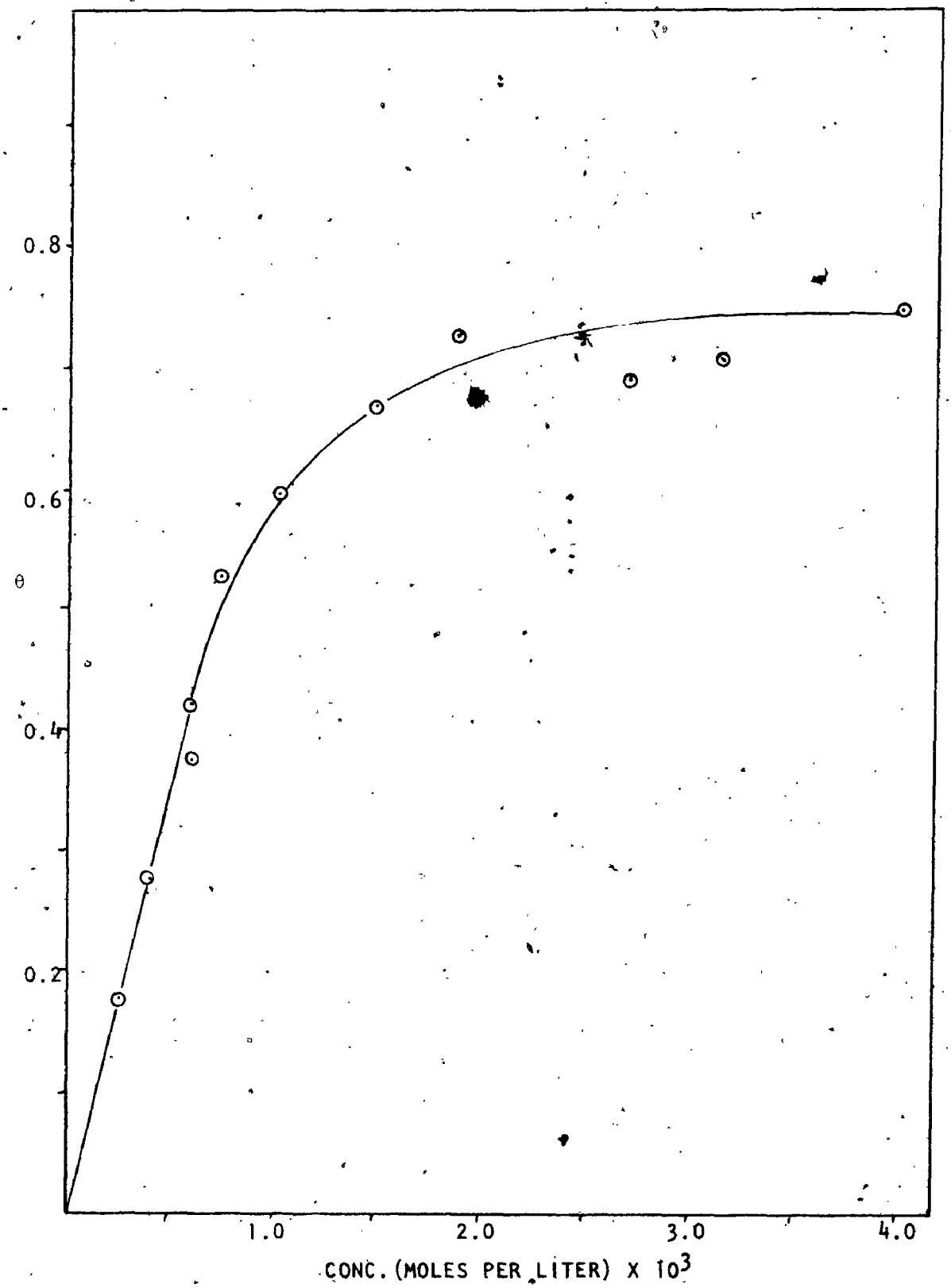

Fig. 27 Surface coverage-concentration relationship for octanedioic acid.

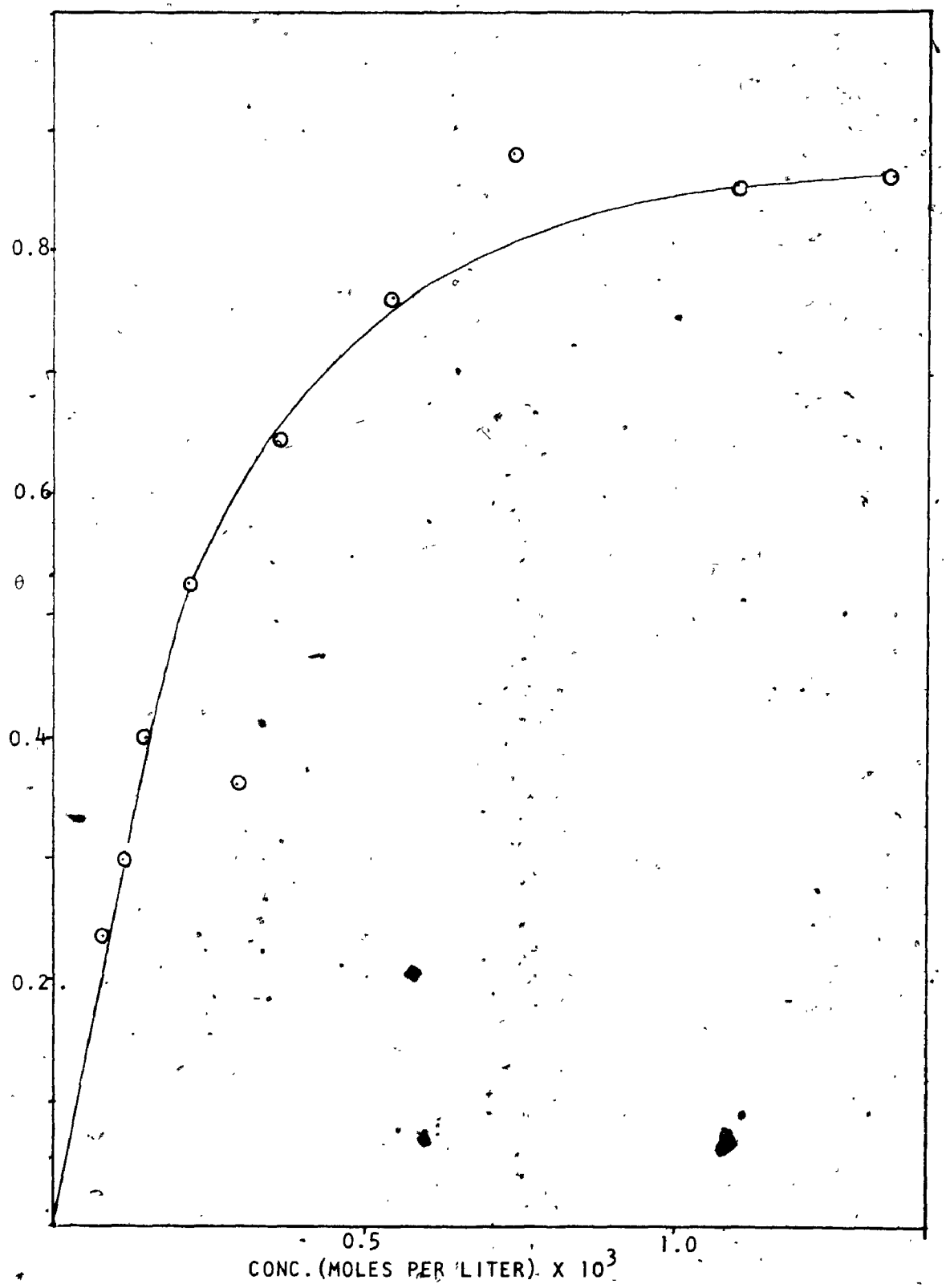

Fig. 28 Surface coverage-concentration relationship for nonanedioic acid.

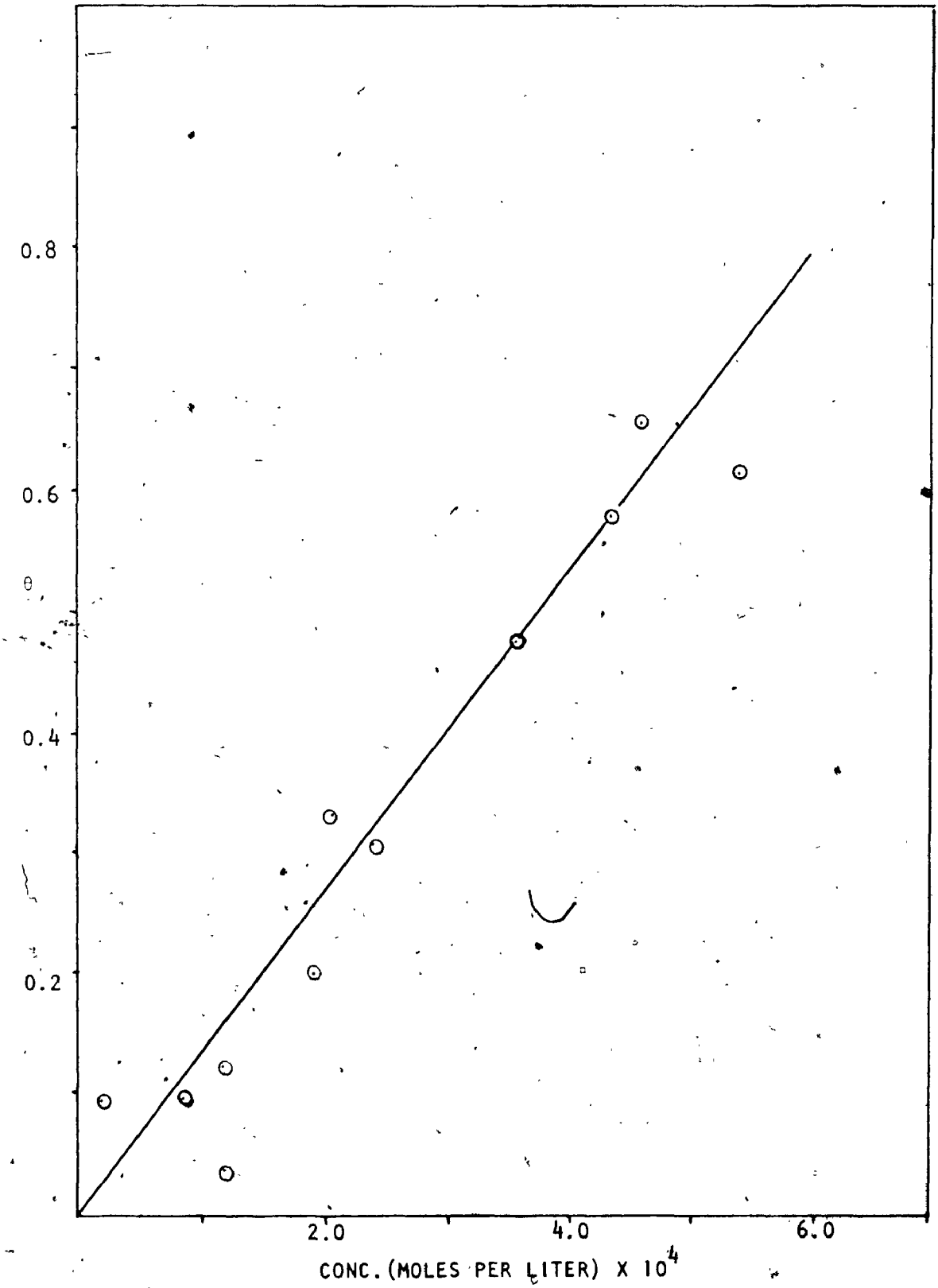

Fig. 29 Surface coverage-concentration relationship for decanedioic acid.

in such a manner that only part of the molecule displaces solvent and the remainder is in an orientation such that it does not displace the primary water layer but lies on top of it, effectively blocking that part of the surface beneath it, then the water displacement number n in the various adsorption isotherms does not conform to the predicted value from the blocking effect. Therefore, it is necessary when using the blocking theory, to differentiate between these n values.

Consider the Bockris-Swinkels Isotherm. Let n be as before, the number of water molecules displaced by each organic molecule on adsorption. Let n^* be the ratio of the projected area of the organic molecule in the orientation of adsorption to the projected area of a water molecule on the surface. Then for the substitution process (24), the standard free energy of adsorption is given by

$$\Delta G^\circ_{ads} = - RT \ln \left[\frac{(Y_{O,ads})(Y_{W,soln})^n}{(Y_{W,ads})^n (Y_{O,soln})} \right] \qquad (28)$$

where $Y_{O,ads}$ and $Y^\circ_{W,ads}$ are the mole fractions of O and W in the interphase and $Y_{O,soln}$ and $Y_{W,soln}$ the mole fractions in solution. As before in dilute solution;

$$Y_{W,soln} = 1 \qquad (30a)$$

$$Y_{O,soln} = C_{org}/55.5 \qquad (30b)$$

and on the surface

$$Y_{O,ads} = \frac{\Gamma_{org}}{\Gamma_{org} + \Gamma_W} \tag{43}$$

Taking θ from blocking theory, then

$$\Gamma_{org} = \theta \Gamma_{max,org} \tag{32}$$

but

$$\Gamma_W = \left[1 - \theta \frac{n}{n^*}\right] \Gamma_{max,W} \tag{105}$$

and

$$\Gamma_{max,W} = n^* \Gamma_{max,org} \tag{106}$$

Substituting (106), (105), and (32) into (43) and rearranging gives

$$Y_{O,ads} = \frac{\theta}{n^* + \theta(1-n)} \tag{107}$$

Similarly for water

$$Y_{W,ads} = \frac{n^* - \theta n}{n^* + \theta(1-n)} \tag{108}$$

Substituting (108), (107), (30b) and (30a) into (28) and rearranging yields

$$\frac{\theta\left[n^*+\theta(1-n)\right]^{n-1}}{(n^*-\theta n)^n} = \frac{C_{org}}{55.5}\exp\left(\frac{-\Delta G_a^\circ}{RT}\right) \qquad (109)$$

The standard free energy of adsorption is markedly dependent on θ for most organic adsorbates. This dependence is generally attributed to lateral interaction in the adsorbed phase [36]. For the purpose of comparison of the adsorbability of different adsorbates, it is therefore necessary to obtain values for ΔG_a° (θ=0).

As C_{org} approaches zero, equation (109) becomes

$$\left(\frac{\theta}{C}\right)_{C\to 0} = \frac{n^*}{55.5}\exp\left(\frac{-\Delta G_a^\circ(0)}{RT}\right) \qquad (110)$$

showing that the initial slope of the θ vs C curve is fixed for any organic adsorbate and for any fixed value of n*.

Values of $\Delta G_a^\circ(0)$ for the aliphatic acids are listed in Tables 5a and b. Values of n* and n for likely orientations of adsorption were determined with space filling molecular models.

4.2.3 Determination of Adsorbate Orientation on the Surface

According to the work of Loutfy [49] and Seto [105], most organic additives adsorb on copper under deposition conditions by a purely physical interaction of the functional group(s) with the surface. Since the experimental conditions employed in this work dictated an electrode potential 250-150 mV anodic to the potential of zero charge, it is reasonable to assume that the carboxyl functions would adsorb

TABLE 5a

Correlation of Solubility with Adsorbability for Various Orientation Effects for the Monocarboxylic Acids

ACID ADDITIVE	n^*	n	$\left[\frac{\theta}{C}\right]_{C\to 0}$	$-\Delta G^\circ_a(0)$ Kcal./mole	SOLUBILITY (m/l)	
a) Adsorbate in Perpendicular Orientation						
Propanoic	2.75	1.93	7.86	3.00	6.46	[49]
Butanoic	2.75	1.93	1.39 x 10	3.34	1.51	[49]
Pentanoic	2.75	1.93	4.95 x 10	4.09	3.62×10^{-1}	[169]
Hexanoic	2.75	1.93	1.60×10^{2}	4.79	8.35×10^{-2}	[169]
Heptanoic	2.75	1.93	4.93×10^{2}	5.39	1.84×10^{-2}	[169]
Octanoic	2.75	1.93	1.60×10^{3}	6.15	4.85×10^{-3}	[169]
b) Adsorbate in Flat Orientation						
Propanoic	2.75	2.75	7.86	3.00	6.46	
Butanoic	3.58	3.58	1.39 x 10	3.18	1.51	
Pentanoic	4.00	4.00	4.95 x 10	3.87	3.62×10^{-1}	
Hexanoic	4.83	4.83	1.60×10^{2}	4.45	8.35×10^{-2}	

TABLE 5a - continued

ACID ADDITIVE	n*	n	$\left[\frac{\theta}{C}\right]_{C\to 0}$	$-\Delta G_a^\circ(0)$ Kcal./mole	SOLUBILITY (m/l)
b) Adsorbate in Flat Orientation - continued					
Heptanoic	5.66	5.66	4.93×10^2	4.96	1.84×10^{-2}
Octanoic	6.49	6.49	1.60×10^3	5.64	4.85×10^{-3}
c) Adsorbate in Parallel Orientation					
Propanoic	2.75	1.93	7.86	3.00	6.46
Butanoic	3.58	1.93	1.39×10	3.18	1.51
Pentanoic	4.41	1.93	4.95×10	3.81	3.62×10^{-1}
Hexanoic	5.24	1.93	1.60×10^2	4.40	8.35×10^{-2}
Heptanoic	6.07	1.93	4.93×10^2	4.92	1.84×10^{-2}
Octanoic	6.90	1.93	1.60×10^3	5.60	4.85×10^{-3}

TABLE 5b

Correlation of Solubility with Adsorption for Various Orientation Effects for the Dicarboxylic Acids

ACID ADDITIVE	n*	n	$\left[\frac{\theta}{C}\right]_{C\to 0}$	$-\Delta G_a^\circ(0)$ (Kcal./mole)	SOLUBILITY (m/l)	
a) Adsorbate in Perpendicular Orientation (one functional group on surface)						
Propanedioic	3.84	1.93	7.70×10	4.15	7.07	[170]
Butanedioic	2.75	1.93	1.52×10	3.39	4.91×10^{-1}	[170]
Pentanedioic	2.75	1.93	7.70×10	4.35	4.84	[170]
Hexanedioic	2.75	1.93	9.88×10	4.50	1.64×10^{-1}	[170]
Heptanedioic	2.75	1.93	1.83×10^{2}	4.86	3.12×10^{-1}	[170]
Octanedioic	2.75	1.93	6.95×10^{2}	5.65	9.10×10^{-3}	[170]
Nonanedioic	2.75	1.93	2.50×10^{3}	6.41	1.28×10^{-2}	[170]
Decanedioic	2.75	1.93	1.30×10^{3}	6.02	4.95×10^{-3}	[170]
b) Adsorbate in Flat Orientation						
Propanedioic	4.46	4.46	7.70×10	4.06	7.07	
**Butanedioic	3.84	3.84	1.52×10	3.19	4.91×10^{-1}	

TABLE 5b - continued

ACID ADDITIVE	n*	n	$\left[\frac{\theta}{C}\right]_{C\to 0}$	$-\Delta G_a^\circ(0)$ (Kcal./mole)	SOLUBILITY (m/l)
b) Adsorbate in Flat Orientation - continued					
Pentanedioic	6.12	6.12	7.70×10	3.87	4.84
Hexanedioic	6.95	6.95	9.88×10	3.95	1.64×10^{-1}
Heptanedioic	7.78	7.78	1.83×10^{2}	4.25	3.12×10^{-1}
Octanedioic	8.61	8.61	6.95×10^{2}	4.98	9.19×10^{-3}
Nonanedioic	9.44	9.44	2.50×10^{3}	5.68	1.28×10^{-2}
Decanedioic	10.3	10.3	1.30×10^{3}	5.24	4.95×10^{-3}
c) Adsorbate in Parallel Orientation (both functional groups on surface)					
Propanedioic	4.46	4.46	7.70×10	4.06	7.07
*Butanedioic	4.67	1.93	1.52×10	3.08	4.91×10^{-1}
**Butanedioic	3.84	3.84	1.52×10	3.19	
Pentanedioic	3.84	3.84	7.70×10	4.15	4.84
Hexanedioic	5.50	3.84	9.88×10	4.09	1.64×10^{-1}
Heptanedioic	6.33	3.84	1.83×10^{2}	4.37	3.12×10^{-1}
Octanedioic	7.16	3.84	6.95×10^{2}	5.08	9.19×10^{-3}

TABLE 5b - continued

ACID ADDITIVE	n*	n	$\left[\frac{\theta}{C}\right]_{C \to 0}$	$-\Delta G^{\circ}_{a}(0)$ (Kcal./mole)	SOLUBILITY (m/l)
c) Adsorbate in Parallel Orientation (both functional groups on surface) - continued					
Nonanedioic	7.99	3.84	2.50×10^{2}	5.78	1.28×10^{-2}
Decanedioic	8.82	3.84	1.30×10^{2}	5.33	4.95×10^{-3}

* Only one functional group displacing water.

** Both functional groups displacing, molecule under stearic strain.

with the oxygens directed toward the surface. This geometric orientation corresponds to a water displacement number (n) of 1.93 for the carboxyl function alone. Most authors have considered the organic to adsorb perpendicular to the surface, one end of the molecule adsorbed on the surface and the hydrocarbon chain extending into the solution. This arrangement would give a blocking projection number (n*) of 2.75 for the monocarboxylic acids.

The effect of the hydrophobic nature of the hydrocarbon chain is ignored when accepting the perpendicular mode of adsorption. There would be a tendency of rejection from solution of the hydrocarbon chain, that is, to lie flat on the surface displacing water in the primary layer. This orientation is called the flat orientation. Bockris, Devanathan, and Müller [14] and Blomgren, Bockris, and Jesch [110], considering the energetics of this orientation for the adsorption of butyl, phenyl, and naphthyl compounds, concluded that, due to the energy required for displacement of the primary water, this orientation is much less favoured than the perpendicular mode.

This raises the possibility of a third mode of adsorption, the parallel mode. In this orientation only the functional groups displace primary water, but the hydrocarbon chain lies parallel to the electrode surface on top of the primary water layer, thus effectively blocking that part of the surface to deposition. The fractional surface coverage calculated from blocking theory would then be larger, depending on the size of the hydrocarbon chain, than the true surface coverage. Gale [172] in a study of the adsorption of amino acids on copper during deposition, employing both radiotracer methods and

blocking theory, reported such a discrepancy. There is further evidence to support the feasibility of this mode of adsorption. Langmuir has shown [173] that for the theoretical proof of Traube's rule one must assume that at degrees of coverage which are not too high, the hydrocarbon chains of the adsorbed molecules lie almost flat on the electrode surface. Under these conditions the polar groups of the adsorbed molecules are within the compact layer and form some fixed angle with the electrode surface which changes little with increasing coverage [174]. Traube's rule is obeyed in the adsorption of normal fatty acids, alchohols, and amines onto mercury [175,176] and for normal fatty acids on copper [103,104].

4.2.4 Components of the Standard Free Energies of Adsorption

Bockris and Swinkels [36] considered adsorption from solution to be influenced by several interactions between the metal, the organic compound and the water both on the surface and in the bulk. Since the adsorption is a replacement process, the thermodynamic cycles of water and the adsorbate must be considered. Considering Fig. 30 for water

$$\Delta G_s(W) = \Delta G_p(W) + \Delta G_v(W) \qquad (111)$$

where $\Delta G_s(W)$ = free energy of adsorption of water from solution; $\Delta G_v(W)$ = free energy of adsorption of water from vapor phase at 1 atm.; $\Delta G_p(W) = RT \ln p_o(W)$ where $p_o(W)$ = vapor pressure of water at temperature T.

FIG. 30

THERMODYNAMIC CYCLE FOR WATER

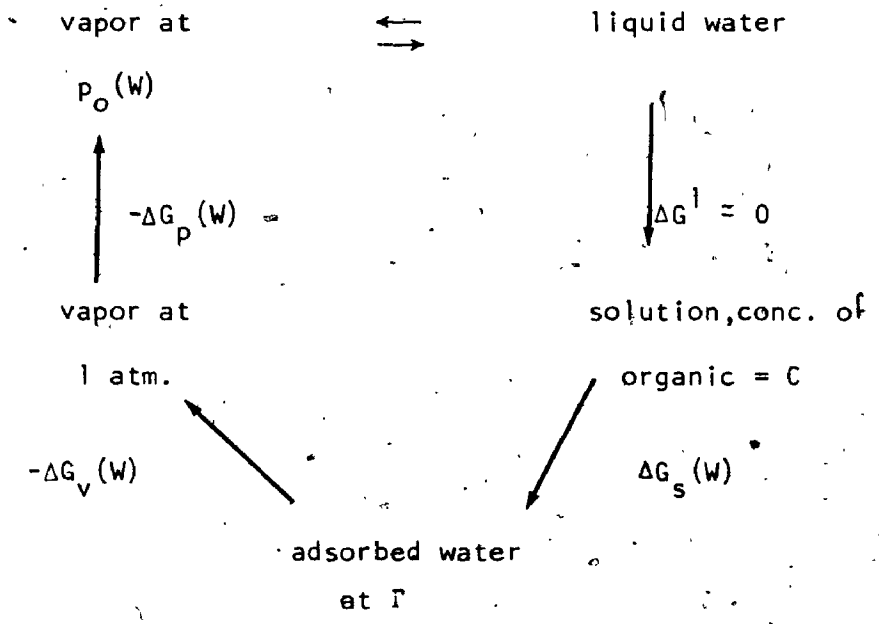

THERMODYNAMIC CYCLE FOR THE ORGANIC MATERIAL

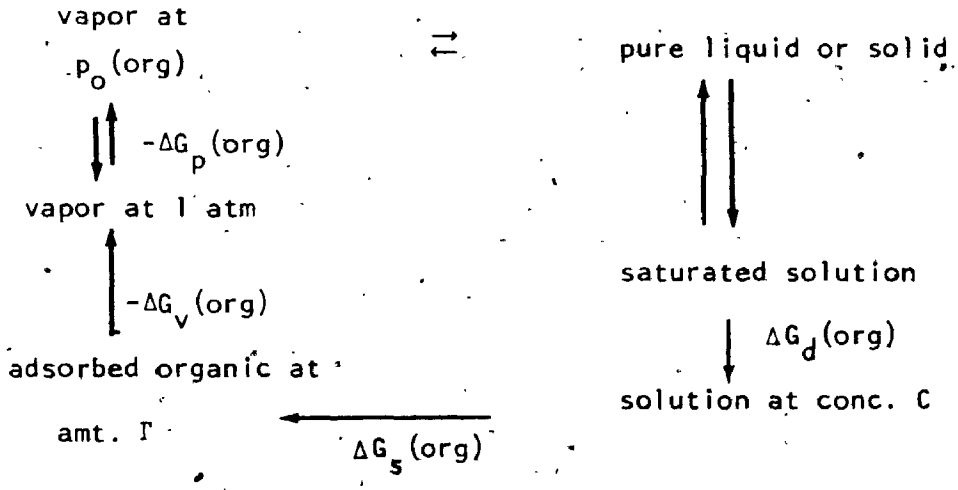

For the organic material at temperature T

$$\Delta G_s(org) = -\Delta G_d(org) + \Delta G_p(org) + \Delta G_v(org) \qquad (112)$$

where $\Delta G_s(org)$ = free energy of adsorption of the organic compound from solution at concentration C and coverage Γ; ΔG_d = free energy of dilution = RT ℓn (C/C_s); C_s = saturation concentration for organic; $\Delta G_p(org) = -RT$ ℓn $p_o(org)$; $p_o(org)$ = vapor pressure of the pure organic material at temperature T; $\Delta G_v(org)$ = free energy of adsorption of the organic compound from the vapor phase at 1 atm.

The free energy of adsorption of the replacement process is

$$\Delta G_a^\circ = \Delta G_s^\circ(org) - n\,\Delta G_s^\circ(W) \qquad (113)$$

Defining the standard state as unit mole fraction of organic material or water at the interface and in solution one has

$$\Delta G_a^\circ = -\Delta G_d^\circ(org) + \Delta G_p^\circ(org) - n\Delta G_p^\circ(W) + \Delta G_v^\circ(org) - n\Delta G_v^\circ(W) \qquad (114)$$

$$= RT\ell n \frac{C_s}{55.5} - RT\ell n \frac{P_o(org)}{P_o^n(W)} + \Delta G_v^\circ(org) - n\Delta G_v^\circ(W) - RT\ell nC \qquad (115)$$

The first two terms of equation (114) do not change with the metal and hence make the same contribution to ΔG_a° for all metals. A notable point of equation (115) is that it predicts that for a given concentration and solvent replacement value, the amount of adsorption increases as the solubility C_s of the adsorbate decreases. There are no published

values available for the solubilities of the carboxylic acids in the electrolyte solution employed. However, the various orientation effects and $\Delta G^{\circ}_{a}(0)$ correlated with solubility in pure water are tabulated in Tables 5a and b.

4.2.5 Lateral Interaction in the Adsorbed Phase

Many attempts have been made at theoretically calculating the lateral interaction free energy ($g(\theta)$) as a function of coverage. The first attempts [36,49,50,105] considered only the interaction between adsorbed solute molecules, neglecting any contributions by solvent. These approximations are valid at the potential of maximum adsorption where net interaction effects associated with solvent dipoles are minimal [177]. At potentials other than this, there is a net orientation of adsorbed solvent dipoles and solvent-solute, solvent-solvent, as well as solute-solute interactions must be considered. In order to make theoretical calculations of lateral interaction free energy involving these three types of interactions it is necessary to know R (net water dipole orientation) at the potential at which one is working. R is usually defined as

$$R = \frac{N_{s\uparrow} - N_{s\downarrow}}{N_{ST}} \qquad (116)$$

where $N_{s\uparrow}$, $N_{s\downarrow}$ are the populations of solvent molecules oriented in "up" ($\uparrow$) or "down" ($\downarrow$) directions [14,178,179] in the electrode field, N_{ST} is the total number of water molecules cm^{-2}. Several authors [177,178,180] have attempted to calculate R as a function of charge

on the mercury surface and have had reasonable success in fitting experimental data. In the present work, conducted on a solid metal surface under galvanostatic conditions, the electrode charge is not known and R cannot be determined theoretically.

The experimental variation of $g(\theta)$ with θ can yield important information on the types of interactions present as well as the degree of localization of the adsorption process. Calculated $g(\theta)$ values** from the data in Table 5a and the smoothed adsorption isotherms for the monocarboxylic acids are plotted versus θ, the coverage calculated from blocking theory, in Figs. 31-33.

There are two types of interactions in the adsorbed phase, dipolar and dispersion. At low surface coverages, dispersion forces may be ignored in comparison to the longer range dipole interactions [36,49,50]. Bockris and Swinkels [36] have shown that the functional dependence of $g(\theta)$ on θ, where θ is the fractional surface coverage of adsorbed dipoles, is

$$g(\theta) = \frac{a\theta}{\varepsilon} \qquad (117)$$

for localized adsorption * and

$$g(\theta) = \frac{a\theta^{3/2}}{\varepsilon} \qquad (118)$$

for non-localized adsorption. ε is the dielectric constant of the

* If adsorption takes place on a surface where potential energy fluctuations are appreciable, the troughs will represent adsorption sites and the adsorption is said to be localized. If, however the fluctuations are so small as effectively to vanish, adsorption is said to be non-localized.

** $g(\theta) = \Delta G^{a}(\theta) - \Delta G^{a}(\theta=0)$; where $\Delta G^{a}(\theta)$ is obtained from equation (109) and $\Delta G^{a}(\theta=0)$ from equation (110), using data from the smoothed adsorption isotherms (Figs. 16-29).

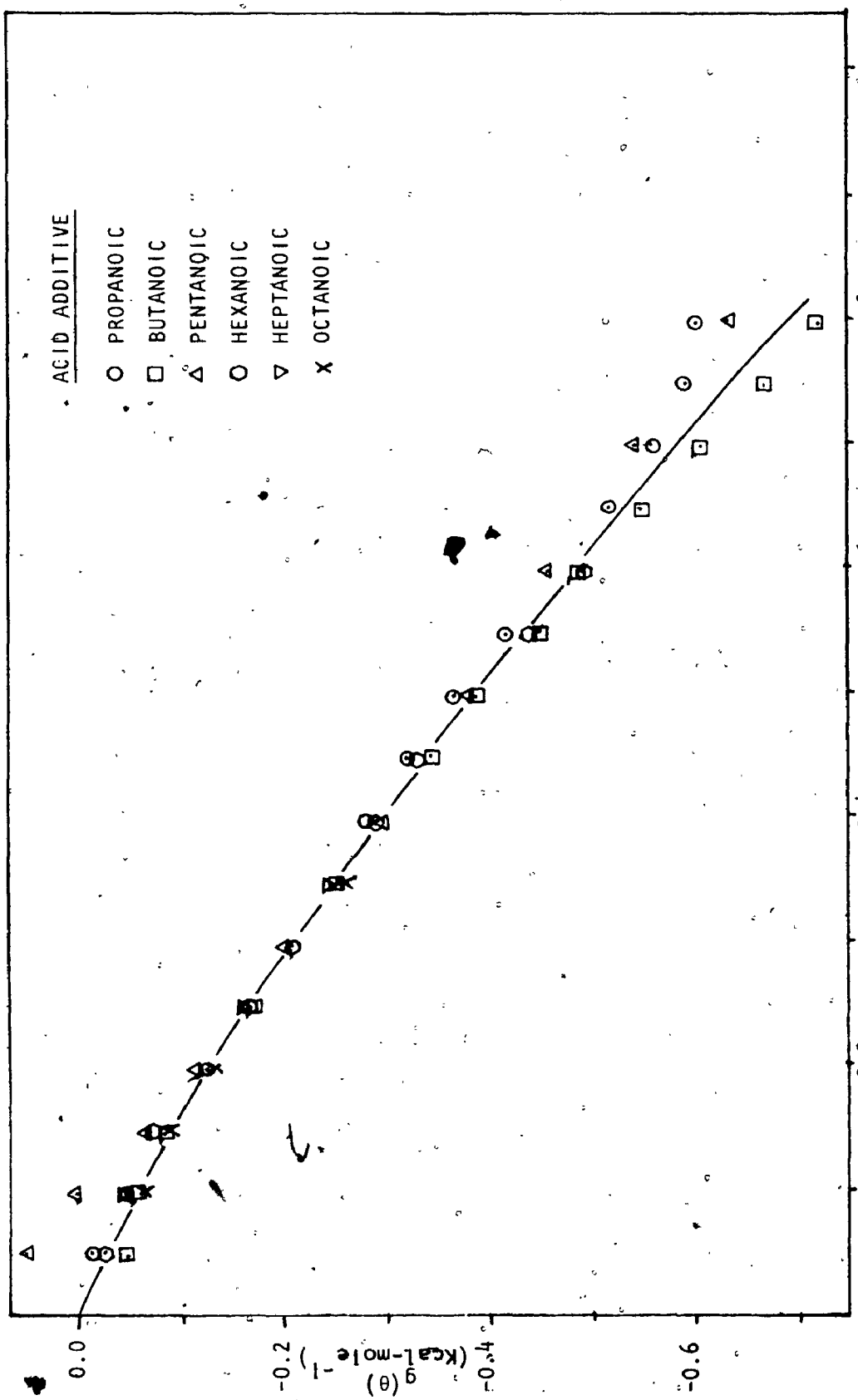

Fig. 31 Lateral interaction free energy-surface coverage relationships for the monocarboxylic acids assuming the perpendicular orientation.

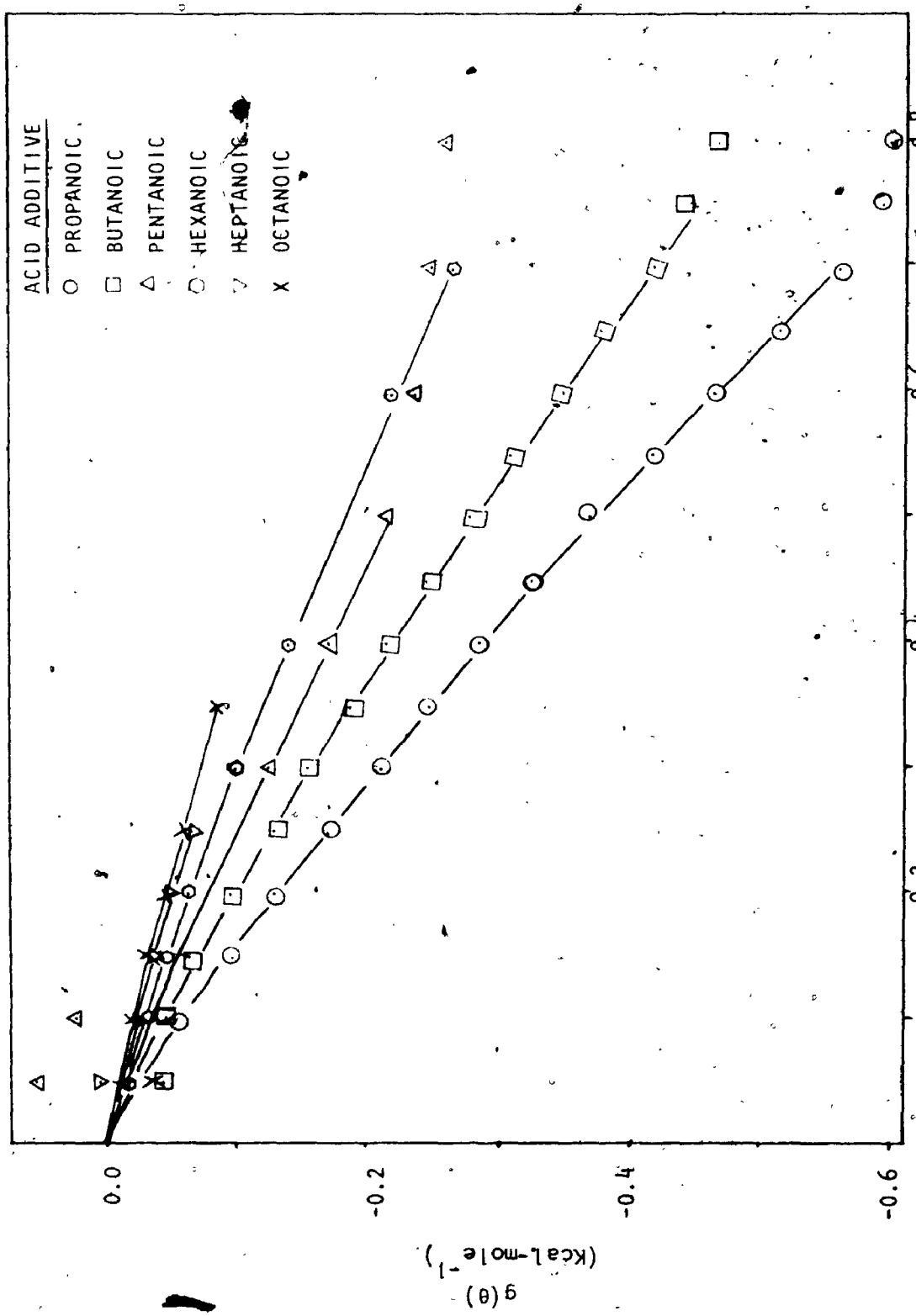

Fig. 32 Lateral interaction free energy-surface coverage relationships for the monocarboxylic acids assuming the parallel orientation.

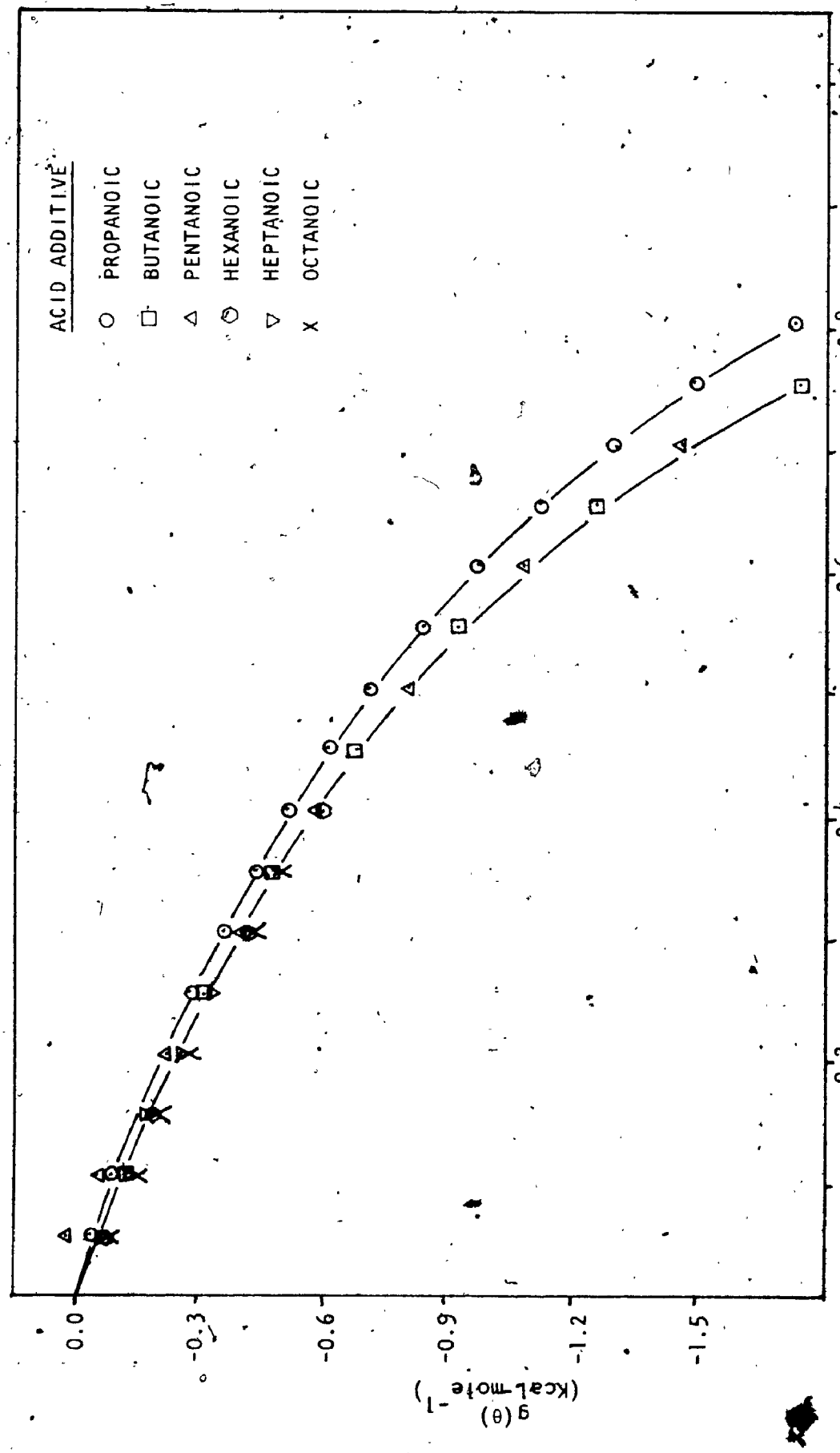

Fig. 33 Lateral interaction free energy-surface coverage relationships for the monocarboxylic acids assuming the flat orientation.

medium, which varies with coverage and a is a constant, the value of which is determined by the dipole moment and the orientation and packing of the dipoles on the surface. At coverages approaching zero, the dielectric constant is that of the water in the primary layer, generally estimated as around 6 [14]. At full coverage the dipoles are separated by organic dipoles (carboxyl functions) and ε will be approximately equal to the pure additive value of 2.5 [49,181]. A linear combination is generally assumed at intermediate coverages [36,174,177] giving

$$\varepsilon = 6 - 3.5\ \theta \tag{119}$$

The fractional surface coverage of adsorbed dipoles is smaller than the surface coverage obtained by blocking theory by the factor $\frac{n}{n^*}$. Therefore the variation of $g(\theta)$ with θ, where θ is the fraction of the surface blocked to deposition is predicted to be

$$g(\theta) = \frac{a\left(\theta \frac{n}{n^*}\right)}{6 - 3.5\ \theta\left(\frac{n}{n^*}\right)} = a\ f(\text{loc}) \tag{120}$$

for localized adsorption, and

$$g(\theta) = \frac{a\left(\theta \frac{n}{n^*}\right)^{3/2}}{6 - 3.5\ \theta\left(\frac{n}{n^*}\right)} = a\ f(\text{non-loc}) \tag{121}$$

for non-localized adsorption.

Figs. 34-39 show the relation for the monocarboxylic acids between calculated $g(\theta)$ values from experimental data and the predicted functional

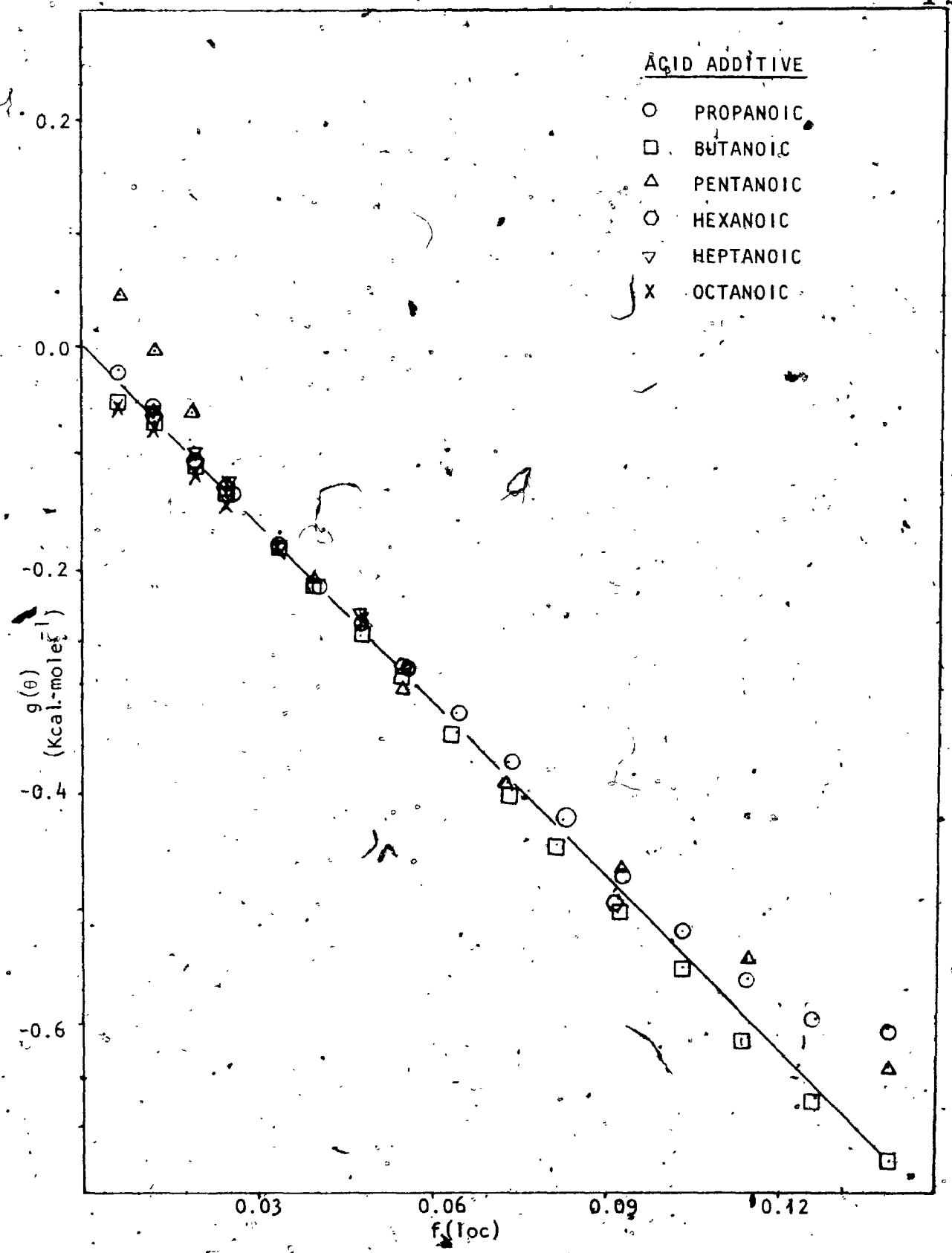

Fig. 34 Lateral interaction free energy-predicted functional dependence relationships for the monocarboxylic acids assuming localized adsorption, perpendicular orientation.

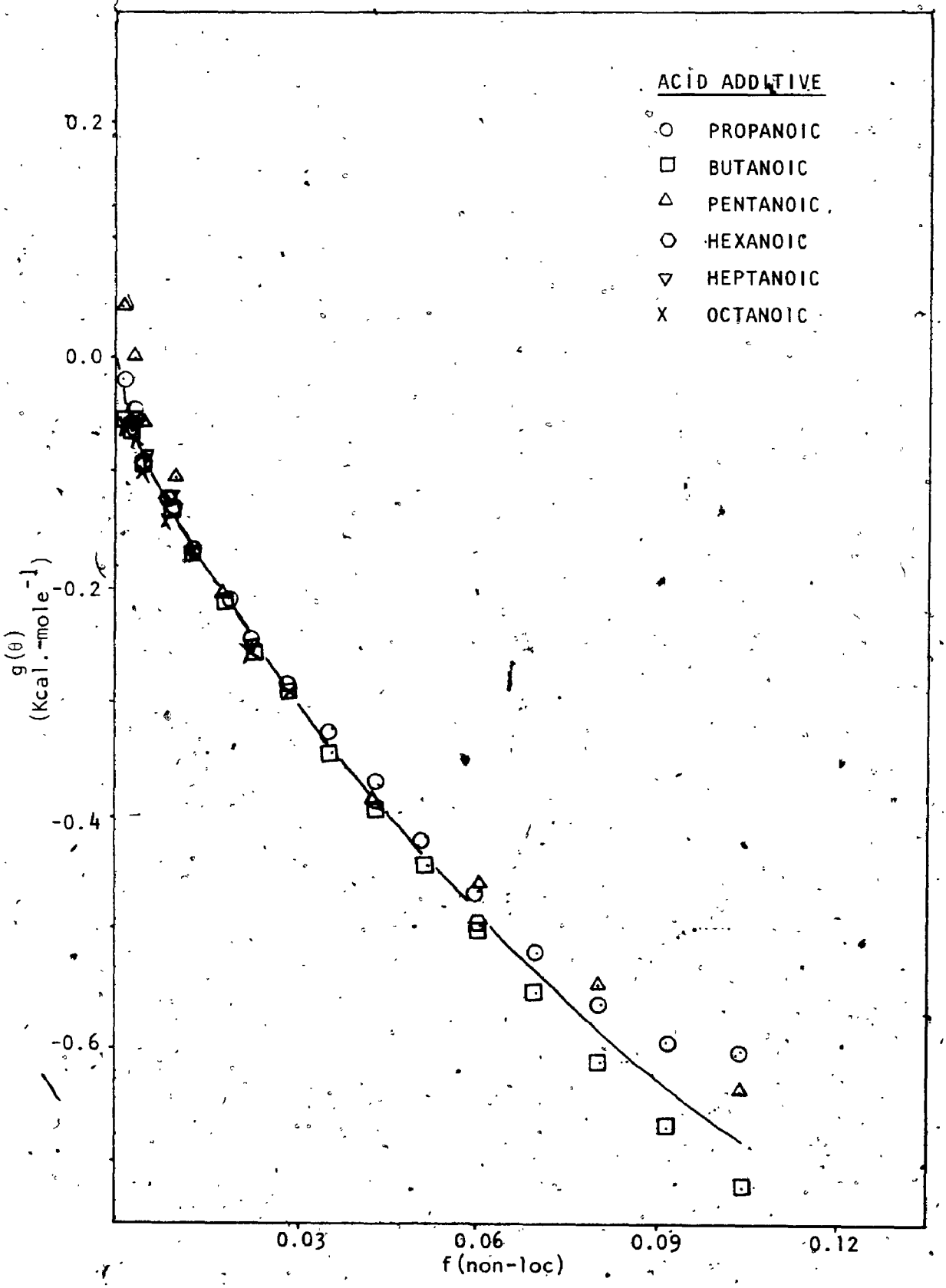

Fig. 35. Lateral interaction free-energy - predicted functional dependence relationships for the monocarboxylic acids assuming non-localized adsorption, perpendicular orientation.

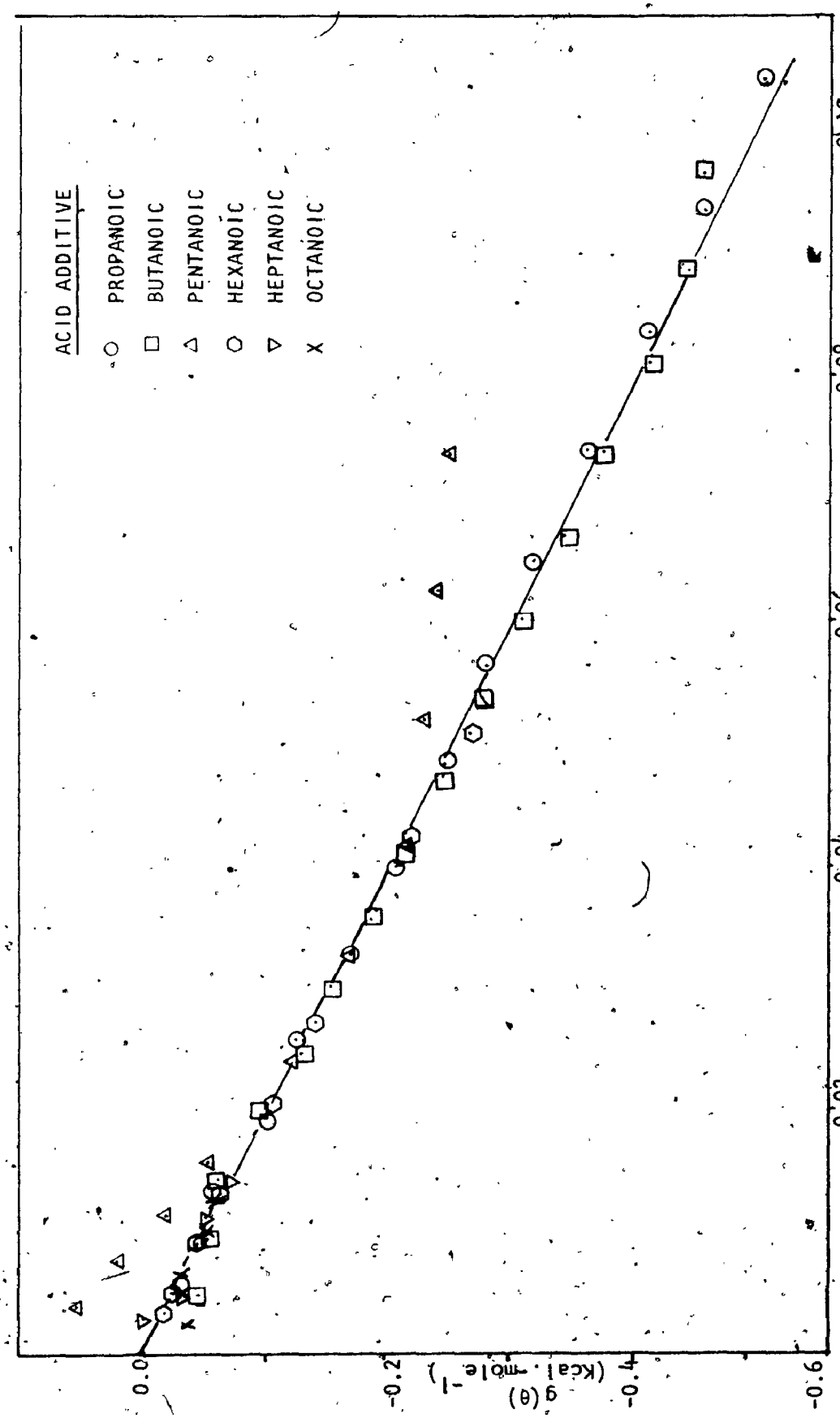

Fig. 36 - Lateral interaction free energy-predicted functional dependence relationships for the monocarboxylic acids assuming localized adsorption, parallel orientation.

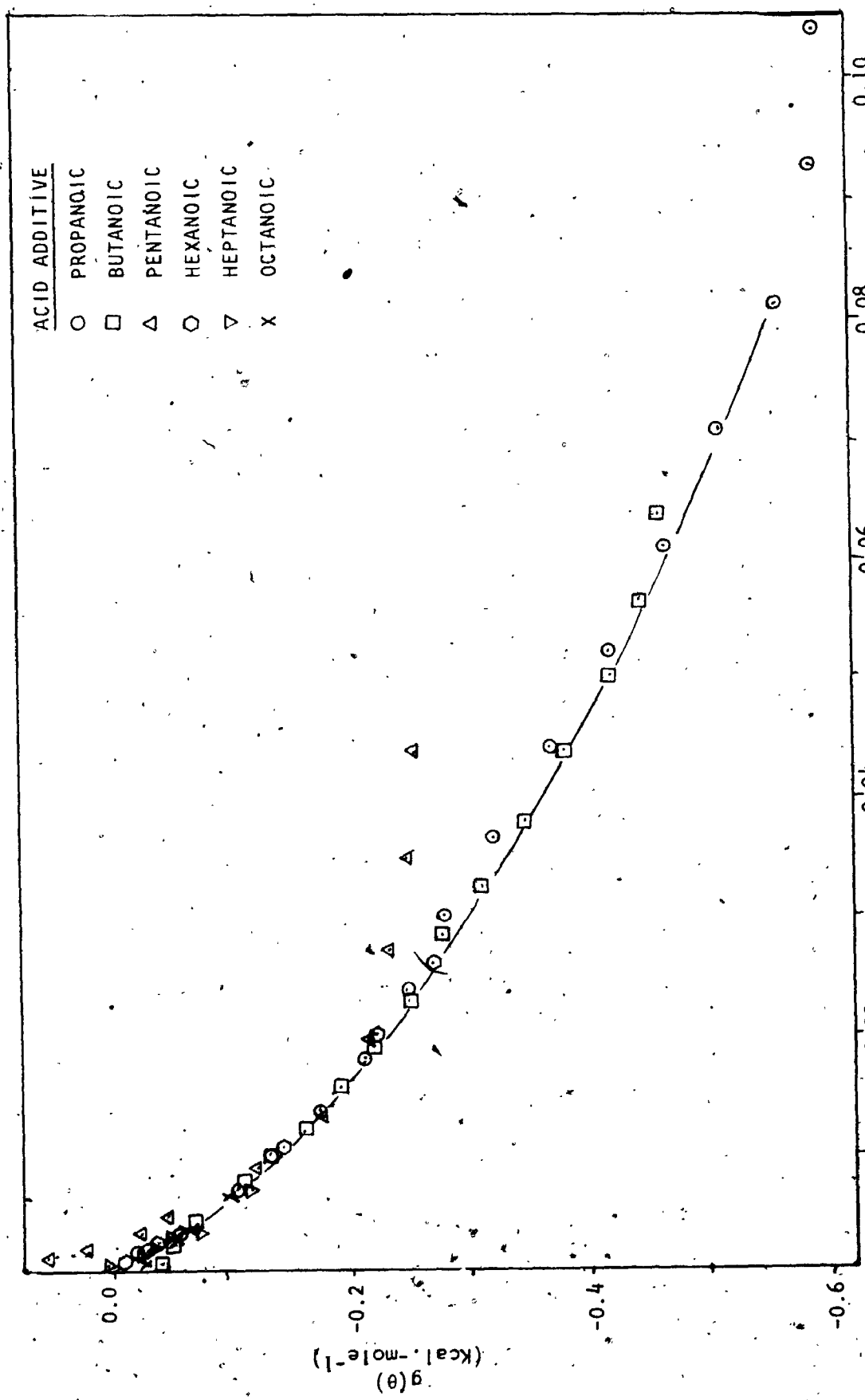

Fig. 37 Lateral interaction free energy-predicted functional dependence relationships for the monocarboxylic acids assuming non-localized adsorption, parallel orientation.

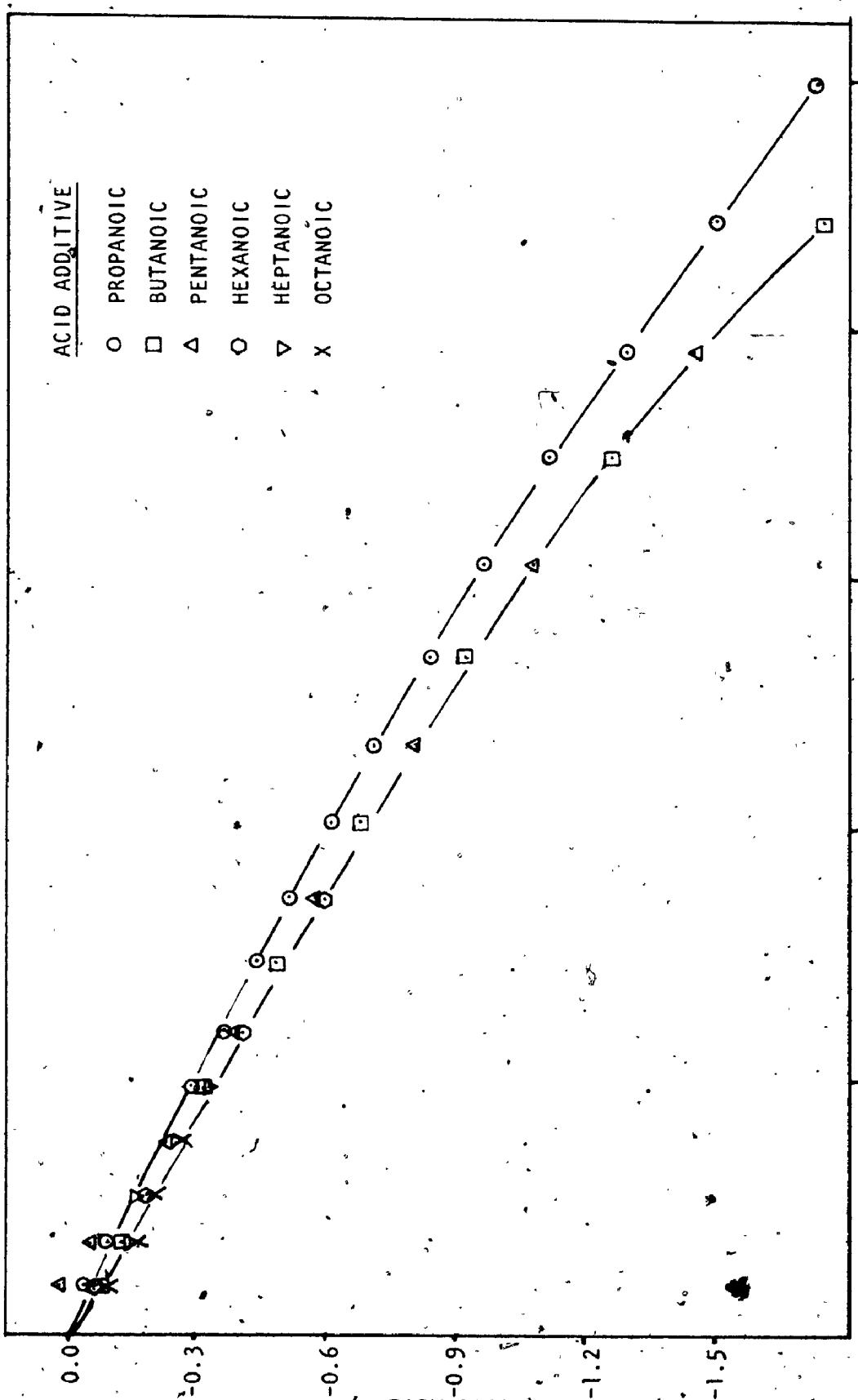

Fig. 38. Lateral interaction free energy-predicted functional dependence relationships for the monocarboxylic acids assuming localized adsorption, flat orientation.

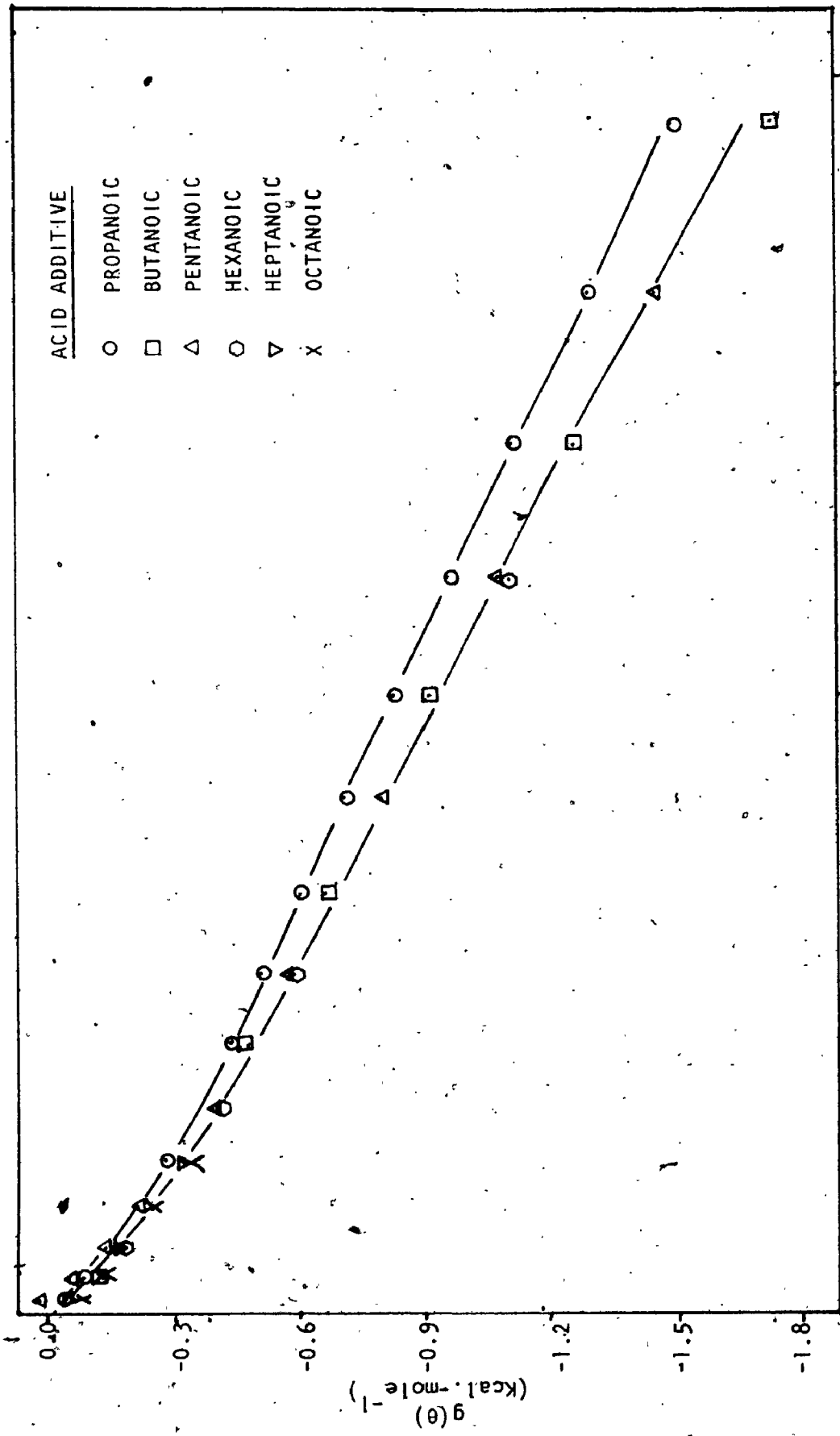

Fig. 39 Lateral interaction free energy-predicted functional dependence relationships for the monocarboxylic acids assuming non-localized adsorption, flat orientation.

dependences of equations (120) and (121) for the three orientations of adsorption. The best linear fit on these "normalized" curves is Fig. 36; localized adsorption, parallel orientation.

Similarly, the data in Table 5b and the experimental adsorption isotherms were used to calculate predicted functional dependences for the lateral interaction free energy in the adsorption of the dicarboxylic acids. Propanedioic acid is unique in that there is only one orientation of adsorption possible ($n = n^* = 4.46$). It can be seen in Fig. 40 that the functional dependence for localized adsorption best accounts for the calculated $g(\theta)$ values. Butanedioic acid is also stearically restricted in its adsorption on a planar surface. For strain-free adsorption only one functional group may be present on the surface at any instant in time. The hydrocarbon chain with the other terminal carboxyl may however either lie parallel to the metal surface, blocking it to deposition, or may rise perpendicular from the surface. Also, orientations between these extremes cannot be excluded due to the conflict between the hydrophobic nature of the methyl groups and the hydrophilic carboxyl character. Fig. 41 shows the variation of $g(\theta)$ with the blocking θ for adsorption in the two orientational extremes. Prediction of the variation of $g(\theta)$ between the non-adsorbed carboxyl functions is extremely difficult due to uncertainty in the value of ε in regions other than in the primary layer and in the orientation of these dipoles with respect to each other.

It has been shown [182-184] that the presence of several functional groups in an organic compound, which are located at different segments in the molecular chain, will produce planar orientation of this molecule

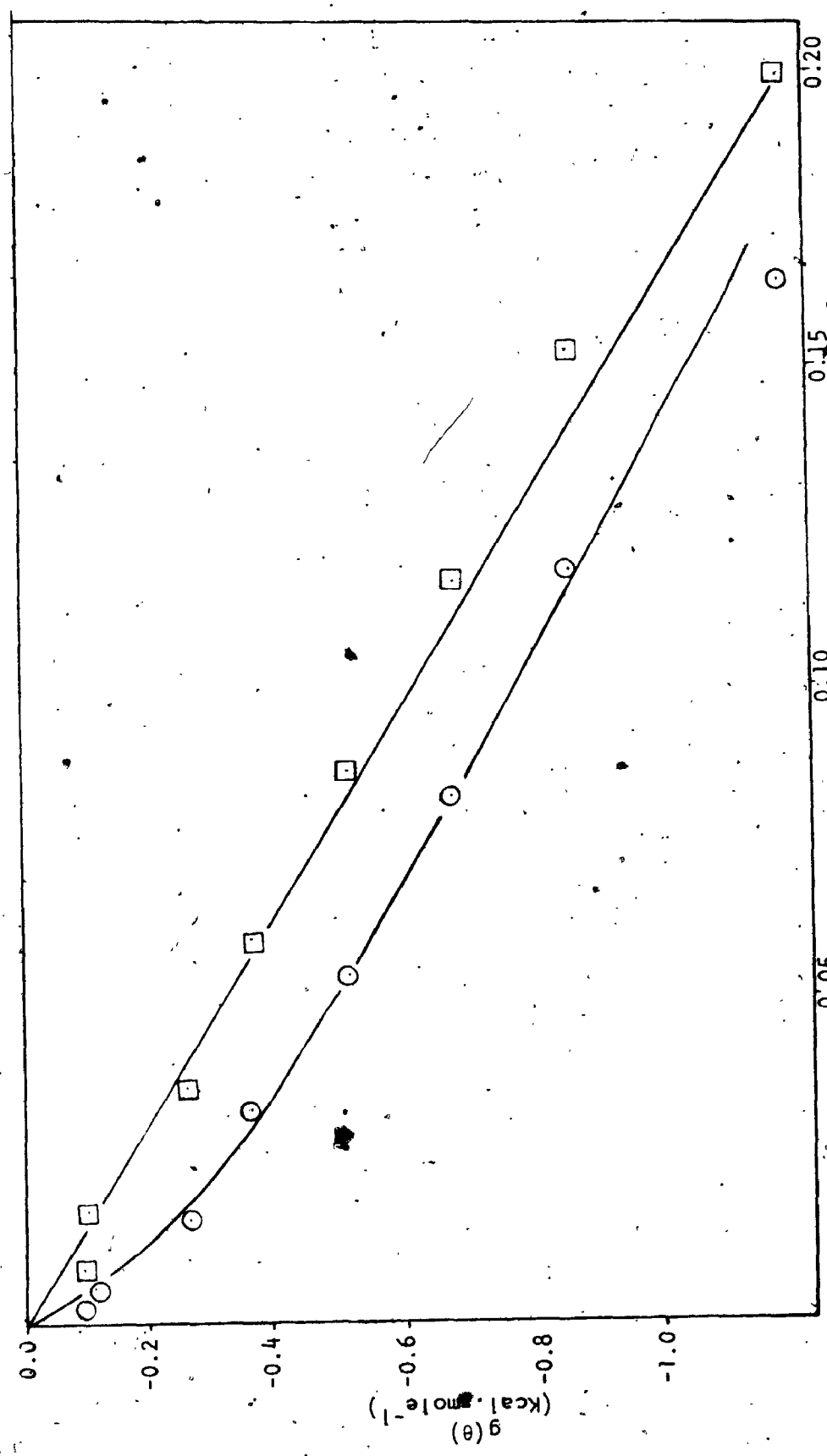

Fig. 40 Lateral interaction free energy-predicted functional dependence relationships for propanedioic acid; ○ non-localized adsorption, □ localized adsorption.

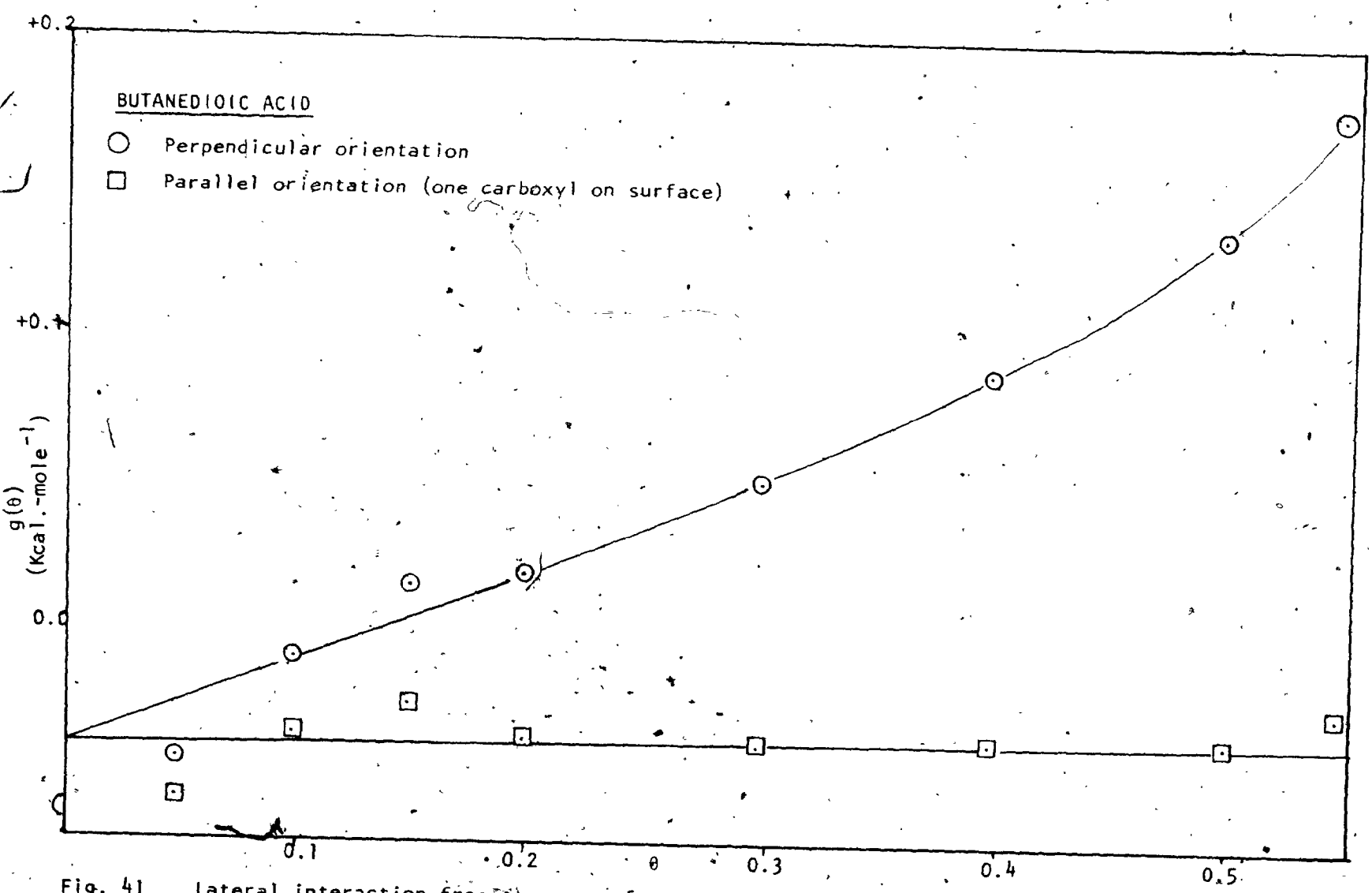

Fig. 41 Lateral interaction free energy-surface coverage relationships for butanedioic acid assuming various orientations.

during its adsorption at the surface of a mercury electrode. Accordingly plots of calculated $g(\theta)$ values versus the appropriate dipole surface coverage functional dependence were prepared for the longer chain dicarboxylic acid additives. Localized adsorption in the flat and parallel orientations were the only conditions which produced linear relationships. This linearity is shown in the initial regions of Figs. 42 and 43.

When the adsorbate is in a flat orientation, the hydrocarbon chain is on the surface displacing oriented dipoles and one would expect an increase in net interaction as the length of this chain is increased. Fig. 42, however, does not show these expected vertical relationships.

Considering adsorption in the parallel orientation (Fig. 43), the deviations from linearity appear to increase in the regions corresponding to high surface coverages. Apart from the lessening applicability of the experimental method in these regions, the deviations may be due to small errors in the determination of the blocking projection and solvent displacement numbers. As the chain length is increased, a greater flexibility is imparted to the compound. When considering adsorption in the parallel mode, this flexibility made the determination of n^* and n from molecular models very difficult and subject to estimation. It can be seen in equation (109) that a decrease in interaction free energy with increasing coverage is predicted by decreasing the ratio $\frac{n}{n^*}$. Since the blocking projection numbers were estimated at their maximum values, this ratio can only be decreased by a decrease in the value of the solvent displacement number. Accordingly, it is proposed that as the coverage of additive

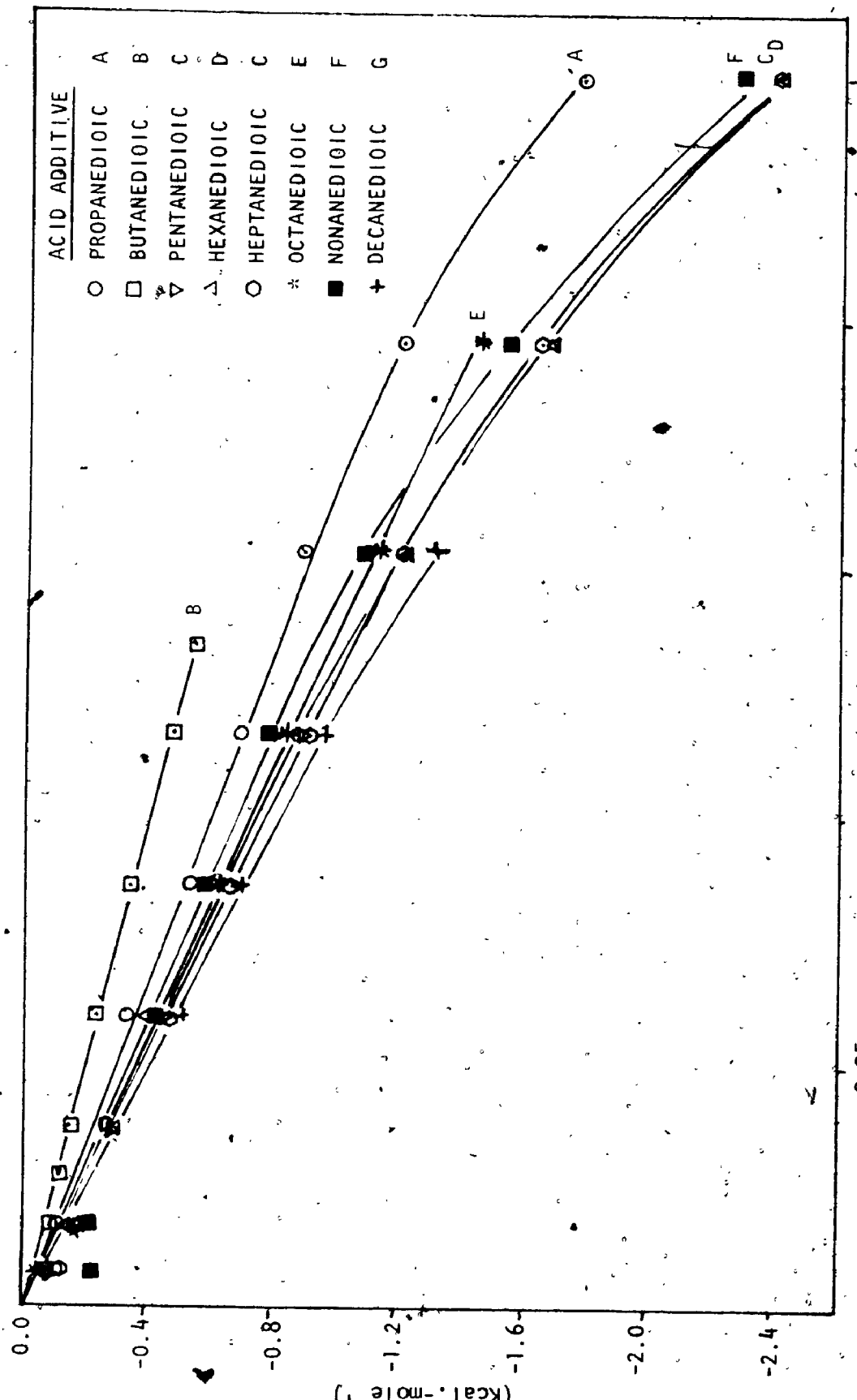

Fig. 42 Lateral interaction free energy-predicted functional dependence relationships for the dicarboxylic acids assuming localized adsorption, flat orientation.

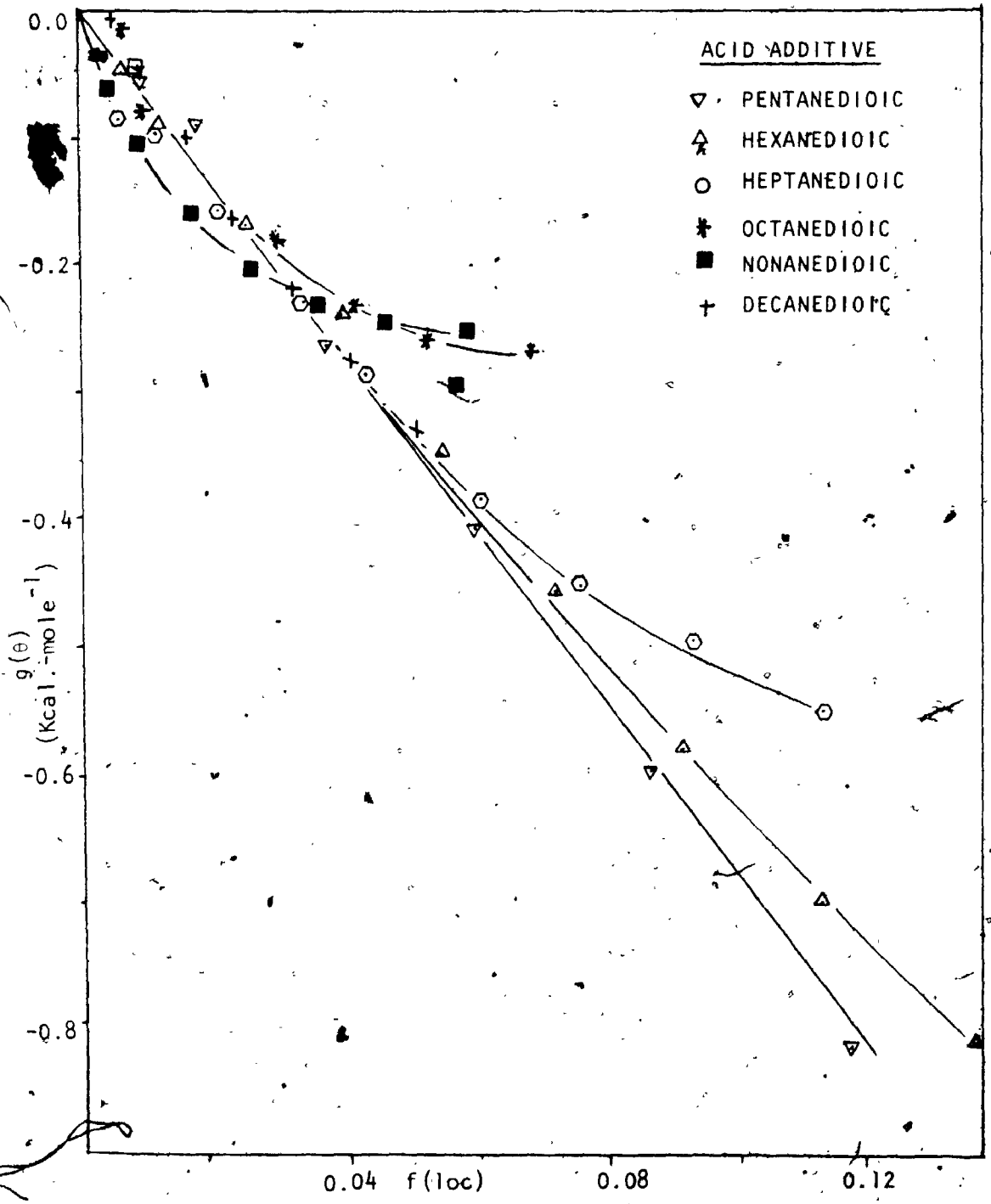

Fig. 43 Lateral interaction free energy-predicted functional dependence relationships for the dicarboxylic acids assuming localized adsorption, parallel orientation.

on the surface is increased, there is an increasing tendency for the molecule to undergo one point attachment to the surface. This conclusion is further supported by the fact that pentanedioic acid shows no deviation from linearity, but as the chain length is increased the deviations become more severe and originate in progressively lower coverage regions.

DISCUSSIONS - PART 3

4.3 THE ELECTROSORPTION OF THE AROMATIC CARBOXYLIC ACIDS

4.3.1 The Experimental Adsorption Isotherms

Fractional surface coverages, calculated from equation (104), are plotted versus the bulk concentration of the aromatic carboxylic acids studied in Figs. 44-47. In all cases the isotherms for stirred and unstirred conditions coincide in the initial, low coverage region, however the isotherms determined under unstirred conditions level off in the high coverage regions below the curves determined under stirred conditions.

The experimental isotherms fall into two classes. Phenyl-acetic acid (PAA) produced an "L" class isotherm similar to the aliphatic acids, while benzoic, 3-phenyl-propanoic (3-PPA), and 4-phenyl-butanoic (4-PBA) acids produced "S" class isotherms characteristic of i) strong solvent adsorption and/or ii) strong intermolecular attraction within the adsorbed layer and/or iii) a single point of attachment in an aromatic or long hydrocarbon chain system. The first possibility can be eliminated since "L" class isotherms were obtained for other adsorbates with the same solvent under similar electrode conditions. Strong intermolecular attraction and single point attachment usually occur simultaneously as has been shown by Lorenz and Muller [185,186] and Shallal et al [187] for the adsorption of t-amyl alcohol and cyclohexanol on mercury producing "S" shape

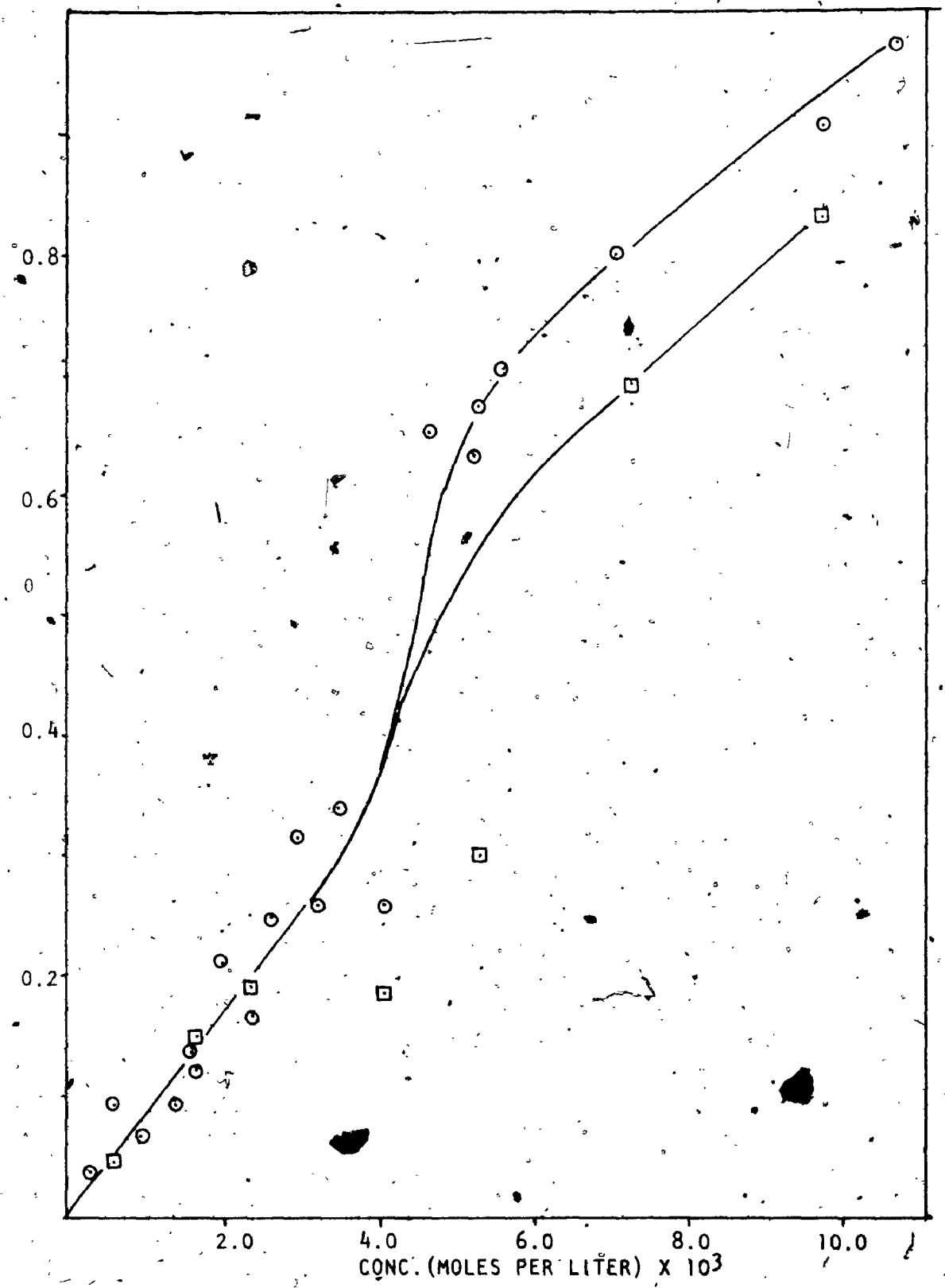

Fig. 44 Surface coverage-concentration relationship for benzoic acid; ○ stirred solutions, □ unstirred solutions.

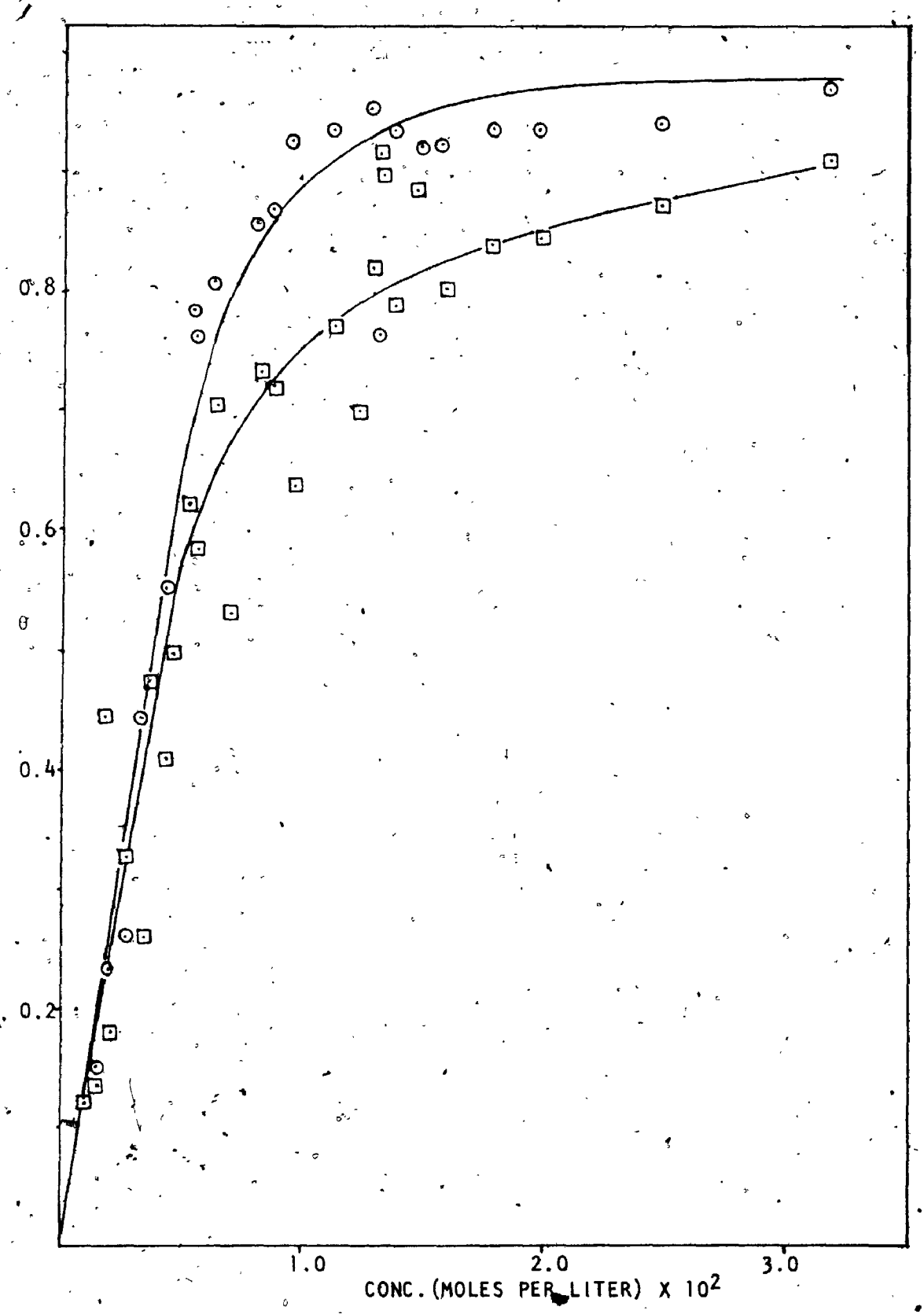

Fig. 45 Surface coverage-concentration relationship for phenyl-acetic acid; O stirred solutions, □ unstirred solutions.

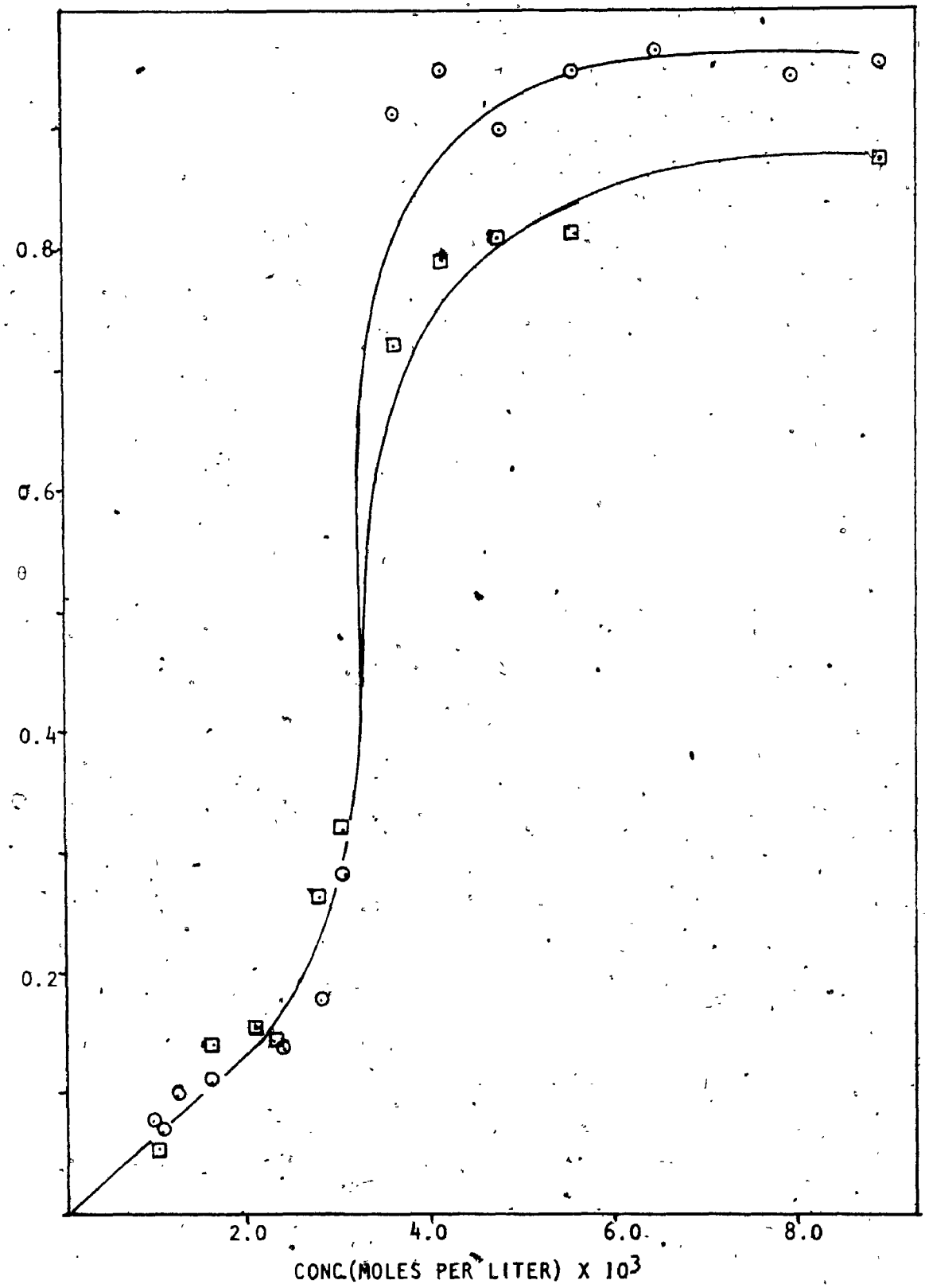

Fig. 46 Surface coverage-concentration relationship for 3-phenyl-propanoic acid; ⊙ stirred solutions, □ unstirred solutions.

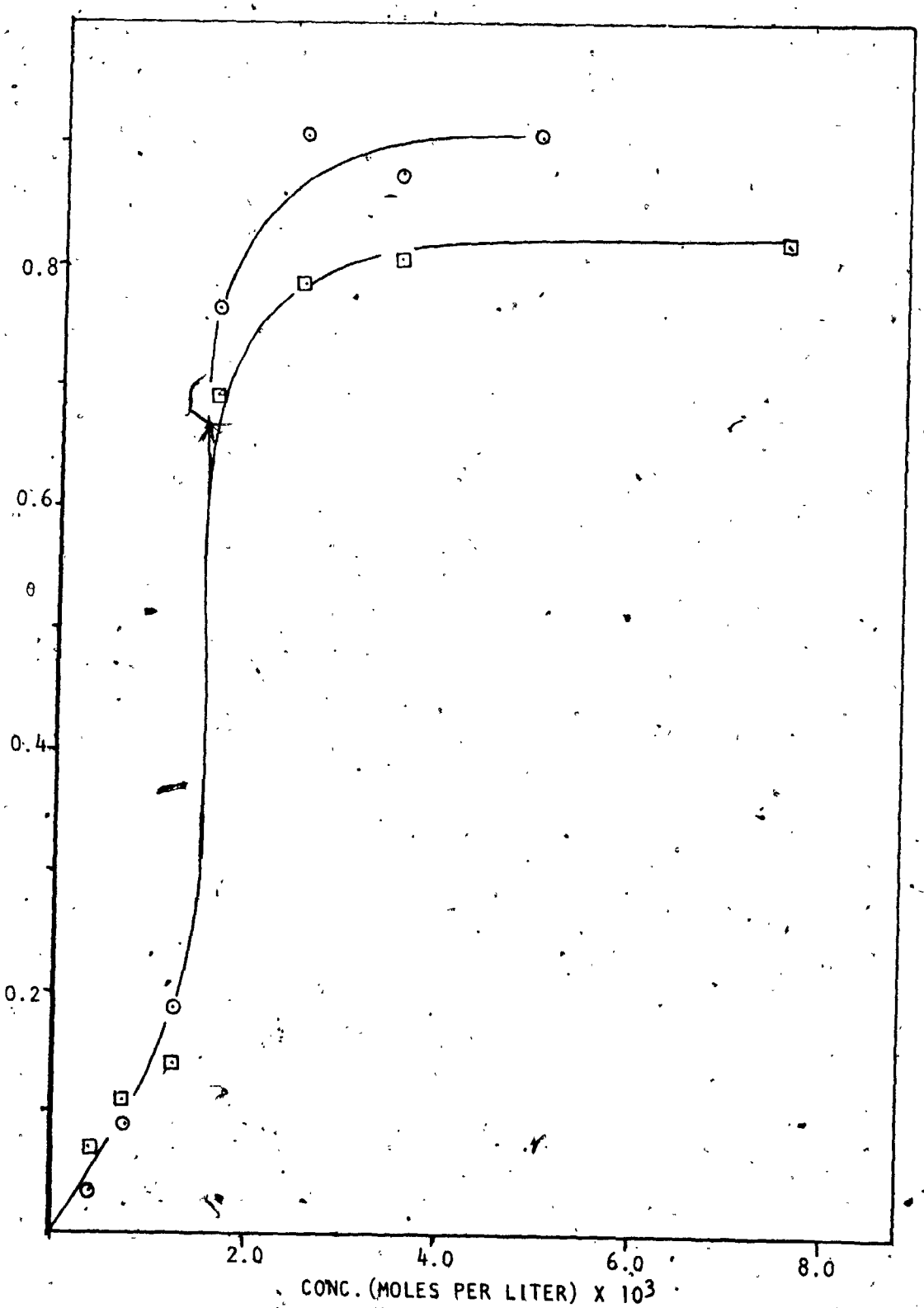

Fig. 47 Surface coverage-concentration relationship for 4-phenyl-butanoic acid; ○ stirred solution □ unstirred solution.

isotherms. A condensation mechanism has been proposed for adsorption showing this type of isotherm. Under equilibrium conditions, the discontinuous region observed is attributed to the transition from a "gaseous" layer with a small coverage to a condensed film, for which θ is close to unity. Unstable states for which $d\theta/dc$ is greater than zero have been experimentally observed in some systems [82]. Evidence of such states was exhibited in the overpotential-time relationships for benzoic acid.

In some systems, for example o-cresoxide ion at Hg [111], the "S" shape isotherm has been attributed to a spontaneous change of orientation of adsorbate on the surface at a coverage corresponding to adsorbate saturation in the original orientation. The adsorbate in the new perpendicular orientation then forms a condensed film due to increased intermolecular attraction.

4.3.2 Adsorbate Orientation and Free Energies of Adsorption

The adsorption of benzoic acid on gold electrodes has been studied by Dahms and Green [43]. Working at potentials 500 to 800 mV anodic to the pzc, they reported adsorption effects consistent with a flat orientation of the benzene ring on the surface at low surface coverages. Similar findings were reported by Blomgren et al [110] for the adsorption of substituted benzene derivatives on Hg. These conclusions are consistent with the predicted strong interaction between π-electrons and the metal.

Since the Langmuir type isotherms are not observed for benzoic acid, 3-PPA and 4-PBA it is unlikely, for these additives, that the

phenyl ring adsorbs flat on the surface over the potential range studied in the present work. Maximum intermolecular attraction is predicted when the aromatic rings are aligned with the planes parallel to each other. The dispersion energy of such interaction between π-bonded systems would show a $(-a\theta)$ functional dependence [177]. "S" shape curves of the type shown in Figs. 44,46 and 47 show a functional dependence of $\Delta G_a^\circ(\theta) = \Delta G_a^\circ(\theta=0) - a\theta$, where a is a constant greater than 0.

Although a change of orientation in the adsorbed phase would also cause "S" shape isotherms, it is unlikely that such an orientation change would be so instantaneous and complete as to cause the discontinuities exhibited in the adsorption isotherms.

Further evidence of a condensation mechanism is exhibited by the behaviour of phenyl-acetic acid. Unlike other aromatic acids, phenyl-acetic acid is not capable of adsorbing with the carboxyl dipole perpendicular to the surface and displacing water while the phenyl ring is also in a perpendicular orientation, the orientation for maximum intermolecular interaction. In order for the carboxyl group to undergo maximum interaction with the electric field, the ring must be in a position parallel to the metal surface but above the primary water layer. In this orientation the expected isotherm would be a Langmuir type, which is found experimentally.

Benzoic acid as well differs from 3-PPA and 4-PBA. The discontinuity is less severe for this additive. The rotation of the benzene ring is restricted in this additive due to the proximity of the functional groups. It is accordingly much more difficult for aromatic

rings on neighbouring adsorbate molecules to come into contact with each other.

On the basis of the above arguments and the studies of the aliphatic carboxylic acids, the number of possible modes of adsorption of these additives may be reduced to a manageable few. It appears that all these compounds adsorb with only the carboxyl dipole on the surface displacing primary water.

Considering benzoic acid first; the phenyl ring is restricted to a perpendicular orientation in relation to the surface, but the plane of the ring may either be in the same plane as the axis between the oxygens in the carboxyl group (orientation A) or at an angle to this axis (orientation B). Orientation B is stearically more favourable.

Two orientations must be considered for 3-PPA and 4-PBA. With the extensions in the hydrocarbon chains and more flexibility in these molecules, condensation mechanisms are possible when the plane of the phenyl ring is perpendicular to the surface (orientation C) and when the plane is parallel to the surface (orientation D). Orientation D, would yield strong π-bond interaction by stacking of the rings on top of each other. A summary of the standard free energies of adsorption, solvent replacement numbers, adsorbate projection numbers, and solubility data for these compounds is given in Table 6.

TABLE 6

Correlation of Solubility with Adsorbability for Various Orientation Effects for the Aromatic Carboxylic Acids.

ACID ADDITIVE	ORIENTATION	n*	$\bar{n}$	$\left(\frac{\theta}{C}\right)_{C\rightarrow O}$	$-\Delta G_a^\circ(0)$ Kcal./mole	SOLUBILITY (m/l)
Benzoic	A	1.93	1.93	85	4.62	2.37×10^{-2} [171]
	B	3.59	1.93	85	4.26	
PAA		5.73	1.93	125	4.20	1.20×10^{-1} [171]
3-PPA	C	5.00	1.93	66	3.90	4.66×10^{-2} [171]
	D	6.56	1.93	66	3.74	
4-PBA	C	5.83	1.93	130	4.22	
	D	7.39	1.93	130	4.07	

CHAPTER 5

SUMMARY AND CONCLUSIONS

5.1 From a theoretical examination of the kinetics of copper deposition under galvanostatic conditions it was shown that the Tafel equation should apply in the overpotential region 60-140 mV. The effects of adsorption of neutral organic compounds on the kinetics of the deposition process were examined and it was shown that the Tafel equation should also apply to deposition from solution containing these additives. On the basis of these Tafel relationships, a modified blocking equation was developed for determining the fractional surface coverage of adsorbed molecules on a copper electrode during the electrodeposition of copper. It was shown that under certain conditions the surface coverage determined by the kinetic method is an apparent value in that the adsorbate may block more of the electrode to reaction than it is physically in contact with. Modifications were made to the Bockris-Swinkels adsorption isotherm to account for this effect.

5.2 The effects of six normal monocarboxylic acids on the electrodeposition of copper at a copper cathode were studied using the galvanostatic method. Adsorption isotherms were deduced from surface coverages calculated from the modified blocking equation. Standard free energies of adsorption at the zero coverage limit were calculated using the initial slopes of these isotherms and assuming different adsorbate orientations. The free energy of adsorption was found to increase with decreasing solubility of the compounds studied for all

orientation effects.

Lateral interaction free energies for the adsorbates were calculated as a function of coverage for the assumed orientations. Graphical comparisons of these values with the predicted theoretical functional dependencies indicated that adsorption is possible in either of two modes: localized adsorption,perpendicular orientation; or localized adsorption,parallel orientation; the latter being the more likely.

5.3 The effects of eight dicarboxylic acids on the electrodeposition of copper were studied using the same techniques. The correlation of standard free energies of adsorption with solubility data indicated that these compounds were adsorbed in different orientations. Structural examinations and lateral free energy calculations then provided the information to arrive at the following conclusions: a) Propanedioic acid is restricted to adsorption with both carboxyl groups on the surface displacing water. b) Butanedioic acid is adsorbed with only one carboxyl displacing water from the primary layer. c) Pentanedioic acid appeared to adsorb in a parallel orientation with both functional groups displacing water at all coverages studied. d) At low surface concentrations, the longer chain dicarboxylic acids appeared to adsorb similar to pentanedioic acid. As the surface coverage increased, indication was noted of a tendency for only one carboxyl to adsorb on the surface. e) Best agreement with theoretical predictions was noted for localized adsorption in all cases.

5.4 The effects of four aromatic carboxylic acids on the kinetics of copper electrodeposition were studied. Phenyl-acetic acid produced an "L" class isotherm, while benzoic acid, 3-PPA, and 4-PBA produced "S" class adsorption isotherms. The structure of the adsorbate molecules was shown to correlate with these findings, in that the aromatic rings in adsorbed PAA molecules cannot orient themselves in a manner which produces strong dispersion interactions*, characteristic of systems showing "S" class isotherms.

Studies of the electrical double layer were carried out on the standard solution and solutions containing these aromatic additives. Inflections in the electrode capacity-concentration relationships were observed at additive concentrations corresponding to the discontinuities in the adsorption isotherms for benzoic acid, 3-PPA, and 4-PBA. As expected, no inflections were evident in the relationship for phenyl-acetic acid.

* In this text dispersion interactions are separated from permanent dipole-permanent dipole interactions. Dispersion interactions refer to interactions attributed to induced charge distribution.

APPENDIX I

CAPACITANCE MEASUREMENTS AT THE COPPER ELECTRODE IN THE PRESENCE OF SOME AROMATIC CARBOXYLIC ACIDS

INTRODUCTION

It has been stated in the main text of this work that a fundamental difference was seen in the effects of phenyl-acetic acid and the other aromatic acids studied on the kinetics of copper deposition. In order to obtain a better understanding of the role of these additives in the double layer, the electrode capacitance was measured as a function of additive concentration for these four compounds.

The potential decay method was used to measure the electrode capacitance and equation (55) was employed to convert the rate of potential decay to capacitance.

EXPERIMENTAL

The electrical circuit employed for these studies is that shown in Fig. 9 and described in Chapter 2 of the main text. The oscilloscope was adjusted to a time scale of 2 μsec cm^{-1} and a potential scale of 2 or 5 mV cm^{-1}.

Overpotential versus time measurements were made during initial overpotential decay, starting at the steady-state. In these experiments, the steady-state overpotential was first established at several different values of the apparent current density for each concentra-

tion of additive, thus giving capacitance data at electrode potentials varying over a narrow range of about 200 mV overall.

RESULTS AND DISCUSSIONS

Typical plots of electrode capacitance versus overpotential for standard solution and solution containing additive are shown in Fig. 48. Due to the error inherent in graphical differentiation, reproducibility in these determinations was restricted to about ± 4 $\mu F\text{-cm}^{-2}$. It appears that no significant potential dependence of the capacitance occurs, within the experimental error, in the range of potentials used. This is in agreement with the results of Loutfy [109] for the adsorption of monocarboxylic acids from the same standard solution and overpotential range as employed in this work. This could mean, presumably, that in these capacitance measurements the experimental potentials correspond approximately to the region of maximum adsorption where coverage changes very little with potential. If this interpretation is correct, then the data in Fig. 48 would appear to show that the potential of maximum adsorption, $\Delta\phi_{max}$, tends to shift in the cathodic direction with increasing coverage.

The apparent potential independence of the capacitance enables the worker to examine electric double layer capacitance as a function of the concentration of additive. Figs. 49-52 show this relationship for the additives studied. In the region of the potential of maximum adsorption, the capacitance-concentration profile for most organic additives is similar to that obtained for phenyl-acetic acid (Fig. 50). Equation (52) can then be employed to calculate θ values and hence

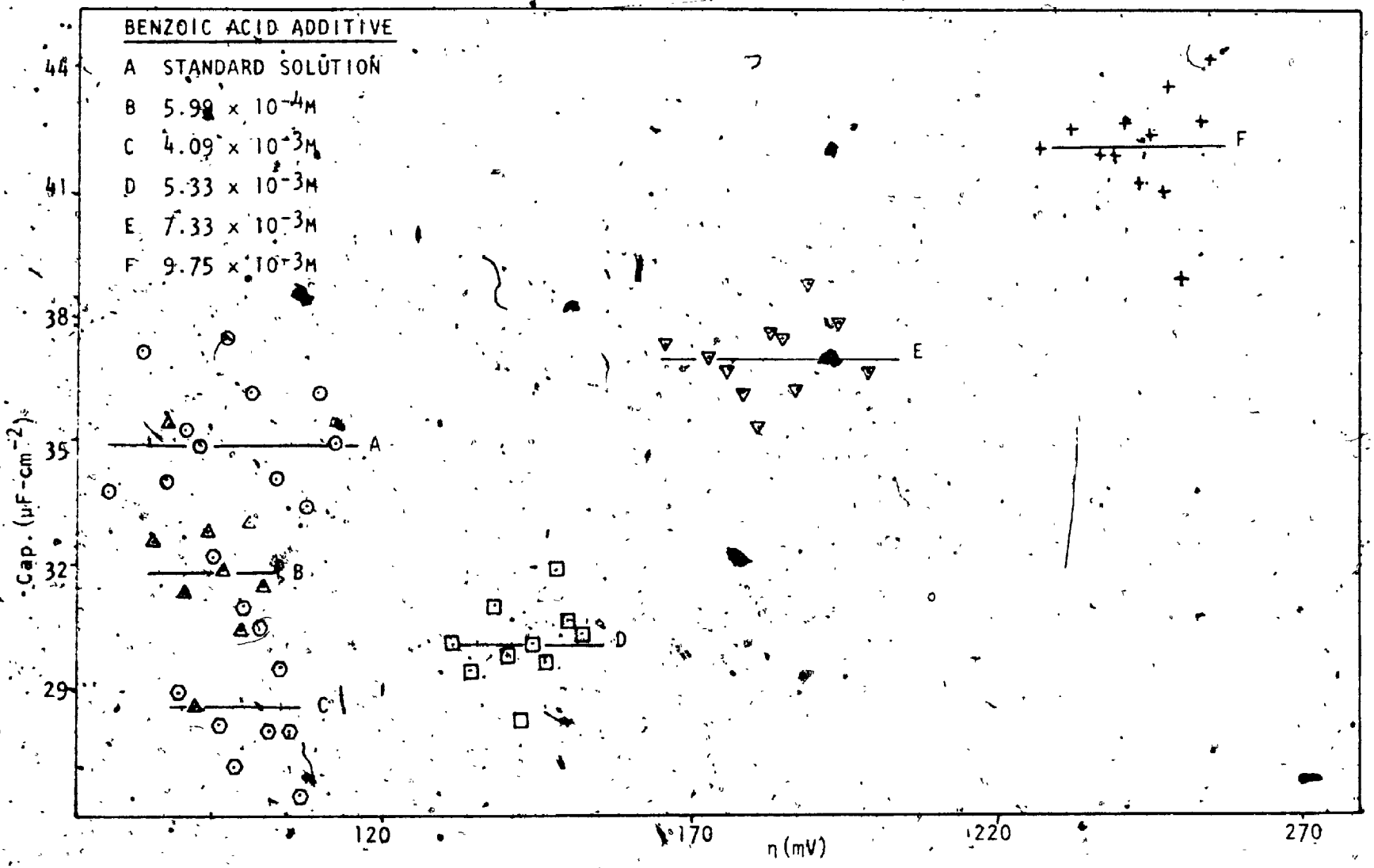

Fig. 48 Electrode capacitance-overpotential relationships for standard solution and solution containing benzoic acid as additive.

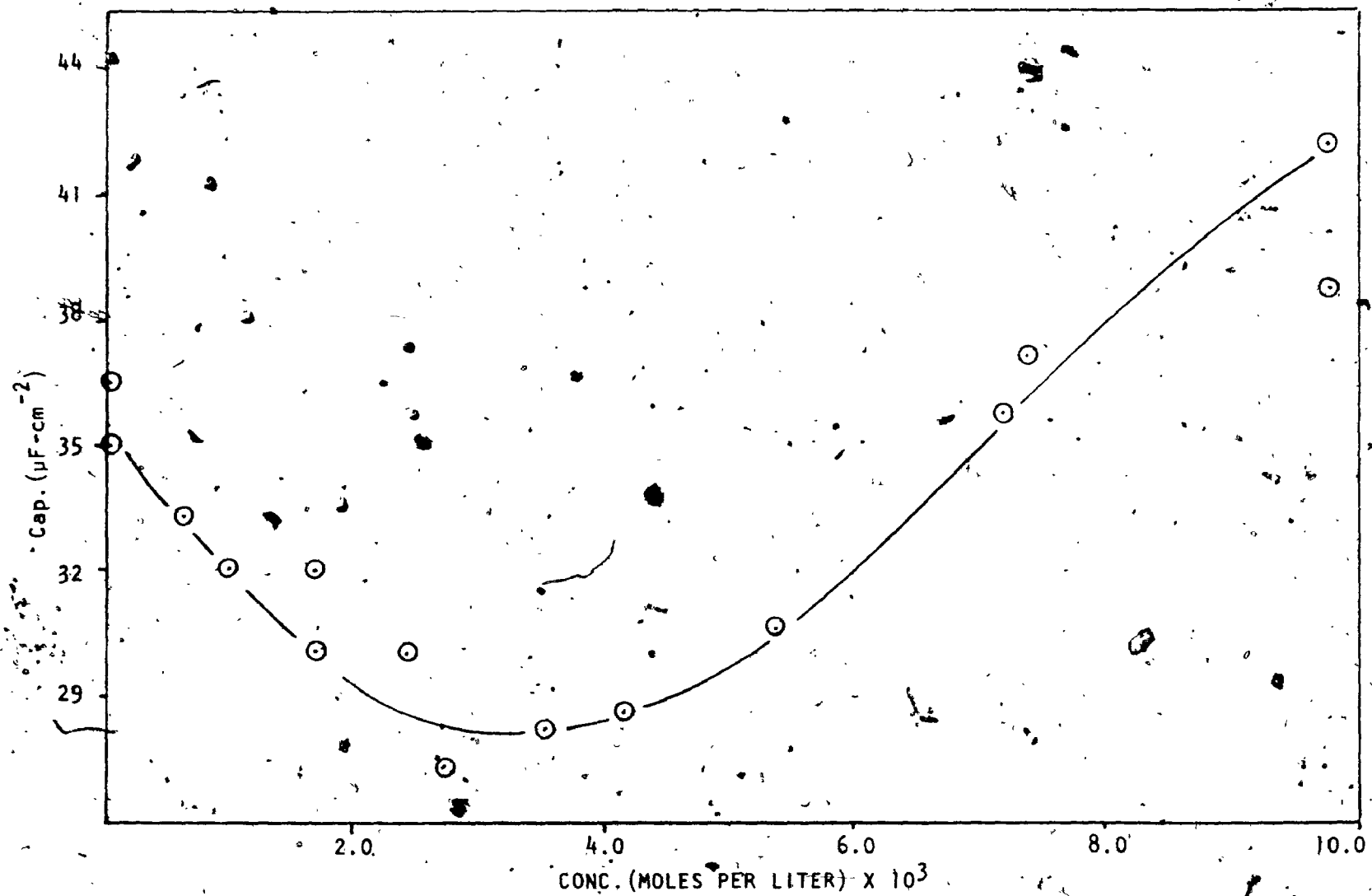

Fig. 49 - Electrode capacitance-concentration relationship for solutions containing benzoic acid as additive..

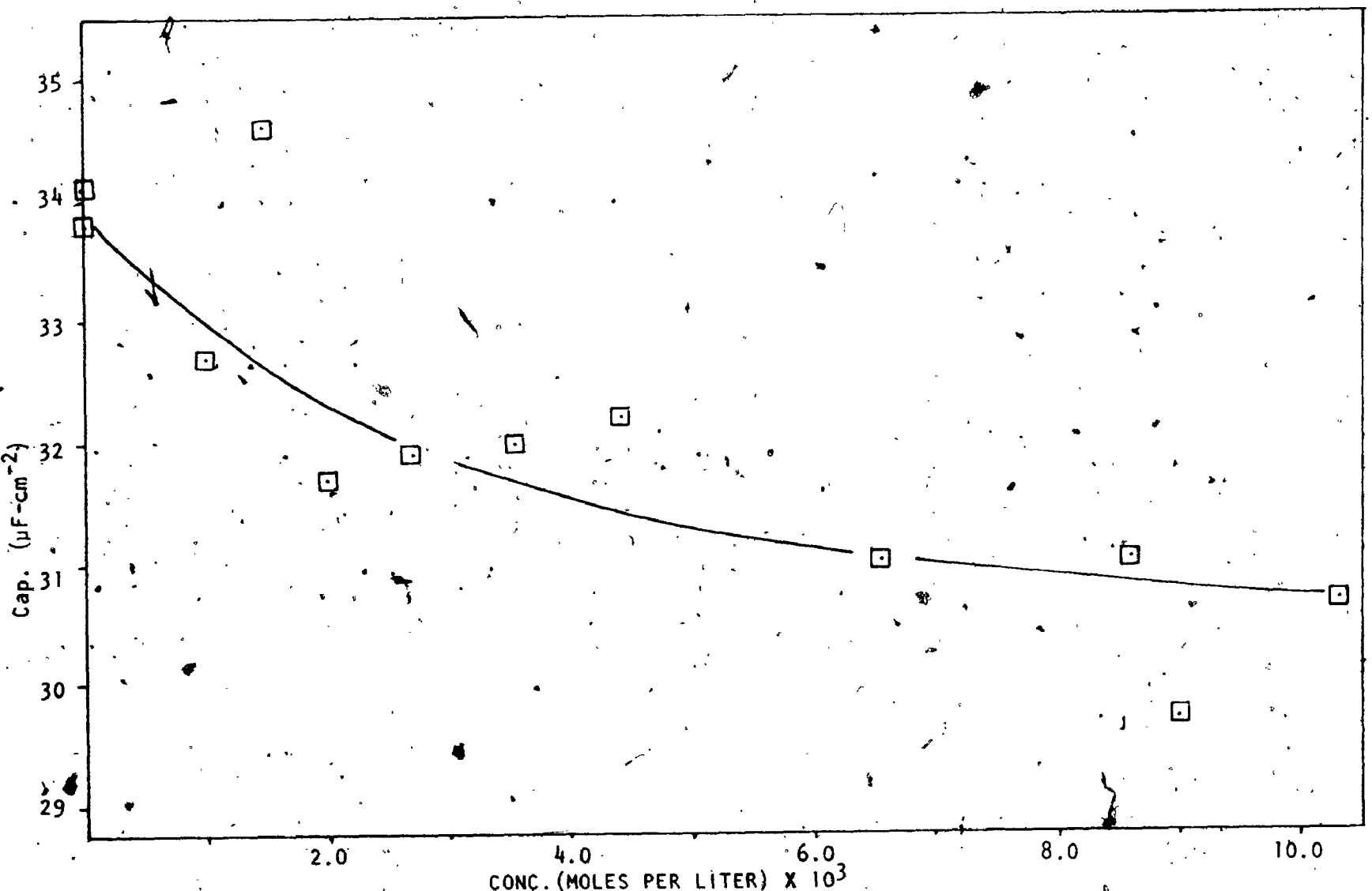

Fig. 50 Electrode capacitance-concentration relationship for solutions containing phenyl-acetic acid as additive..

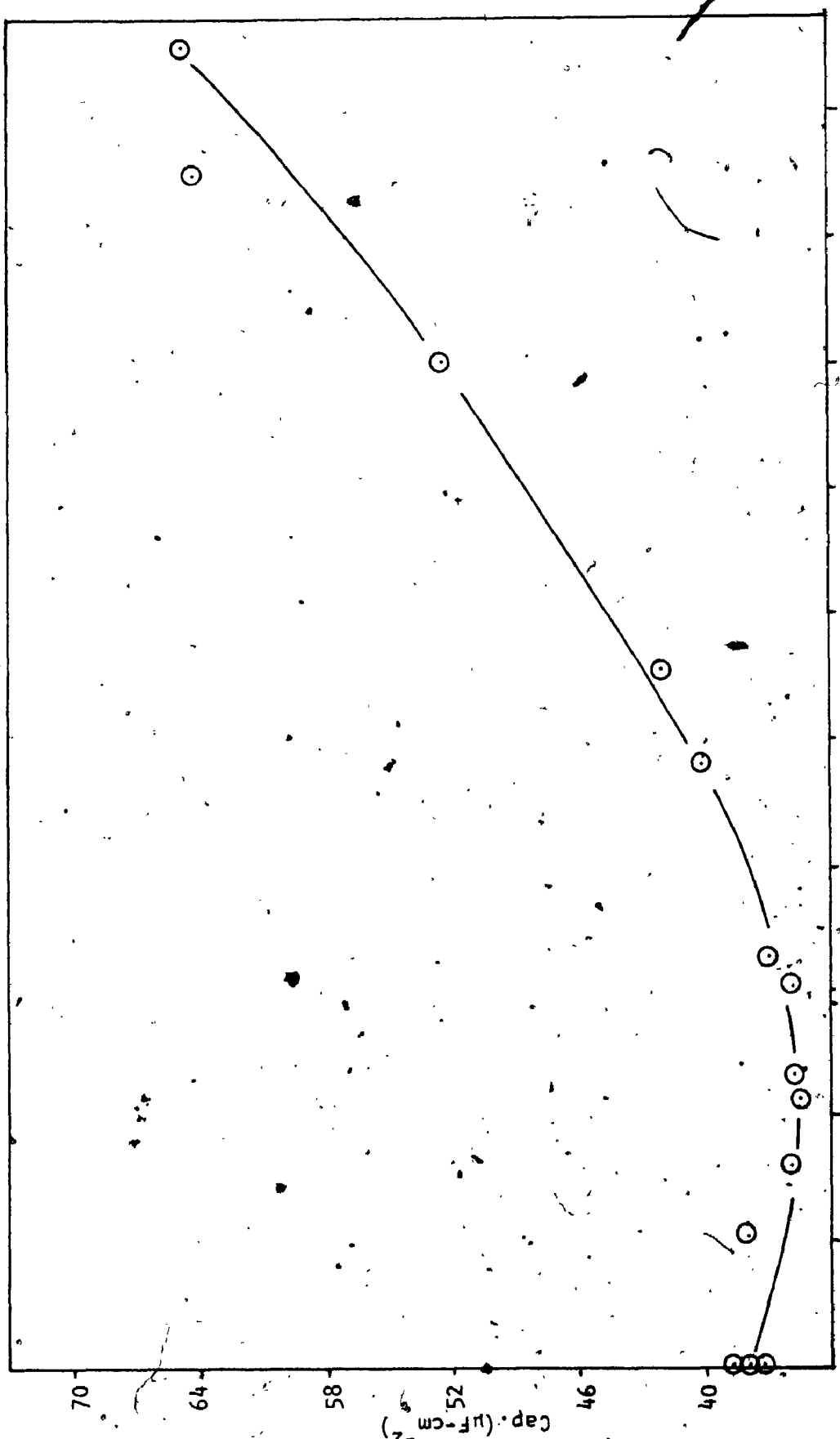

Fig. 51 Electrode capacitance-concentration relationship for solutions containing 3-phenyl-propanoic acid as additive.

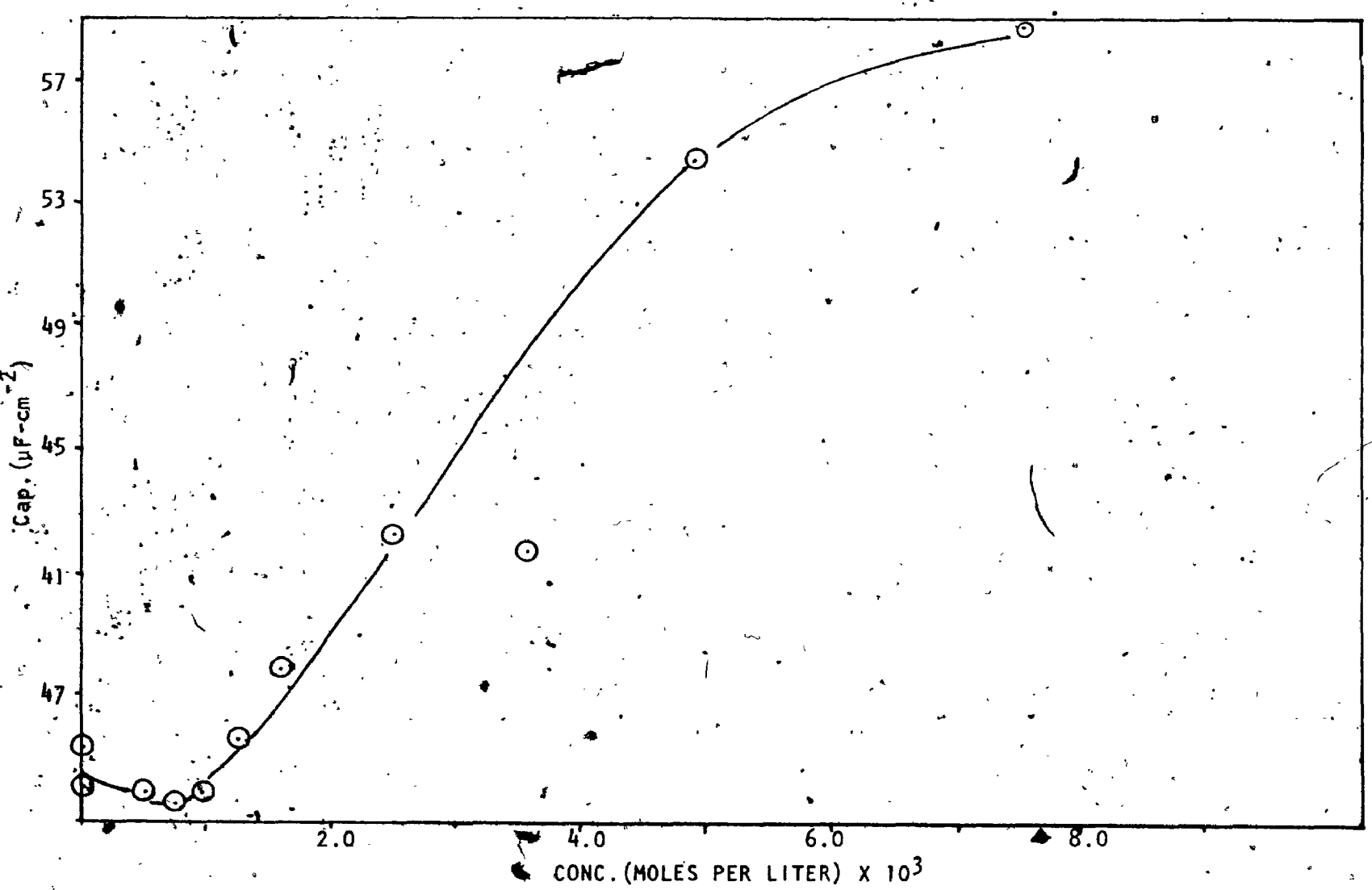

Fig. 52 Electrode capacitance concentration relationship for solutions containing 4-phenyl-butanoic acid as additive.

obtain adsorption isotherms. This technique was used by Loutfy [109] in a study of the adsorption of the monocarboxylic acids on copper during deposition.

The "U" shaped curves found for benzoic; 3-PPA, and 4-PBA are quite unusual. The minima in capacitance occurs at the same concentration, within experimental error, as the discontinuity in the adsorption isotherms. Capacitance minima can be attributed to either a reorientation of adsorbate or to the effect of an adsorption pseudo capacitance. Parsons and Bockris [141] showed that the double layer capacitance is inversely proportional to the double layer thickness, while the Tafel slope is directly proportional to the double layer thickness. It was pointed out in Chapter III of the main text that the Tafel slope after initially increasing at low additive concentration, rapidly decreased for the higher concentrations of these additives. Thus it would appear that a reorientation of additive in the double layer so as to decrease the thickness of the double layer would explain this behaviour. However, the facts that the capacitance rises to values far above the standard solution value and the Tafel slope decreases to a value far below the standard value, cannot be explained by reorientation.

In the case of processes involving deposition of adsorbed intermediates (adions), the measured (pseudo) capacitance may be much larger than the true double layer capacitance and usually depends on the value of $\frac{d\Delta\phi}{dt}$ owing to relaxation effects [188-190] associated with the finite rates of electrochemical deposition or desorption of ad-species generated at the electrode surface. The formation of a condensed film

of adsorbate on the surface must have a significant effect on the electrochemical deposition process. The reversibility of the adsorption process will be greatly diminished by the strong intermolecular attractions between individual adsorbate molecules. Thus the rate of mass transport and surface diffusion would also be affected and hence the Tafel slope and electrode capacitance. It may therefore be concluded that the kinetic and capacitance effects of the presence of aromatic carboxylic acids on the deposition of copper can be attributed to the irreversibility of the adsorption process brought on by strong intermolecular attraction in the adsorbed phase.

APPENDIX II

EXPERIMENTAL DATA FOR CARBOXYLIC ACID ADDITIVES

SYMBOLS

Concentration	(mole $-l^{-1}$)
b_θ (mv)	Tafel slope for solution containing additive.
η_{c_0} (mV)	Cathodic overpotential of solution containing additive at i_g = 20 ma-cm^{-2}
η_c (mV)	Cathodic overpotential of standard solution at i_g = 20 ma-cm^{-2} to which acid was added.
b (mV)	Tafel slope of standard solution to which acid was added.
θ	Fractional surface coverage calculated from blocking equation (104)
NS	Solutions studied under conditions of free convection
*	Complexing or recrystallization after initiation of deposition.
**	Grey-black cathodic deposit
***	Solution showed step η vs time relationship.

NOTE: All overpotentials are negative quantities. The sign has been dropped for reasons of convenience.

CONCENTRATION	b_0	η_{c0}	η_c	b	θ
Propanoic Acid					
8.51×10^{-3}	41.9	93.8	89.1	41.9	0.106
1.70×10^{-2}	41.9	94.1			0.112
2.55×10^{-2}	41.9	95.5			0.142
3.40×10^{-2}	41.9	98.1			0.193
4.26×10^{-2}	42.9	100.0			0.328
5.11×10^{-2}	42.9	102.8			0.370
5.70×10^{-2}	43.2	105.0			0.425
5.96×10^{-2}	58.5	116.5	95.5	52.6	0.568
7.24×10^{-2}	62.5	119.9			0.680
7.99×10^{-2}	58.8	120.0			0.600
8.51×10^{-2}	64.2	122.1			0.721
1.06×10^{-1}	63.9	125.5			0.731
1.28×10^{-1}	65.9	126.5			0.761
1.70×10^{-1}	69.5	130.0			0.809
4.19×10^{-3}	39.5	91.3	89.6	39.5	0.042
8.38×10^{-3}	39.5	93.3			0.089
1.26×10^{-2}	39.5	94.6			0.119
2.09×10^{-2}	39.5	95.6			0.141
2.93×10^{-2}	39.5	97.0			0.171
3.50×10^{-2}	39.5	102.3			0.275
5.44×10^{-2}	39.5	102.5			0.279

CONCENTRATION	b_Θ	n_{c_Θ}	$^\circ n_c$	b	Θ
Propanoic Acid - continued					
2.16×10^{-3}	36.9	87.4	86.4	36.9	0.027
6.48×10^{-3}	36.9	88.2			0.048
8.64×10^{-3}	36.9	89.5			0.081
1.08×10^{-2}	36.9	87.6			0.032
1.08×10^{-2}	36.9	88.1			0.045
1.41×10^{-2}	36.9	89.6			0.083
7.58×10^{-2}	40.1	105.8	90.3	37.7	0.547
1.33×10^{-1}	46.9	108.8			0.822
2.05×10^{-1}	48.1	115.3			0.863
4.10×10^{-1}	62.6	128.9			0.964
6.15×10^{-1}	48.3	140.0			0.919
9.22×10^{-1}	182.3	196.5			0.997
Butanoic Acid					
2.20×10^{-3}	37.5	87.6	87.0	37.5	0.016
3.12×10^{-3}	37.5	88.4			0.037
4.22×10^{-3}	37.5	90.0			0.077
5.51×10^{-3}	37.5	90.5			0.089
9.18×10^{-3}	37.5	90.8			0.094
7.35×10^{-3}	38.4	91.1	85.8	38.4	0.130
1.36×10^{-2}	38.4	92.0			0.150
1.84×10^{-2}	39.3	95.8			0.336

CONCENTRATION	b_θ	$n_{c\theta}$	n_c	b	Q
Butanoic Acid - continued					
3.67×10^{-2}	39.3	99.3			0.393
5.51×10^{-2}	44.1	105.3			0.733
7.35×10^{-2}	51.3	111.3			0.890
8.26×10^{-3}	38.4	88.8			0.076
7.27×10^{-3}	36.2	91.3	87.5	36.2	0.100
5.45×10^{-3}	39.9	90.5	85.9	39.9	0.109
9.09×10^{-3}	39.9	91.7			0.135
1.18×10^{-2}	39.9	93.0			0.163
1.60×10^{-2}	40.3	93.5			0.225
1.82×10^{-2}	41.0	93.7			0.306
2.50×10^{-2}	41.1	95.5			0.350
2.73×10^{-2}	43.0	96.0			0.506
2.73×10^{-3}	38.8	90.5	90.5	38.8	0.000
5.45×10^{-3}	38.8	92.0			0.038
1.09×10^{-2}	38.8	94.6			0.100
1.36×10^{-2}	38.8	97.5			0.165
1.82×10^{-2}	38.8	97.5			0.165
3.90×10^{-2}	41.9	102.6			0.540

CONCENTRATION	b	n_{c_0}	n_c	b	θ
Pentanoic Acid					
1.04×10^{-3}	30.3	88.5	87.3	30.3	0.039
2.09×10^{-3}	30.3	90.8			0.109
3.13×10^{-3}	30.3	92.5			0.158
3.00×10^{-2}	59.4	120.2	89.7	35.0	0.971
4.31×10^{-2}	47.7	164.0			0.970
7.98×10^{-3}	40.3	95.6	94.9	37.3	0.405
1.10×10^{-2}	41.8	99.0			0.561
1.20×10^{-2}	41.8	99.0			0.561
1.40×10^{-2}	44.3	99.5			0.689
1.60×10^{-2}	44.1	100.0			0.685
1.02×10^{-3}	42.3	89.9	89.6	42.3	0.007
2.04×10^{-3}	42.7	89.9			0.062
4.07×10^{-3}	42.7	90.6			0.077
6.11×10^{-3}	43.5	91.5			0.190
8.14×10^{-3}	44.3	90.8			0.260
1.02×10^{-2}	47.0	91.7			0.479
1.63×10^{-2}	52.0	94.2			0.705
Hexanoic Acid					
4.83×10^{-4}	38.6	90.2	87.0	38.6	0.080
7.24×10^{-4}	38.6	91.5			0.110

CONCENTRATION	b_0	η_{c_0}	η_c	b	0
Hexanoic Acid - continued					
9.65×10^{-4}	39.0	90.5			0.146
1.45×10^{-3}	39.0	94.3			0.225
1.93×10^{-3}	39.5	95.6			0.310
2.41×10^{-3}	39.7	99.6			0.395
3.86×10^{-3}	41.0	109.8			0.613
2.33×10^{-4}	71.5	123.0	123.8	68.1	0.134
7.00×10^{-4}	72.4	124.1			0.180
1.17×10^{-3}	73.4	121.5			0.185
2.33×10^{-3}	73.4	140.4			0.370
Heptanoic Acid					
1.97×10^{-4}	65.0	104.3	100.5	64.4	0.089
3.94×10^{-4}	64.8	114.2			0.210
5.42×10^{-4}	66.1	114.8			0.270
6.90×10^{-4}	69.3	113.7			0.369
8.38×10^{-4}	70.7	112.2			0.397
9.85×10^{-4}	73.0	116.3			0.486
1.48×10^{-3}	73.0	154.6			0.696
Octanoic Acid					
5.93×10^{-5}	42.2	88.7	89.8	41.2	0.114
1.19×10^{-4}	42.8	89.0			0.192
1.78×10^{-4}	43.9	87.0			0.273

CONCENTRATION	b_0	η_{c0}	η_c	b	0
Octanoic Acid - continued					
2.37×10^{-4}	45.0	86.0			0.357
5.93×10^{-5}	41.2	92.8	91.4	41.2	0.033
2.60×10^{-4}	45.0	93.0			0.425
Propanedioic Acid					
1.18×10^{-2}	51.5	96.5	80.5	48.4	0.473
2.10×10^{-2}	53.4	107.8			0.641
2.80×10^{-2}	70.0	116.5			0.890
3.74×10^{-2}	80.5	124.2			0.935
5.02×10^{-2}	68.2	131.2			0.903
7.70×10^{-2}	71.4	139.8			0.926
1.04×10^{-1}	75.7	144.5			0.941
NS 8.92×10^{-4}	62.1	105.7	103.3	62.1	0.038
NS 2.41×10^{-3}	65.0	110.1			0.244
NS 5.86×10^{-3}	69.7	115.8			0.454
NS 8.40×10^{-3}	70.1	119.1			0.489
NS 1.05×10^{-2}	71.9	122.6			0.551
NS 2.56×10^{-2}	90.4	143.0			0.811
NS 5.05×10^{-2}	105.7	155.0			0.878
Butanedioic Acid					
NS 3.72×10^{-3}	66.4	107.5	104.0	66.4	0.051

3 3

OF/DE

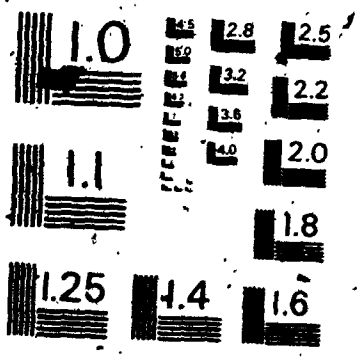

MICROCOPY RESOLUTION TEST CHART
NATIONAL BUREAU OF STANDARDS - 1963 - A

ARC - 374

CONCENTRATION	b_θ	$n_{c\theta}$	n_c	b	θ
Butanedioic Acid - continued					
NS 4.85×10^{-3}	66.4	112.5			0.120
NS 8.63×10^{-3}	66.4	116.0			0.165
NS 2.47×10^{-2}	68.4	123.5			0.254
1.35×10^{-2}	51.8	83.3	74.8	51.8	0.151
2.33×10^{-2}	51.8	91.2			0.271
3.59×10^{-2}	51.8	100.5			0.391
4.97×10^{-2}	51.8	105.8			0.450
5.65×10^{-2}	51.8	109.0			0.483
6.44×10^{-2}	51.8	113.0			0.522
7.85×10^{-2}	51.8	119.1			0.575
Pentanedioic Acid					
2.89×10^{-3}	48.3	90.2	80.0	48.0	0.218
3.71×10^{-3}	48.7	92.2			0.281
5.08×10^{-3}	49.8	93.5			0.376
5.80×10^{-3}	51.1	94.8			0.465
6.96×10^{-3}	50.2	96.2			0.432
1.04×10^{-2}	52.4	97.8			0.553
1.21×10^{-3}	63.7	97.0	90.7	63.7	0.094
1.65×10^{-3}	63.7	101.1			0.151
5.07×10^{-3}	64.1	136.0			0.509
8.00×10^{-3}	68.9	142.2			0.650

CONCENTRATION	b_θ	η_{c_θ}	η_c	b	θ
Pentanedioic Acid - continued					
9.30×10^{-3}	73.8	152.9			0.751
1.22×10^{-2}	74.7	159.8			0.780
Hexanedioic Acid					
4.03×10^{-3}	34.2	91.1	89.1	33.2	0.248
8.56×10^{-3}	38.5	97.0			0.720
1.27×10^{-2}	42.6	101.8			0.866
1.64×10^{-2}	47.0	104.8			0.926
2.31×10^{-2}	49.1	109.7			0.947
2.84×10^{-2}	49.1	112.2			0.949
3.33×10^{-2}	49.1	115.2			0.952
3.03×10^{-3}	57.8	83.9	81.0	52.1	0.424
3.30×10^{-3}	56.2	84.3			0.351
6.11×10^{-3}	60.4	90.0			0.572
1.20×10^{-3}	66.3	95.2	94.9	64.1	0.125
2.04×10^{-3}	66.7	95.5			0.149
3.79×10^{-3}	67.8	99.2			0.242
8.39×10^{-3}	72.6	106.7			0.463
Heptanedioic Acid					
1.12×10^{-3}	37.9	95.4	91.2	37.9	0.105
1.93×10^{-3}	39.4	98.0			0.349

CONCENTRATION	b_Θ	$n_{c\Theta}$	n_c	b	Θ
Heptanedioic Acid - continued					
3.02×10^{-3}	43.7	98.8			0.656
4.31×10^{-3}	44.3	98.6			0.680
5.20×10^{-3}	45.8	99.3			0.738
7.42×10^{-3}	48.2	103.2			0.815
1.08×10^{-2}	50.4	107.5			0.864
8.34×10^{-4}	65.1	100.1	93.1	65.1	0.102
3.67×10^{-3}	74.0	116.8			0.545
4.97×10^{-4}	47.3	91.4	84.2	47.3	0.141
1.15×10^{-3}	48.7	94.2			0.307
1.53×10^{-3}	48.5	95.5			0.312
1.87×10^{-3}	50.5	96.7			0.450
3.63×10^{-3}	51.3	102.8			0.547
3.70×10^{-3}	51.3	102.8			0.547
5.72×10^{-3}	78.7	119.0			0.930
8.91×10^{-3}	60.5	153.0			0.904
5.24×10^{-5}	66.4	109.5	109.3	66.4	0.003
9.49×10^{-5}	66.4	109.7			0.006
1.50×10^{-4}	66.4	110.2			0.013
2.25×10^{-4}	66.4	111.3			0.030
4.17×10^{-4}	66.4	114.2			0.071
1.54×10^{-3}	68.0	122.3			0.241

CONCENTRATION	b_Θ	$n_{c\Theta}$	π_c	$_4b$	Θ
Octanedioic Acid					
6.09×10^{-4}	42.4	87.0	67.1	42.4	0.375
7.76×10^{-4}	43.7	91.1			0.525
1.05×10^{-3}	44.6	93.0			0.596
1.50×10^{-3}	45.8	95.1			0.667
1.89×10^{-3}	47.3	95.9			0.725
2.72×10^{-3}	45.7	98.9			0.690
4.06×10^{-3}	46.4	105.0			0.750
2.50×10^{-4}	48.5	85.9	79.2	48.0	0.178
4.06×10^{-4}	49.1	89.0			0.277
3.18×10^{-3}	56.6	101.3			0.709
Nonanedioic Acid					
9.14×10^{-5}	49.5	91.5	78.2	49.5	0.236
3.00×10^{-4}	50.0	98.0			0.362
3.55×10^{-4}	57.2	96.1			0.647
5.42×10^{-4}	58.1	115.1			0.762
7.37×10^{-4}	65.4	132.8			0.884
1.09×10^{-3}	57.2	148.0			0.858
1.34×10^{-3}	55.3	158.1			0.866
1.15×10^{-4}	46.0	101.5	85.0	46.0	0.301
1.50×10^{-4}	46.1	108.1			0.401
2.19×10^{-4}	45.9	119.7			0.525

CONCENTRATION	b_Θ	η_{c_Θ}	η_c	b	Θ
Decanedioic Acid					
1.78×10^{-5}	65.9	112.7	111.3	64.5	0.094
8.50×10^{-5}	66.5	110.7			0.096
1.17×10^{-4}	67.3	109.8			0.121
1.92×10^{-4}	69.1	109.8			0.198
2.43×10^{-4}	71.3	112.5			0.305
3.60×10^{-4}	75.0	121.2			0.474
4.37×10^{-4}	77.3	131.2			0.577
1.17×10^{-4}	63.2	101.8	101.8	62.6	0.036
2.08×10^{-4}	69.1	104.0			0.329
4.63×10^{-4}	74.4	134.8			0.655
5.42×10^{-4}	79.9	110.0			0.613
7.44×10^{-4}	74.2	102.5			0.462
Benzoic Acid					
5.99×10^{-4}	41.4	91.8	87.7	41.4	0.094
1.64×10^{-3}	41.4	93.2			0.124
2.39×10^{-3}	41.4	95.2			0.166
4.09×10^{-3}	41.4	100.1			0.259
5.33×10^{-3}	34.4	170.0			0.672
7.33×10^{-3}	32.1	185.0			0.705
9.75×10^{-3}	32.1	217.1			0.904

	CONCENTRATION	b_Θ	n_{c_Θ}	n_c	b	Θ
	Benzoic Acid - continued					
	2.91×10^{-4}	37.4	102.8	101.4	37.4	0.037
	1.40×10^{-3}	37.6	103.7			0.095
	2.02×10^{-3}	38.3	104.7			0.213
	3.03×10^{-3}	39.4	103.2			0.315
	5.25×10^{-3}	42.1	112.5			0.630
**	6.91×10^{-3}	42.6	109.0			0.624
	9.47×10^{-4}	38.1	94.6	93.0	37.9	0.070
	1.64×10^{-3}	38.3	96.0			0.138
	2.67×10^{-3}	38.9	97.4			0.248
	3.25×10^{-3}	38.9	98.2			0.258
	3.48×10^{-3}	39.5	98.7			0.340
***	4.74×10^{-3}	40.5	118.6			0.654
	7.13×10^{-3}	32.0	184.0			0.800
	1.11×10^{-2}	37.7	235.7			0.976
NS	5.99×10^{-4}	60.0	113.8	111.0	60.0	0.046
NS	1.64×10^{-3}	60.0	120.8			0.150
NS	2.39×10^{-3}	60.4	122.0			0.190
*** NS	4.09×10^{-3}	55.3	140.7			0.184
NS	5.33×10^{-3}	47.6	176.7			0.301
NS	7.33×10^{-3}	48.1	214.5			0.693
NS	9.75×10^{-3}	45.4	248.4			0.829

CONCENTRATION	b_θ	ηc_θ	η_c	b	θ
Phenyl-Acetic Acid					
5.84×10^{-3}	56.9	103.0	83.8	46.1	0.758
9.80×10^{-3}	73.1	117.0			0.922
1.40×10^{-2}	66.2	145.0			0.930
1.59×10^{-2}	59.9	154.3			0.917
1.80×10^{-2}	59.7	165.7			0.931
2.00×10^{-2}	57.6	172.2			0.931
2.48×10^{-2}	52.2	193.2			0.937
3.18×10^{-2}	50.2	227.2			0.964
2.02×10^{-3}	45.2	86.3	89.1	42.8	0.227
3.54×10^{-3}	47.6	87.8			0.439
6.57×10^{-3}	55.2	104.7			0.805
8.34×10^{-3}	57.5	110.5			0.852
1.33×10^{-2}	55.2	109.0	89.9	44.9	0.756
1.51×10^{-2}	68.0	128.9			0.919
1.43×10^{-3}	44.2	91.0	89.9	43.3	0.147
2.71×10^{-3}	45.2	91.9			0.255
4.40×10^{-3}	49.1	93.8			0.547
5.38×10^{-3}	56.0	99.0			0.781
8.99×10^{-3}	59.3	112.1			0.863
1.15×10^{-2}	69.2	118.3			0.929
1.29×10^{-2}	70.5	135.5			0.947

CONCENTRATION	b_Θ	c_Θ	n_c	b	Θ
Phenyl-Acetic Acid - continued					
NS 5.84×10^{-3}	80.6	135.9	108.6	68.4	0.579
NS 9.80×10^{-3}	76.9	156.0			0.632
NS 1.40×10^{-2}	85.1	180.3			0.782
NS 1.59×10^{-2}	82.9	189.7			0.795
NS 1.80×10^{-2}	87.1	199.0			0.832
NS 2.00×10^{-2}	85.3	206.5			0.841
NS 2.48×10^{-2}	81.7	225.5			0.864
NS 3.18×10^{-2}	81.0	254.0			0.903
NS 1.91×10^{-3}	63.1	118.3	115.3	55.1	0.440
NS 3.73×10^{-3}	63.5	120.8			0.473
NS 4.78×10^{-3}	64.1	121.0			0.492
NS 7.07×10^{-3}	63.9	125.8			0.524
NS 1.24×10^{-2}	71.7	130.0			0.691
NS 1.33×10^{-2}	106.0	139.0			0.893
NS 1.33×10^{-2}	106.0	157.5			0.910
NS 1.51×10^{-2}	85.1	170.5			0.881
NS 1.01×10^{-3}	66.0	106.5	107.5	63.5	0.120
NS 2.02×10^{-3}	66.1	110.4			0.175
NS 3.54×10^{-3}	66.6	115.4			0.254
NS 6.57×10^{-3}	80.8	133.5			0.676
NS 8.34×10^{-3}	82.5	145.8			0.736

	CONCENTRATION	b_0	nc_0	n_c	b	θ
	Phenyl-Acetic Acid - continued					
	NS 1.43×10^{-3}	66.5	111.0	107.5	64.9	0.132
	NS 2.71×10^{-3}	70.9	113.0			0.322
	NS 4.40×10^{-3}	70.7	123.0			0.406
	NS 5.38×10^{-3}	78.8	132.2			0.618
	NS 8.99×10^{-3}	83.4	145.0			0.718
	NS 1.15×10^{-2}	83.4	160.0			0.764
	NS 1.29×10^{-2}	86.9	173.0			0.815
	3-Phenyl-Propanoic Acid					
	NS 1.59×10^{-3}	63.5	109.5	106.8	61.7	0.141
	NS 2.33×10^{-3}	63.5	109.5			0.141
	NS 2.80×10^{-3}	65.2	113.2			0.264
	NS 3.62×10^{-3}	73.6	154.8			0.722
	NS 4.16×10^{-3}	78.3	163.8			0.789
	NS 5.58×10^{-3}	75.1	181.5			0.815
	NS 8.95×10^{-3}	58.2	242.8			0.878
	NS 1.10×10^{-2}	61.8	262.1			0.919
	NS 1.04×10^{-3}	66.4	106.7	105.0	65.8	0.057
	NS 2.13×10^{-3}	68.2	108.0			0.159
	NS 3.05×10^{-3}	70.0	116.4			0.318
	NS 4.79×10^{-3}	86.3	173.0			0.810
**	NS 6.53×10^{-3}	62.8	194.6			0.714
**	NS 7.99×10^{-3}	47.6	226.1			0.681

	CONCENTRATION	b_Θ	nc_Θ	η_c	b	Θ
3-Phenyl-Propanoic Acid - continued						
** NS	1.05×10^{-2}	78.2	132.0			0.604
	9.99×10^{-4}	42.6	83.1	79.8	42.6	0.075
	1.59×10^{-3}	42.6	84.8			0.111
	2.33×10^{-3}	42.6	86.2			0.139
	2.80×10^{-3}	42.6	88.2			0.179
	3.62×10^{-3}	60.9	114.8			0.914
	4.16×10^{-3}	66.6	126.5			0.948
	5.58×10^{-3}	59.0	151.5			0.948
**	8.95×10^{-3}	39.5	222.2			0.955
**	1.10×10^{-3}	94.7	243.9			0.994
	1.04×10^{-3}	43.4	91.0	87.9	43.4	0.069
	1.25×10^{-3}	43.4	92.5			0.100
	3.05×10^{-3}	46.0	87.6			0.281
	4.79×10^{-3}	56.9	135.4			0.894
	6.53×10^{-3}	41.6	236.9			0.964
	7.99×10^{-3}	34.8	239.4			0.944
**	1.05×10^{-2}	40.5	100.3			-
4-Phenyl-Butanoic Acid						
NS	3.87×10^{-4}	63.6	109.8	105.0	63.6	0.073
NS	7.48×10^{-4}	64.3	109.8			0.112
NS	1.24×10^{-3}	64.5	111.5			0.142

	CONCENTRATION	b_0	n_{c_0}	n_c	b	θ
	4-Phenyl-Butanoic Acid - continued					
	NS 1.58×10^{-3}	81.4	132.2			0.688
	NS 2.48×10^{-3}	82.2	160.3			0.784
	NS 3.55×10^{-3}	83.9	175.0			0.827
*	NS 4.90×10^{-3}	58.8	204.7			0.750
*	NS 7.51×10^{-3}	64.4	212.2			0.819
	3.87×10^{-4}	44.6	85.0	83.4	44.6	0.035
	7.48×10^{-4}	44.9	85.9			0.091
	1.24×10^{-3}	45.6	87.0			0.188
	1.58×10^{-3}	55.9	97.0			0.762
	2.48×10^{-3}	63.8	120.9			0.906
	3.55×10^{-3}	52.5	144.8			0.872
	4.90×10^{-3}	48.8	174.2			0.906
*	7.51×10^{-3}	37.0	172.0			0.694

REFERENCES

[1] R.E. Bates, Techniques of Electrochemistry, (eds. Yeager and Salkind), Wiley-Interscience, New York, 1972. Chapter 1.

[2] P. Van Rysselberghe, Electrochim. Acta, 9, 1343 (1964).

[3] E. Lange and B. Miscenko, Z. Physik. Chem., 149, 1 (1930).

[4] N.K. Adam, Physics and Chemistry of Surfaces, 3rd ed., Oxford University Press, London, 1941. p. 300

[5] J. Perrin, J. Chim. Phys., 2, 601 (1904).

[6] A. Helmholtz, Wiss. Abb. Phys. Tech., Reichonst, 1, 925 (1879).

[7] G. Gouy, J. Phys. Rad., 9, 457 (1910).

[8] D.L. Chapman, Phil. Mag., 25, 475 (1913).

[9] O. Stern, Z. Elektrochem., 30, 508 (1924).

[10] R. Parsons, Modern Aspects of Electrochemistry, Vol. 1 (eds. Bockris and Conway), Butterworths, London, 1954. Chapter 3.

[11] J. Malsch, Z. Physik, 29, 770 (1928).

[12] F. Booth, J. Chem. Phys., 19, 391 (1951).

[13] D.C. Grahame, Chem. Rev., 41, 441 (1947).

[14] M.A.V. Devanathan, J.O'M. Bockris and K. Müller, Proc. Royal Soc., London, A274, 55 (1963).

[15] J.R. MacDonald, J. Chem. Phys., 22, 1857 (1954).

[16] N.F. Mott and R.J. Watts - Tobin, Electrochim. Acta, 4, 79 (1961).

[17] E.C. Potter, Electrochemistry, Cleaver-Hume, London, 1956.

[18] S. Glasstone, K.J. Laidler and H. Eyering, The Theory of Rate Processes, McGraw-Hill, New York, 1941.

[19] K.J. Vetter, Electrochemical Kinetics (Transl. ed. S. Bruckenstein and B. Howard), Academic Press, New York, 1967.

[20] J. Tafel, Z. Physik. Chem., 50, 641 (1905).

[21] T. Erdey-Gruz and M. Volmer, Z. Phys. Chem., 150A, 203 (1930).

[22] J.O'M. Bockris, Modern Aspects of Electrochemistry, Vol. 3 (eds, Bockris and Conway), Butterworths, New York, 1964. Chapter 4.

[23] B.E. Conway and J.O'M. Bockris, Proc. Royal Soc., A248, 394 (1958).

[24] B.E. Conway and J.O'M. Bockris, Electrochim. Acta, 3, 340 (1960).

[25] E. Mattson and J.O'M. Bockris, Trans. Faraday Soc., 55, 1586 (1959).

[26] R.W. Gurney, Ionic Processes in Soltuion, McGraw-Hill, New York, 1953.

[27] N.S. Hush, Trans. Faraday Soc., 57, 557 (1961).

[28] W.F. Libby, J. Phys. Chem., 56, 863 (1952).

[29] R.A. Marcus, Can. J. Chem., 37, 155 (1959).

[30] H. Gerischer, Z. Electrochem., 62, 256 (1956).

[31] H. Kita, M. Enyo and J.O'M. Bockris, Can. J. Chem., 39, 1670 (1961).

[32] A. Damjanovic and J.O'M Bockris, J. Electrochem. Soc., 110, 1035 (1963).

[33] J.J. Kipling, Adsorption from Solutions of Non-Electrolytes, Academic Press, London, 1965. Chapter 7.

[34] C.H. Giles, T.H. MacEwan, S.N. Nakhwa, and D. Smith, J. Chem. Soc., 3973 (1960).

[35] T. Cummings, H.C. Garven, C.H. Giles, S.M.K. Rahman, J.G. Sneddon and C.E. Steward, J. Chem.Soc., 535 (1959).

[36] D.A. Swinkels and J.O'M. Bockris, J. Electrochem.Soc., 111, 736 (1964).

[37] J.O'M. Bockris, M. Green and D.A. Swinkels, J. Electrochem. Soc., 111, 743 (1964).

[38] B.B. Damaskin, Electrokhimiya, 3, 1390 (1967).

[39] H.P. Dhar, B.E. Conway, and K.M. Joshi, Electrochim. Acta, 18, 789 (1973).

[40] P.J. Flory, J. Chem. Phys., 10, 51 (1942).

[41] M.L. Huggins, Ann. N.Y. Acad. Sci., 43, 1 (1942).

[42] B.E. Conway, H. Angerstein-Kozlowska, and H.P. Dhar, Electrochim. Acta, 19, 455 (1974).

[43] H. Dahms and M. Green, J. Electrochem. Soc., 110, 1075 (1963).

[44] N. Tompa, Polymer Solutions, Butterworths, London, 1956. p.78.

[45] T.L. Hill, Introduction to Statistical Thermodynamics, Addison-Wesley, San Francisco, 1962.

[46] R. Parsons, J. Electroanal. Chem., 8, 93 (1964).

[47] E.A. Guggenheim, Mixtures, Clarendon Press, Oxford, 1952. Chapter 10.

[48] J.M. Honig, Solid-Gas Interface (ed. E.A. Flood), Marcel Dekker, New York, 1967. p.371.

[49] R.O. Loutfy, Electrosorption Effects of Organic Additives on the Cathode-Overpotential of Copper Electrodeposition, Ph.D. Thesis, University of Western Ontario, 1971.

[50] K.M. Joshi, M.R. Bapat, and S.W. Dhawale, Electrochim. Acta, 15, 1519 (1970).

[51] I. Langmuir, J. Am. Chem. Soc., 40, 1361 (1918).

[52] B.E. Conway, Techniques of Electrochemistry (eds. Yeager and Salkind, Wiley-Interscience, New York, 1972. Chapter 5.

[53] F.C. McCrackin, E. Passaglia, R.R. Stromberg, and H.L. Steinberg, J. Res. Natl. Bur. Stds., A. Phys. and Chem., 67A, 363 (1963)

[54] K.H. Zaininger and A.G. Revesz, R.C.A. Review, 25, 85 (1964).

[55] P.H. Berning, Physics of Thin Films (ed. G. Hass), Academic Press, New York, 1963. Vol. 1, p. 69.

[56] L. Laliberte and B.E. Conway, Report to the Defence Research Board, Canada, Grant No. 5412-01, September 1970.

[57] F.O. Koenig, J. Phys. Chem., 38, 339 (1934).

[58] S.R. Craxford, O. Gatty, and J. Philpot, Phil. Mag., 7, 19, 965 (1935).

[59] D.C. Grahame and R.B. Whitney, J. Am. Chem. Soc., 64, 1548 (1942).

[60] R. Parsons and M.A.V. Devanathan, Trans. Faraday Soc., 49, 404 (1953).

[61] G. Lippmann, Ann. Chim. Phys., 5, 494 (1875)

[62] G. Gouy, Ann. Chim. Phys., 7, 29, 145 (1903).

[63] B.E. Conway, Theory and Principles of Electrode Processes, Ronald Press, New York, 1965.

[64] P. Delahay, Double Layer and Electrode Kinetics, Interscience, New York, 1965. Chapter 5.

[65] S.R. Craxford and H.A.C. McKay, J. Phys. Chem., 39, 545 (1935).

[66] P. Corbusier and L. Gierst, Anal. Chim. Acta, 15, 254 (1956).

[67] R.G. Barradas and F.M. Kimmerle, Can. J. Chem., 45, 109 (1967).

[68] A.Y. Gokshtein, Soviet Electrochemistry, 2, 1318 (1966); Dokl. Akad. Nauk. SSR, 174, 394 (1967).

[69] T.R. Beck, J. Phys. Chem., 73, 466 (1969).

[70] P.A. Rebinder and N.A. Kalinovskaya, Zh. Fiz. Khim., 5, 332 (1934).

[71] J.O'M. Bockris and R. Parry-Jones, Nature, 17, 930 (1953).

[72] P.A. Rebinder and E.K. Venstrem, Zh. Fiz. Khim., 19, 1 (1945).

[73] B.B. Damaskin, O.A. Petrii and V.V. Batrakov, Adsorption of Organic Compounds on Electrodes, Plenum Press, New York, 1971. p. 187.

[74] N.A. Balashova, Z. Physik. Chem., 207, 340 (1957).

[75] N.A. Balashova and N.S. Merkuleva, Trudy Chet. Soveshchaniya po Electrokhimii, 1959. p. 48.

[76] E. Blomgren and J. O'M. Bockris, Nature, 186, 305 (1960).

[77] H. Wroblowa and M. Green, Electrochim. Acta, 8, 679 (1963).

[78] E. Gileadi, B.T. Rubin, and J.O'M. Bockris, J. Phys. Chem., 69, 3335 (1965).

[79] W. Heiland, E. Gileadi, and J.O'M. Bockris, J. Phys. Chem., 70, 1207 (1966).

[80] N. Hackerman and S.J. Stephens, J. Phys. Chem., 58, 904 (1954).

[81] M. Green, D.A.J. Swinkels, and J. O'M. Bockris, Rev. Sci. Instr., 33, 20 (1961).

[82] A.N. Frumkin and B.B. Damaskin, Modern Aspects of Electrochemistry, (eds. J.O'M. Bockris and B.E. Conway), Vol. 3, Butterworths, London, 1964. Chapter 3.

[83] G.J. Hills and R. Payne, Trans. Faraday Soc., 61, 316 (1965).

[84] G.H. Nancollas and P. Vincent, J. Sci. Inst., 40, 306 (1963).

[85] D.C. Grahame, J. Am. Chem. Soc., 63, 1207 (1941); 71, 2975 (1949).

[86] R.N. O'Brien and P. Seto, J. Electroanal. Chem., 18, 219 (1968).

[87] M.A. Proskurnin and A.N. Frumkin, Trans. Faraday Soc., 31, 110 (1935).

[88] A.N. Frumkin, Electrochim. Acta, 9, 465 (1964).

[89] T. Biegler and H.A. Laitinen, J. Electrochem. Soc., 113, 852 (1966).

[90] K. Niki and N. Hackerman, J. Electroanal. Chem., 32, 257 (1971).

[91] A. Aramata and P. Delahay, J. Phys. Chem., 68, 880 (1964).

[92] K. Asada, P. Delahay, and A.K. Sundasam, J. Am. Chem. Soc., 83, 3396 (1961).

[93] K. Niki and N. Hackerman, J. Phys. Chem., 73, 1023 (1969).

[94] R.W. Schmid and C.N. Reilley, J. Am. Chem. Soc., 80, 2087 (1958).

[95] J. Koryta and K. Holub, J. Electroanal. Chem., 9, 169 (1965).

[96] H.A. Laitinen, K. Eda, and N. Nakanishi, Talanta, 11, 321 (1964).

[97] V.K. Venkatesan, B.B. Damaskin, and N.V. Nikolaeva-Fedorovich, J. Electroanal. Chem., 25, 85 (1970).

[98] F.A. Ammar, S. Darwich, and M.W. Khalil, Electrochim. Acta, 12, 657 (1967).

[99] L. Gierst, J. Tondeur, and E. Nicolas, J. Electroanal. Chem., 10, 397 (1965).

[100] A.N. Frumkin, Trans. Faraday Soc., 55, 156 (1959).

[101] S. Sathyanarayana, J. Electroanal. Chem., 10, 119 (1965).

[102] E.J. Duwell, J. Electrochem. Soc., 109, 1013 (1962).

[103] A.K.P. Chu and A.J. Sukava, J. Electrochem. Soc., 116, 1188 (1969).

[104] R.O. Loutfy and A.J. Sukava, J. Electrochem. Soc., 118, 216 (1971).

[105] P.F.L. Seto, Electrosorption Effects of Amino Acids on the Rate of Copper Electrodeposition, Ph.D. Thesis, University of Western Ontario, 1972.

[106] R.S. Hansen and B.H. Clampett, J. Phys. Chem., 58, 908 (1954).

[107] R.S. Salter, P. Seto, and A.J. Sukava, J. Electrochem. Soc., 119, 852 (1972).

[108] A.J. Sukava, H. Schneider, D.J. McKenney, and A. T. McGregor, J. Electrochem. Soc., 112, 571 (1965).

[109] R.O. Loutfy, J. Electroanal. Chem., 38, 282 (1972).

[110] E. Blomgren, J.O'M. Bockris, and C. Jesch, J. Phys. Chem., 65, 2000 (1961).

[111] S. Sathyanarayana and G. Manohar, J. Electroanal. Chem., 51, 151 (1974).

[112] G. Horanyi and F. Nagy, J. Electroanal. Chem., 32, 275 (1971).

[113] D.R. Turner and G.R. Johnson, J. Electrochem. Soc., 109, 798 (1962).

[114] R. Parsons and J.T. Reilly, J. Electroanal. Chem., 24, App. 23 (1970).

[115] K.M. Joshi, W. Mehl, and R. Parsons, Trans. Symp. on Electrode Processes (ed. Yeager), John Wiley, New York, 1959. p.249.

[116] M.A.V. Devanathan, J.O'M. Bockris, and W. Mehl, J. Electroanal. Chem., 1, 143 (1959).

[117] J.J. McMullen and N. Hackerman, J. Electrochem. Soc., 106, 341 (1959).

[118] C.A. Winkler, Can. J. Chem., 31, 306 (1953).

[119] G.C. Barker, Trans. Symp. on Electrode Processes (ed. Yeager), John Wiley, New York, 1959. p. 366.

[120] D.A. Jenkins and C.J. Weedan, J. Electroanal. Chem., 31, App. 13 (1961).

[121] A. Damjanovic, M. Paunovic, and J. O'M. Bockris, J. Electroanal. Chem., 9, 93 (1965).

[122] H. Fischer, Electrochim. Acta, 2, 50 (1960).

[123] J. O'M. Bockris and G.A. Razumney, Fundamental Aspects of Electrocrystallization, Plenum Press, New York, 1967.

[124] O. Volk and H. Fischer, Electrochim. Acta, 5, 112 (1961).

[125] H. Schneider, A.J. Sukava, and W.J. Newby, J. Electrochem. Soc., 112, 568 (1965).

[126] A.N. Frumkin, Z. Physik Chem., 164, 121 (1933).

[127] R. Parsons, Advances Electrochem. and Electrochem. Engineering (eds. Delahay and Tobias), Vol. 1, Interscience, New York, 1961, p. 1.

[128] M.A.V. Devanathan, Electrochim. Acta, 17, 1683 (1972).

[129] R. Parsons, J. Electroanal. Chem., 21 35 (1969).

[130] B.E. Conway, R.G. Barradas, and P.G. Hamilton, Collect. Czech. Chem. Commun., 32, 1790 (1967).

[131] B.E. Conway, H.P. Dhar, and S. Gottesfeld, J. Colloid Interface Sci., 43 303 (1973).

[132] N.S. Hush, J. Chem. Phys., 28, 962 (1958).

[133] R. Guidelli, J. Electroanal. Chem., 53, 205 (1974).

[134] W.R. Fawcett, J. Electroanal. Chem., 22, 19 (1969).

[135] W.R. Fawcett and S. Levine, J. Electroanal. Chem., 43, 175 (1973).

[136] A. Frumkin, B. Damaskin, and O. Petrii, J. Electroanal. Chem., 53, 57 (1974).

[137] D. C. Grahame, J. Electrochem. Soc., 98, 343 (1951).

[138] A.N. Frumkin, Z. Elektrochem., 59, 807 (1955).

[139] L. Gierst, Trans. Symposium on Electrode Processes (ed. Yeager), John Wiley, New York, 1959. p. 143.

[140] H.H. Bauer, J. Electroanal. Chem., 16, 419 (1968).

[141] R. Parsons, Trans. Faraday Soc., 47, 1332 (1951).

[142] C. Perrin, Progr. Phys. Org. Chem., 3, 165 (1965).

[143] J.A.V. Butler, Trans. Symposium Electrode Processes, John Wiley, New York, 1961.

[144] J.A.V. Butler, Trans. Faraday Soc., 19, 729 (1924).

[145] J.A.V. Butler, Trans. Faraday Soc., 19, 734 (1924).

[146] F.P. Bowden, Proc. Royal Soc. London, A126, 107 (1929).

[147] B. Breyer and H. H. Bauer, Alternating Current Polarography and Tensammetry, Interscience, New York, 1963.

[148] T. Erdey-Gruz and H. Wick, Z. Physik. Chem., A162, 53, (1932).

[149] H. Eyring, S. Glasstone, and K.J. Laidler, J. Chem. Phys., 7, 1053 (1939).

[150] H. Eyring, S. Glasstone, and K. J. Laidler, Trans. Electrochem. Soc., 76, 145 (1939).

[151] M. Volmer and H. Wick, Z.Physik. Chem., A172, 429.(1935).

[152] A.R. Despic and J. O'M. Bockris, J. Chem. Phys., 32, 389 (1960).

[153] V.G. Levich, Dokl. Akad. Nauk SSSR, 67, 309 (1949); Physiochemical Hydrodynamics, 2nd edn., Academy of Sciences, Moscow (1959).

[154] L. Gierst, Proc. Meeting CITCE 1955, Butterworths, London, 1957, p. 49.

[155] R. Parsons, Advances in Electrochemistry and Electrochemical Engineering (eds. P. Delahay and C.W. Tobias), Wiley, New York, 1961. Vol. 1, p. 1.

[156] A. Frumkin, Advances in Electrochemistry and Electrochemical Engineering (eds. P. Delahay and C.W. Tobias), Wiley, New York, 1961. Vol. 1, p. 65.

[157] K.B. Oldham, J. Electroanal. Chem., 16, 125 (1968).

[158] A. Damjanovic, T.H.V. Setty, and J. O'M. Bockris, J. Electrochem. Soc., 113, 429 (1966).

[159] D.A. Vermilyea, J. Electrochem. Soc., 106, 66 (1959).

[160] P.B. Price, D.A. Vermilyea, and M.B. Webb, Acta Met., 6, 524 (1958).

[161] S.D. Argade and E. Gileadi, Electrosorption (ed. Gileadi), Plenum, New York, 1967. Chapter 5.

[162] L. Egorov and I. Novosel'skii, Soviet Electrochem., 6, 845 (1970).

[163] S. Trasatti, J. Electroanal. Chem., 33, 351 (1971).

[164] L. Egorov and I. Novosel'skii, Soviet Electrochem., 6, 869 (1970).

[165] J. Clavilier and Nguyen van Huong, C.R. Ser. C, 270, 982 (1970).

[166] A. Frumkin, J. Chem. Phys., 7, 552 (1939).

[167] Klein and Lange, Z. Electrochem., 43, 570 (1947).

[168] Latimer, Pfizer, and Slansky, J. Chem. Phys., 7, 108 (1939).

[169] Lange, Handbook of Chemistry, 3rd ed., McGraw-Hill, U.S.A., 1967.

[170] K.S. Markley, Fatty Acids, Interscience, New York, 1949.

[171] A. Seidell, Solubilities of Inorganic and Organic Compounds, D. Van Nostrand, New York, 1952.

[172] R.J. Gale, Amino Acids as Additives in Copper Electrodeposition, Ph.D. Thesis, McGill University, 1972.

[173] I. Langmuir, J. Am. Chem. Soc., 39, 1848 (1917).

[174] V.A. Kir'yanov, V.S. Krylov, and B.B. Damaskin, Soviet Electrochem., 6, 521 (1970).

[175] R.I. Kaganovich, V.M. Gerovich, and T.G. Ostova, Dokl. Akad. Nauk SSR, 155, 893 (1964).

[176] R.I. Kaganovich and V.M. Gerovich, Elektrokhimiya, 2, 977 (1966).

[177] R.G. Barradas and J.M. Sedlak, Electrochim. Acta, 16, 2091 (1971).

[178] B.E. Conway and H.P. Dhar, Electrochim. Acta, 19, 445 (1974).

[179] B.E. Conway and H.P. Dhar, Croatica Chem. Acta (Proc. Conference on Surface Chemistry, Rovinj, Yugoslavia, 1972), 45, No. 1 (1973).

[180] J. O'M. Bockris, E. Gileadi, and K. Müller, Electrochim. Acta, 12, 1301 (1967).

[181] A.A. Maryatt and E.R. Smith, Table of Dielectric Constants of Pure Liquids, National Bureau of Standards Circular.

[182] G.A. Dobren'kov and L.T. Guseva, Soviet Electrochem, 10, 110 (1974).

[183] R.I. Kaganovich, B.B. Damaskin, and I.M. Gahzhina, Elektrokhimiya, 4, 867 (1968).

[184] R.I. Kaganovich, B.B. Damaskin, and M.M. Andrusev, Elektrokhimiya, 5, 745 (1969).

[185] Lorenz, Mockel, and Muller, Z. Phys. Chem. (N.F.), 25, 145 (1960).

[186] Lorenz and Müller, Z. Phys. Chem. (N.F.), 25, 161 (1960).

[187] A.K. Shallal, H.H. Bauer, and D. Britz, Collect. Czech. Chem. Commun., 36, 767 (1971).

[188] P. Dolin and B.V. Ershler, Acta Physicochim. URSS, 13, 747 (1940).

[189] B.E. Conway, J. Electroanal. Chem., 8, 486 (1964).

[190] B.E. Conway, E. Gileadi, and H.A. Kozlowska, J. Electrochem. Soc., 112, 341 (1965).